TUD | Technische Petrologie | Schnittspahnstraße 9 | 64287 Darmstadt

TUD | Technische Petrologie | Schnittspahnstraße 9 | 64287 Darmstadt

Final Report

Thermal Integrity of Clay and Claystones - Experiment and Coupled THMC – Simulations

Sub-project: ***Analysen_THMC-Sim***

Ferreiro Mählmann Rafael	TU-Darmstadt
Hoang-Minh Thao	VNU, Hanoi University of Sciences
Kasbohm Jörn	Jörn-Kasbohm-Consulting, Greifswald
Nguyen-Thanh Lan	TU-Darmstadt
Van Bui Dong	VNU, Hanoi University of Sciences
Scheuvens Dirk	TU-Darmstadt
Ukrainczyk	TU-Darmstadt

June, 2024

Content

List of Symbols and Abbreviations

%S	proportion of smectitic layer in mixed layer phases
1w-smectite	Monovalent interlayer cation smectite (Na-smectite
2w-smectite	Divalent interlayer cation smectite (Ca-smectite)
BET	Brunauer–Emmett–Teller surface area
BM	beidellite-montmorillonite intergrowth
BMI-ml	beidellite-montmorillonite-illite interstratification
calc.	calculation
CEC	Cation exchange capacity
diVS-ml	K- and/or charge deficit dioctahedral vermiculite-smectite interstratification
DTA	differential thermal analysis
FTIR	Fourier Transform Infrared
IS-ml	normal charged illite-smectite interstratification
IV	tetrahedral layer
KS GLY R0	kaolinite- one water layer smectite mixed layer
KSS GL R0	kaolinite – one water layer smectite – two water layer smectite mixed layer
KSV-ml	kaolinite-smectite-dioctahedral vermiculite interstratification
meas.	measurement
SEM-EDX	Scanning Electron Microscopy linked with energy dispersive X-ray spectroscopy
SSA	specific surface area
TA	Thermal analysis
TEM-EDX	Transmission Electron Microscropy linked with energy dispersive X-ray spectroscopy
TG	thermogravimetric
Tmean	thickness of particles
VI	octahedral layer
XII	interlayer charge
XRD	X-ray diffraction
XRF	X-ray Fluoresence
Δ%S	Specific Dissolution Potential

Part I. INITIAL MATERIALS

1. Introduction

This report presents results from a joint research project on smectite-rich clay minerals with respect to their use as buffer and backfill materials in a repository for high-level radioactive waste. The project "Thermal Integrity of Clay and Claystones - Experiment and Coupled THMC Simulations" is initiated and funded by the Bundesgesellschaft für Endlagerung (BGE). The Gesellschaft für Anlagen- und Reaktorsicherheit (GRS) was commissioned with its realisation.

In this report, a clay-rich rock of a commercial high-quality bentonite from Bavaria in Germany (B25 bentonite), Opalinus clay from the Opalinus deposit, and Friedland clay are characterized from a mineralogical perspective as starting materials in THMC experiments. Different methods are used, including geochemical composition analysis via X-ray Fluorescence (XRF) for whole rocks (<40 µm fraction) of initial materials. Additionally, whole rocks are characterized by X-ray Diffraction (XRD), Infrared Spectroscopy (IR), and Thermal Analysis (TA), as well as cation exchange capacity (CEC) and specific surface area (SSA). Surface charge for powder materials and scanning electron microscopy (SEM-EDX) for claystone and compacted clay specimens are also investigated. The < 2 µm fractions are carefully examined by additional methods, including Transmission Electron Microscopy linked with Energy Dispersive X-ray Spectroscopy (TEM-EDX) and oriented mount specimens from XRD.

The application of above-mentioned analytical methods follows the principle of differential diagnostics. Differential diagnostics is a typical methodology to investigate clay minerals. Different analytical methods are combined to verify, validate and complete results of the main analytics. X-ray diffraction of bulk powder is a typical commonly applied mineralogical method. This analysis offers an overview of mineral matter (qualitative and quantitative) and describes additionally selected parameters of certain clay minerals (e.g. polytype of mica, differentiation between di- or trioctahedral clay minerals). X-ray diffraction on oriented specimen of fraction < 2 µm gives information about degree of expandability, e.g. to distinguish between smectite and mixed layer phases. Differential thermogravimetric analysis (DTA/TG) let recognize the possible occurrence of amorphous phases, which are mostly not to detect by XRD. The particle-by-particle determination of chemistry of phases by transmission electron microscopy (TEM-EDX) visualizes possible alteration processes in the composition of certain mineral phases (e.g. smectite), which are not to recognize by XRD. The verification of clustered chemical TEM-EDX-results with expandability detected by oriented XRD is to consider as further validation of TEM-data clustering and additionally an indicator to distinguish between montmorillonite and beidellite. Fourier transform infrared spectroscopy (FTIR) offers even indications to distinguish between montmorillonite and beidellite and to characterize the Al/Fe-ratio in octahedral layer of smectite (confirming the results by TEM-EDX).

Meleshyn et al. (2024) offer a description of applied samples: The solids analysed are Bavarian bentonite (Calcigel), Opalinus clay from the clayey facies and Friedland clay. The Bavarian bentonite, which has already been successfully used in the Salzdetfurth shaft seal at a density of 1.6 g/cm³ and at a fluid pressure load of up to 70 bar (Breidung, 2002; Sitz et al., 2003), was provided by Stephan Kaufhold (BGR) and comes from batch sample B25. The Opalinus clay was obtained in the Mont Terri rock laboratory (Switzerland) (borehole BLT-A7 from 2013 (Laurich et al., 2019) and borehole BFS-B12 from 31 October 2022; the sample material from borehole BLT-A7 was used for the development of the method and the first tests, while the results documented below were obtained with the sample material from borehole BFS-B12). The Friedland clay comes from the Siedlungsscholle clay pit near Friedland in Mecklenburg-Western Pomerania (sample material extracted in the 'Ost-Feld' in September/October 2022, sampling in the external storage facility on 12 January 2023). For the main tests,

cylindrical test specimens with a height of 20 mm and a diameter of 22 mm were produced from the three materials. A slightly different sample preparation procedure was required for each material.

The results revealed that the three starting materials are composed of a high amount of clay minerals. Smectite is the main mineralogical phase, which determines the swelling behaviour of clays and bentonites. In B25 bentonite and Friedland Clay, smectite is distributed in three different groups of smectite-bearing phases (Ca-smectite, diVS-ml, KS-ml), in Opalinus Clay only in two groups (diVS-ml, KS-ml).

Smectite is present in B25 bentonite as beidellite-rich Ca-smectite and furthermore as montmorillonite in illite-smectite mixed layer phases with K- and/or charge deficiency (diVS-ml) and in kaolinite-smectite mixed layer phases (KS-ml). Further minor phases are illite ($2M_1$, $1M$), kaolinite, quartz, and feldspar. 86% of mineral matter in initial B25 bentonite are clay mineral phases. Illite in fraction < 2 µm of original material occurs in two clusters: (i) reduced K in interlayer as well as octahedral layer is Al-rich (octahedral Al/Fe-ratio ~ 4.6) and (ii) high reduced K in interlayer and octahedral layer is Al-poor and Fe-rich (octahedral Al/Fe-ratio ~ 1.1).

Smectite is mainly found in the Friedland clay series (sum of clay mineral phases: 78%) in illite-smectite mixed layers (a minor phase) with K- and/or charge deficiency (diVS-ml) and in Ca-smectite as well as kaolinite-smectite mixed layer phases (both are trace phases). Beidellite is only a minor component of smectite in diVS-ml phases, whereas in Ca-smectite, it is the dominant smectite component. The main phase in Friedland clay is illite (1M), accompanied by illite ($2M_1$), kaolinite and quartz as minor phases. Illite in fraction < 2 µm is characterized by a reduced K in interlayer and its octahedral layer is Al- and Fe-rich. Friedland clay also contains traces of chlorite, feldspar, pyrite, calcite, and anatase. Calcite occurs as crystalline calcite and probably also as amorphous calcium carbonate.

Smectite is found in the Opalinus clay series (sum of clay mineral phases: 61%) in illite-smectite mixed layers with K- and/or charge deficiency (diVS-ml, a minor phase) and especially in kaolinite-smectite mixed layer phases (KS-ml, the main phase). Montmorillonite is the dominant smectite component. Illite ($2M_1$) and kaolinite (including KS-ml) are the main phases in Opalinus clay, accompanied by illite (1M), diVS-ml, quartz, and calcite as minor phases and traces of chlorite, feldspar, pyrite, siderite, dolomite, and anatase. Illite in fraction <2 µm of borehole BLT-A7 is characterized by high reduced K in interlayer and its octahedral layer is Al- and Fe-rich. Illite in fraction <2 µm of borehole BFS-B12 has a higher amount of K in interlayer (similar to Friedland clay) than in illite from borehole BLT-A7. Furthermore, borehole BFS-B12 shows three groups of illite in fraction < 2 µm differentiated mainly by specific octahedral Al/Fe-ratio.

Following the analytical principle of differential diagnostics for clay minerals, the results of XRD, as main analytical method, of the three bulk samples are consistent with IR, TA and TEM-EDX-results. The <2 µm fraction shows the highest frequency of smectite, dioctahedral vermiculite-smectite mixed layer (diVS-ml), illite-smectite mixed layer (IS-ml), and illite with a significant amount of interlayer K and a high content of Fe in the octahedral sheet, as well as significant substitution of Al for Si in the tetrahedral sheet. The same finding of high octahedral Fe is also observed in IR results. The TEM-EDX results are comparable with the oriented mount of XRD by classification into two and partially three clusters.

After the experimental runs, smectites remain the main phases, determining the swelling behaviour of clays. Each smectite-bearing group showed specific behaviour during the experiments. The role and behaviour of KS-ml remain largely unclear. The analytical evidence is mostly the result of modelling of X-ray diffractograms (oriented specimen) and indirect evaluation of thermogravimetry in comparison to powder X-ray diffractometry. Finally, in the experiments with increased thermal load, sample B25 showed slight "illitization," but Opalinus indicated contrasting behaviour of largely stability and

unchanged conditions. Friedland clay is even stable in the development of %S in sum. In detail, %S of diVS-ml phases is increasing with rising thermal load in the experiments. It seems, this development is compensating the loss of Ca-smectite in treated Friedland clay in experiments higher than 60°C.

Additional overhead shaking experiments were applied to evaluate the specific dissolution potential of B25 and Opalinus clay according to Nguyen-Thanh et al. (2014). As Ca-Mg-interlayer type, the results suggested that Opalinus clay is characterized by slow-reacting smectites under limited reaction conditions, but under strong conditions (e.g. high temperature, high ionic strength of solution, 'fast' mass transport in sample body and only Na can act as protecting interlayer type, but Na is not really available there), it will turn to very fast reacting by losing most of the smectitic layer in smectite. The presence of pyrite especially acts as a strong influence on this behaviour. It is expected that the same behaviour would be found in Friedland clay. Otherwise, the specific dissolution potential of B25 bentonite showed as moderately reactive smectite, but under mentioned strong experimental conditions, this clay can react strongly and quickly, causing a complete loss of the smectitic layer in smectite phases.

2. Analytical Methods

2.1 X-ray diffraction (XRD)

Three clay materials of B25 bentonite, Opalinus and Friedland clays are analyzed both as random powders of the bulk materials (<40 µm) and oriented mounts of the clay fraction (< 2µm) by use of a Bruker Diffractometer D8 at Department of Material Sciences, Technical University Darmstadt. The equipment was operated at 30 mA and 40 kV, Cu-K$\alpha_{1,2}$ radiation, 0.5/25 soller collimator, automatic divergence slit, X'Celerator line focus detector. The data were recorded in the range of 4 to 70 °2Θ for randomly oriented powder samples and 4 to 40 °2Θ for oriented mounts.

2.1.1 Random oriented powders

The bulk samples were dried at 50 °C and ground in an agate mortar until the particles were as small as possible. The sample was brushed through a <0.4 µm sieve and carefully packed into the sample holder to avoid the preferred orientation of the particles. A glass slide was used to pack the sample firmly and create a smooth surface to minimize deformation during the rotation of the sample while measuring. A step size of 0.008° 2Θ, and 20 total added seconds for each measurement step were applied.

After identifying the main mineral components by comparison with the ICDD/PDF-4 Minerals database, the mineral phases were refined using the Rietveld program BGMN and the Profex user interface by Taut et al. (1998) and Doebelin and Kleeberg (2015). The B25, Opalinus, and Friedland clays contain a mixture of disordered phases (smectite, IS-ml). The smectite phase content is considered as 1w-smectite for Na-smectite and 2w-smectite for Ca-smectite. These results are then cross-checked with TEM-EDX results, XRF data, and DTA-TG to achieve the best fit for the quantification of mineral phases.

2.1.2 Oriented mounts

The clay suspension of the <2 µm fraction was prepared by Atterberg sedimentation. Oriented mounts were prepared by dispersing 45 mg of clay in 1.5 mL of deionized water and pipetting the dispersion onto glass slides. The mounts of oriented clays were scanned with a step size of 0.02° from 4° to 40° 2Θ. Clay minerals were identified according to the criteria of Brindley and Brown (1980), which are based on the reactions of clays to the following treatments:

- The swelling behaviour was tested by saturating the clay with ethylene glycol at 60 °C for at least 48 hours.
- Illite/smectite interstratification (IS-ml) was identified according to Moore and Reynolds (1989) and quantified using Sybilla© software.
- Heating the materials at 550 °C for 4 hours allowed for the identification and distinction of kaolinite and chlorite.

In addition, the XRD patterns of oriented specimens were modelled, in both air-dried and ethylene glycol-saturated states, with the Sybilla© software developed by Chevron™ (Aplin et al., 2006). This software is designed to calculate theoretical XRD patterns of the basal reflections of discrete clay minerals and interstratification structures. Sybilla©, based on the program designed by Drits and Sakharov (1976), allows direct comparison between experimental and calculated XRD profiles. Instrumental and experimental parameters of the goniometer were introduced but not further refined. The amount of interlayer species, octahedral iron, and the main value of coherent scattering domain sizes (T_{mean}) were considered as variable parameters during the fitting process.

2.2 X-ray Fluoresence (XRF)

Bulk samples were analysed for chemical composition using an X-ray fluorescence spectrometer S8 Tiger (Bruker). The samples were prepared as glass disks with a fully automated fusion technique. Loss on ignition (LOI) was determined at 1100 °C as an approximate measure of volatile H_2O. This method was applied only for the initial materials and these data were used to characterize the chemical composition of the bulk rocks and to cross-check the results of quantitative mineralogical composition identified by XRD of randomly oriented materials.

2.3 Fourier Transform Infrared (FTIR)

A Fourier Transform Infrared (FT-IR) spectroscopic study was conducted using the Varian 670-IR series FT-IR spectrometer. Powder samples (bulk samples) of approximately 1 to 2 mg were mixed homogeneously with 120 mg of KBr, which was pre-dried at 80 °C for at least 6 hours, and then pressed into a dye to form a pellet with a diameter of 13 mm. The spectra were recorded in the mid-infrared range, extending from 400 cm^{-1} to 4000 cm^{-1}, with multiple scans (e.g., 64 scans and 4 cm^{-1} resolution) at room temperature. Detailed investigations focused on the OH-stretching region between 3800 cm^{-1} and 3200 cm^{-1} and the OH-bending region between 1000 cm^{-1} and 750 cm^{-1}.

The FT-IR spectra were deconvoluted using Origin 2021 Peak Fitting software. A Gaussian distribution function was applied to smooth the spectra and to determine the exact values of peak position, full width at half maximum (FWHM), intensity, and area. The interpretation of the absorption spectra was primarily based on the works of Farmer (1974) and Farmer and Russell (1964).

2.4 Thermal analysis (TA)

Thermal analysis, including thermogravimetric (TG) investigation and differential thermal analysis (DTA), was performed using a NETZSCH STA 449 C at 3.5 kVA under an Ar atmosphere. The materials were milled to 40 µm and then dried at 35 °C for 1 hour. A 40 mg sample was heated to 1100 °C with a heating segment (S1) from around 35 °C up to 1100 °C, followed by an isothermal segment (S2) with a holding time of 20 minutes. Finally, the sample was rapidly cooled down to 1000 °C. Al_2O_3 was used as the reference material. The results were evaluated using NETZSCH Proteus Software.

2.5 Cation exchange capacity (CEC) and Brunauer–Emmett–Teller (BET) surface area and surface charge analysis

CEC measurements were conducted according to Gillman (1979). A 0.5 g sample of air-dried clay was mixed with 30 mL of 0.1 M aqueous $BaCl_2$ solution and shaken slowly on an end-over-end shaker (15 rpm) for 5 hours. The supernatant was removed by centrifugation and filtered with Whatman No. 41 filter paper. This procedure was repeated 5 times, and after each ion exchange, all liquid fractions were combined and analysed using atomic absorption spectroscopy (AAS) and ion chromatograph (IC) for Ca, Mg, K, Na, Al, Fe, and Mn. Finally, the concentrations of Ca, Mg, Na, and K were used for CEC calculation.

The surface charges of initial and reaction products were determined by polycation titration combined with streaming potential measurements using a particle charge detector (PCD-06) at the Department of Applied Geosciences, TU Darmstadt.

The Brunauer-Emmett-Teller specific surface area (SSA) was measured by N2 adsorption at 77 K in the relative pressure range of 0.05 to 0.3 (Quantachrome Autosorb-3B, USA) after degassing for 22 hours at 80 °C at the Department of Material Sciences, TU Darmstadt.

2.6 Scanning Electron Microscopy (SEM)

The scanning electron microscopy (SEM) analysis was conducted using an FEI Quanta 400 ESEM FEG instrument (FEI, Eindhoven, the Netherlands) equipped with an energy-dispersive X-ray detector (Oxford, Oxfordshire, UK). The analyses were performed manually, referred to as operator-controlled SEM. An acceleration voltage of 15 kV and a sample chamber pressure of around 1×10^{-5} mbar were used. The Oxford software Aztec was used for single EDX-point and EDX-mapping to control the measurements. Each measurement was conducted with a counting time of 5 to 10 seconds for X-ray microanalysis.

2.7 Transmission Electron Microscropy linked with energy dispersive X-ray spectroscopy (TEM-EDX)

The clay mineral phases in untreated and treated B25, Opalinus, and Friedland clays were characterized using transmission electron microscopy with energy-dispersive X-ray spectroscopy (TEM-EDX). The different clay mineral phases were identified and described based on their chemical composition variability, morphology, specific dissolution potential, and additional parameters. Parameters such as the distribution of smectite layers probability (%S) and the distribution of charges caused by exchangeable cations in the interlayer space were used as indicators for mineralogical alterations in subsequent treatment experiments with B25 and Opalinus clays.

The samples were suspended in deionized water and dispersed using ultrasonic treatment for approximately 20 minutes. The clay fraction (<2 µm) was separated by sedimentation and diluted with deionized water to obtain a clear suspension. This suspension was dropped onto carbon-coated Cu grids, air dried, and stored under controlled environmental conditions at 45% humidity.

TEM-EDX investigations were conducted on the <2 µm fraction using a FEI TECNAI G2 20 transmission electron microscope at the VNU University of Science, Vietnam National University, Hanoi. This equipment, operated at 200 kV with a LaB6 cathode, was equipped with an S-TWIN objective, a windowless EDAX energy-dispersive X-ray system, and a FEI Eagle 2k CCD TEM camera.

Approximately 200 individual clay particles per sample were characterized by TEM-EDX for crystal size, crystal habit, particle morphology, and element distribution. Crystal size, crystal habit, and particle morphology were described according to Henning & Störr (1986). Element distribution was quantified using calibrated k factors, following methods by Cliff & Lorimer (1975), Lorimer & Cliff (1976), and Mellini & Menichini (1985). These k values account for particle-specific behaviour against possible irradiation damage.

The elements O, Na, Mg, Al, Si, K, Ca, and Fe were quantified using the EDAX GENESIS–TEM Quant Materials procedure. This involved correcting acquired EDX spectra through background subtraction, Gaussian deconvolution, and applying k-factor corrections based on standards such as phyllosilicate (muscovite) and selected non-phyllosilicate standards. The average errors in element analysis, expressed as atomic proportions using the phyllosilicate standard, were approximately 10 (Na), 5 (Fe, Mg, K, Ti, Ca), and 1 (Si, Al).

Measurement parameters included a reduced time of 20 seconds per particle and a limited exposed area of 50 nm in diameter to avoid potential irradiation damage to particles. Particle stability during this measurement time was verified at the beginning of each measurement campaign.

Additional methodological details regarding TEM-EDX measurements and mathematical procedures for calculating mineral formulae can be found in Hoang-Minh et al. (2019). These procedures were further extended by applying the k-means clustering method to identify subgroups of observations within the dataset. Data were standardized (scaled) to ensure comparability, and Euclidean distances

were employed as classical methods for distance measures. Optimal clusters were determined using the Elbow method and Gap statistics[1].

[1] *https://uc-r.github.io/kmeans_clustering*

3. Mineralogical Characterization of Initial Materials

3.1 Chemical composition (XRF)

The bulk chemical composition of the three initial powder materials (B25 bentonite, Opalinus, and Friedland clays), as analysed by XRF spectroscopy, is presented in Tab 3.1. The Opalinus clay contains a lower amount of SiO_2 and Fe_2O_3 but higher contents of TiO_2, MgO, CaO, Na_2O, K_2O, and P_2O_5 compared to B25 clay. Friedland clay shows less MgO but higher Fe_2O_3 and K_2O, with CaO and Fe_2O_3 being higher than in the other two clays. Otherwise, the other elements, such as Al_2O_3, are quite consistent among the three clays. The presence of calcite in Opalinus clay, as reported in XRD measurements, could explain the high amount of CaO, while the high sulphur content is due to the presence of pyrite in Opalinus and Friedland clays compared to B25 clay. The lower content of SiO_2 in Opalinus and Friedland clays is consistent with the mineralogical composition of clay minerals, where smectite is mostly absent, but micaceous minerals (illite, illite-ml) dominate in both materials.

Tab 3.1 *Chemical composition (XRF) of untreated materials of Opalinus and B25 clay*

Element (wt%)	SiO_2	TiO_2	Al_2O_3	Fe_2O_3	MnO	MgO	CaO	Na_2O	K_2O	P_2O_5	sum	LOI	total sum
B25 bentonite													
XRF	60.97	0.58	19.50	6.08	0.03	2.35	1.37	0.53	1.93	0.08	93.42	8.46	101.88
XRF[(a)]	61.50	0.50	21.10	6.40	0.10	4.00	3.80	0.40	2.00	0.10	100.00		
Opalinus clay													
XRF	45.95	0.84	19.60	5.86	0.05	2.57	9.00	0.64	2.87	0.19	87.57	14.43	102.00
XRF[(b)]	53.10	1.00	19.70	6.20	<0.1	2.30	3.00	0.60	2.60		91.00		
Friedland clay													
XRF[(c)]	56.7	0.94	18.09	7.31	0.035	2.01	0.54	0.96	3.01	0.11	88.21	9.12	99.32
XRF[(d)]	58.6	0.10	18.20	11.50	2.70	0.70	0.20	3.40	-	-	-	-	-
XRF	54.6	0.94	17.81	6.35	0.02	1.80	0.36	1.08	3.12	0.08	86.15	13.64	99.79
Element (ppm)	S	Cl	V	Cr	Ni	Cu	Zn	Rb	Sr	Zr			
XRF Opalinus	3172	380	179	489	94	56	190	1	279	130			
XRF B25 bentonite	132	0	0	474	79	77	129	1	50	274			

Note: (a) from Matschiavelli et al., 2019, (b) from Pearson et al., 2003, (c) from Hoang-Minh, 2006; (d) from Kasbohm, 2003

3.2 X-ray Diffraction (XRD)

3.2.1 B25-bentonite

The mineralogical composition of B25 bentonite was determined by BGMN-Rietveld refinement and is shown in Tab 3.2 and Fig 3.1A. The analysis revealed the presence of Illite 1*M* and $2M_1$ as the second most abundant phases (15% and 17%) after Ca-smectite (32%). Other clay mineral phases include illite-smectite mixed layers (10%) and highly ordered kaolinite (14%). Non-clay mineral phases include quartz (10%) and traces of feldspar from orthoclase and albite (4%). The quantitative mineralogical composition analysis of the untreated B25 material showed results comparable to Ufer et al. (2008), although the amount of smectite (Ca-smectite + IS-ml) was lower than reported by Matschiavelli et al. (2019). However, our measurements indicated a higher content of illite (illite 1*M* and illite $2M_1$), particularly illite 2M1, which is identified at 3.32, 3.20, 2.99, and 2.79 Å. The content of kaolinite is comparable to that in Matschiavelli et al. (2019) and lower than in Ufer et al. (2008). The amount of non-clay minerals (feldspar, quartz) is mostly consistent with both previous studies.

Tab 3.2. *Mineralogical composition of randomly oriented powder of B25, Opalinus and Friedland clays (original and compacted)*

B25 bentonite	***own results***	Ufer et al. 2008	Matschiavelli et al., 2019	***Opalinus clay***	***own results***	Gaucher et al., 2003	Bossart & Thury, 2008 *(min-best-max)*	Nagara, 2002
Ca-smectite	32%	43.2%	55%	Ca-smectite				
IS-ml	10%			IS-ml	3%	11 - 20%	5 - 11 - 20%	11%
Illite_1M	15%			Illite_1M	4%	17 - 40%	15 - 23 - 30%	23%
Illite_2M1	17%	16.6%	15%	Illite_2M1	18%			
Chlorite				Chlorite	12%	5 - 20%	3 - 10 - 18%	10%
Kaolinite	14%	21.9%	12%	Kaolinite	25%	15 - 32%	15 - 22 - 37%	22%
Σ clay	***86%***	***82%***	***82%***	***Σ clay***	***61%***		***28 - 66 - 93%***	***66%***
Quartz	10%	13.2%	10%	Quartz	13%	6 - 17%	10 - 14 - 32%	14%
Orthoclase	2%	1.7%		Orthoclase	1%	1 - 2%	0 - 1 - 6%	1%
Albite	2%	3.5%	3%	Albite	4%	1 - 2%	0 - 1 - 2%	1%
Pyrite				Pyrite	1%	1 - 2%	0 - 1 - 3%	1%
Calcite			1%	Calcite	17%	11 -28%	4 - 13 - 22%	13%
Siderite				Siderite	1%	1 - 4%	0 - 3 - 6%	3%
Dolomite			4%	Dolomite	2%	≤ 2%	≤ 1%	
Rutile			1%	Rutile				
Gypsum				Gypsum			≤ 0.5%	
Σ total	***100%***	***100%***	***100%***	***Σ total***	***100%***			***99%***

Friedland clay

Phases	Henning, 1971	Hoang, 2006	Karnland et al. (2006)	FIM (2009)	***own results (No19 initial)***	***Tonmehl Juli 2021 – Burg-scholle***
Ca-smectite					5%	
Illite-smectite mixed layer structure	44%	40%	56%	33-42%	14%	12%
Illite 2M1	12%	14%	7%	25-30%	6%	33%
Illite 1M					34%	
Kaolinite (+ Chlorite)	11%	12%				
Kaolinite			11%	10-13%	16%	17%
Chlorite				3-4%	3%	5%
Σ clay	***67%***	***66%***	***74%***		***78%***	***67%***
Quartz	24%	27%	20%	16-20%	15%	16%
Feldspar	5%					
Plagioclase				0-2%	3%	2%
K-feldspar		2%	1%	0-1%	3%	1%
Anatase, Rutile		1%			1%	1%
Gypsum			1%			2%
Pyrite	1%	traces	1%		>1%	1%
Σ total	***97%***	***96%***	***97%***		***100%***	***99%***

In the same refinement, Ca-smectite and two kinds of illite and Ca-smectite are identified as following:

Smectite: $Al_{2.9}\ Ca_{1.46}\ Fe_{1.2}\ Mg_{0.4}\ Si_{7.5}\ O_{32.76}$

Illite $2M_1$: $Al_{11.68}\ Fe_{0.32}\ K_{4.0}\ Si_{12}\ O_{48}$

Illite $1Mt$: $Al_{5.98}\ K_{1.4}\ Si_{6.0}\ O_{24}$

The oriented mount preparation for fraction <2µm indicated that B25 bentonite is dominated by 15Å-montmorilonite (divalent cation of Ca and/or Mg in the interlayer sheet) with specific peak at 15.4Å of the XRD-diffractogram from air-dried specimen (Fig. 1B). After ethylene-glycol saturation, the interlayer sheet was fully expanded to 17Å peak as well as the (001)/(002)-interference appeared at 8.59Å and (002)/(003) peak 5.63Å (Fig. 1B). It showed that smectite (montmorillonite, beidellite, etc.) is the dominant component in the clay fraction (<2µm) instead of IS-ml as expected. Moreover, the distance between (002) and (003) orders also confirmed the presence of this smectite phase.

Otherwise, the composition of clay minerals phases (<2 µm) of smectite, illite and kaolinite as well as mixed layer phases are modelled by Sybilla (Tab. 3.3, Fig. 3.2) and showed that there are two varieties of IS-ml: (1) IS R0 GLY (1) is pure montmorillonite and/or beidellite with 99% smectitic layer whereas distance of (002)/(003) at 5.42°2thetha, (2) IS R0 (2) contains 55% smectitic layer and 45% illitic layer where distance of (002)/(003) is 6.26°2thetha (Moore and Reynolds, 1997). In addition, the clay fraction contains 9% illite (d_{001}=9.99 Å, d_{002} = 4.97 Å and d_{003} = 3.31 Å) and 5% kaolinite at 7.17 Å, 3.57 Å together with 23% kaolinite-smectite mixed layer (KS-ml) with smectitic layer is 45% at 17.2 Å, 8.26 Å, 5.7 Å and 3.43 Å and distance of (001/002)/(002/005) = 15.24°2thetha.

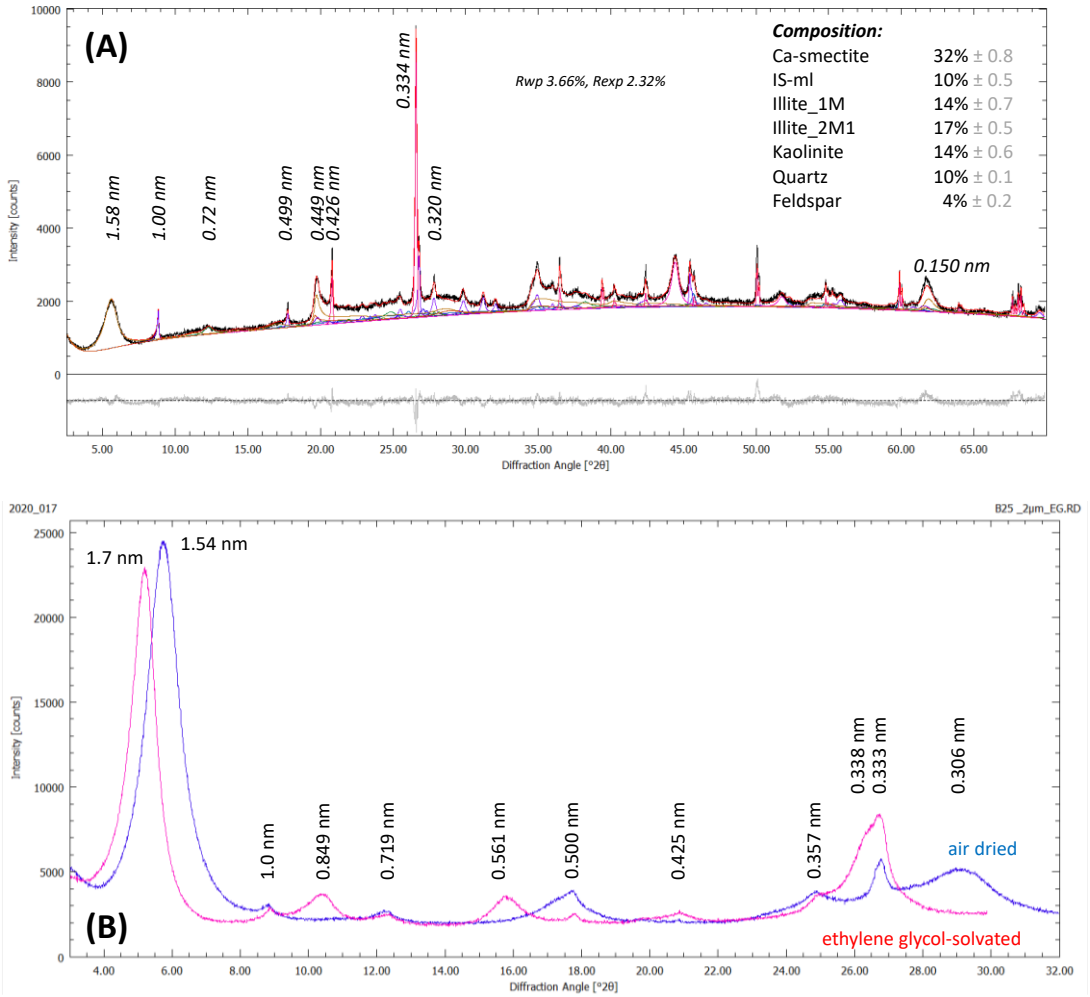

Fig 3.1 *(A) Diffractograms of randomly oriented powder (<40 µm) and oriented mount specimens (< 2 µm) (B) of B25 bentonite and interpretation of phases according to Profex-BGMN refinement (Rwp and Rexp are fitting parameters of refinement)*

Tab 3.3*Clay mineral matter of fraction < 2 µm by Syblla-modelling of XRD-oriented specimen of B25 bentonite, Opalinus, and Friedland clays*

Phases	content (%)	%S	T_{mean} (nm)	a(XII) phfu	Fe(VI) phfu
Oriented specimen of B25 bentonite, misfit = 11.28%					
IS R0 GLY(1)	47	99	4,4	0,06	0,24
IS R0 GLY(2)	16	55	14,4	0,21	0,03
Illite	9	-	13,1	0,3	0
Kaolinite	5	-	14,9	-	-
KS GL R0	n.d.	-	-	-	-
KS GL R1	23	45	11,2	0,15	0,38
Oriented specimen of Opalinus clay, misfit = 17.3%					
IS R0 GLY	10	11	24,4	0,59	0,00
ISS R0 GLY	8	29	12,5	0,50	0,17
Illite	12	18	0,56	0,00	-
Chlorite	7	18	-	-	-
Kaolinite	14	27	-	-	-
KS GL R0	14	16	23,7	0,05	0,00
KSS GL R0	36	44	18,5	0,11	0,00
Oriented specimen of Friedland clay (No19), misfit = 8.10%					
IS R0 GLY					
ISS R1 GLY	54	39	10.6	0.61	0.44
Illite	16	-	23.2	0.86	0.54
Chlorite	2	-	9.6	-	2.48
Kaolinite	10	-	17.3	-	-
KS GL R0	17	48	3.9	0.10	0.13

Note: Tmean – thickness of particles, %S-proportion of smectitic layer in mixed layer phases, a(XII) – interlayer charge, Fe(VI) – octahedral Fe, KS GLY R0 – kaolinite- one water layer smectite mixed layer, KSS GL R0 – kaolinite – one water layer smectite – two water layer smectite mixed layer

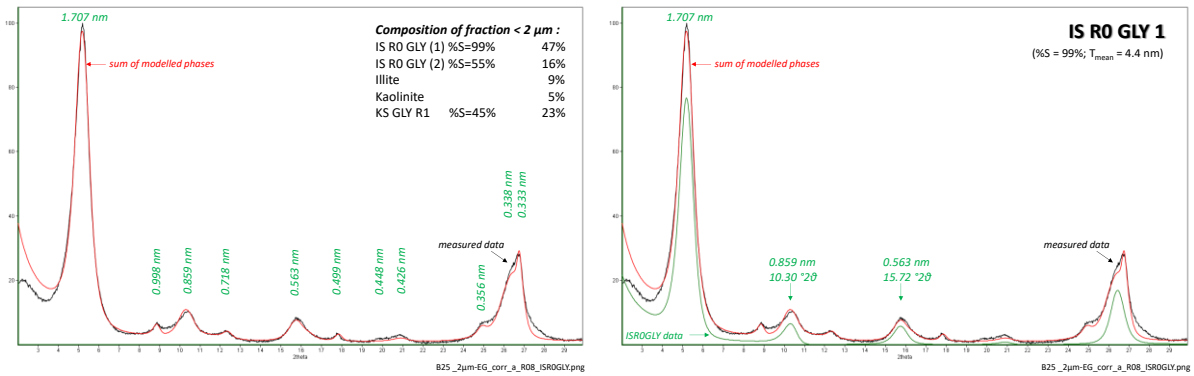

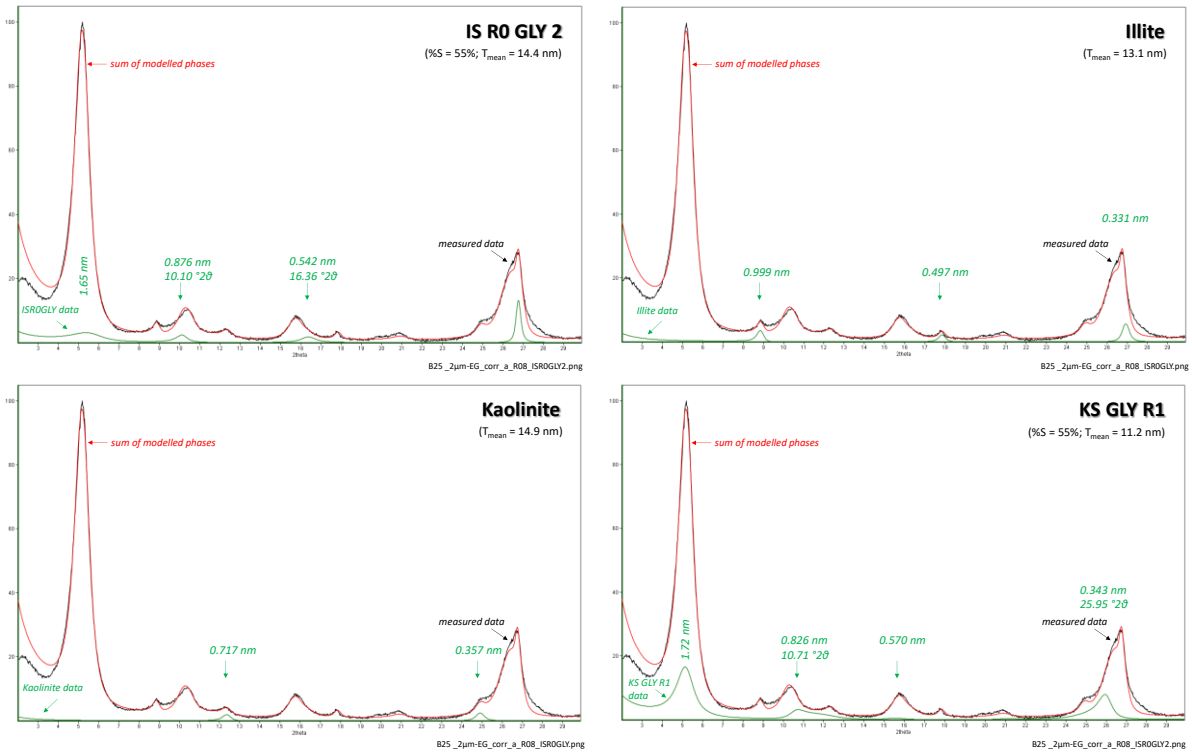

Fig 3.2. *Sybilla modelling of oriented mount specimen (XRD) of B25 bentonite*

3.2.2 Opalinus clay

The visual XRD patterns of randomly oriented material showed the presence of the following minerals: kaolinite, chlorite, illite, and illite-smectite mixed layers, with a total concentration of 62%. Quartz and calcite were found as the main non-clay minerals, along with traces of feldspar, pyrite, siderite, and dolomite. The quantitative amount of each phase was refined using BGMN Rietveld refinement, as shown in Fig 3.3A and Tab 3.2. This method also allowed for the modelling of the quantitative structural formulae of each phase:

IS-ml: $Al_{3.08}\ Fe_{0.28}K_{0.82}Mg_{0.8}Si_{7.84}O_{27.2}$

Illite 1*M*t: $Al_{5.98}K_{1.4}Si_6O_{24}$

Illite $2M_1$: $Al_{11.68}Fe_{0.32}K_{2.97}Si_{12}O_{48}$

Due to a variable mineralogical composition of Opalinus (Bossart and Thury, 2008), the amount of total clay in our own sample is comparable with Nagara (2002) but the amount of non-clay minerals is changed from deposit to deposit /Tab 3.2/.

XRD-measurement with oriented samples, including air dried and ethylene glycol saturation, was used to characterize the expandable layers (Fig 3.3B). In the air-dried diffractogram, the IS-ml shows as broad/diffuse interference at ~ 11.6 Å peak and illite at 10 Å, 4.99 Å, kaolinite appeared at 7.17 Å, 3.57 Å and chlorite at 14.2 Å, 4.73 Å and 3.55 Å. Under ethylene glycol saturation, this clay indicated a strong limit of expandability due to a small amount of illite-smectite mixed layer. The small humps of 9.2 and 5.28 Å (Fig 3.3B) could suggest a presence of illite-smectite mixed layer with proportion of smectitic layer is ~25% (%S=25%).

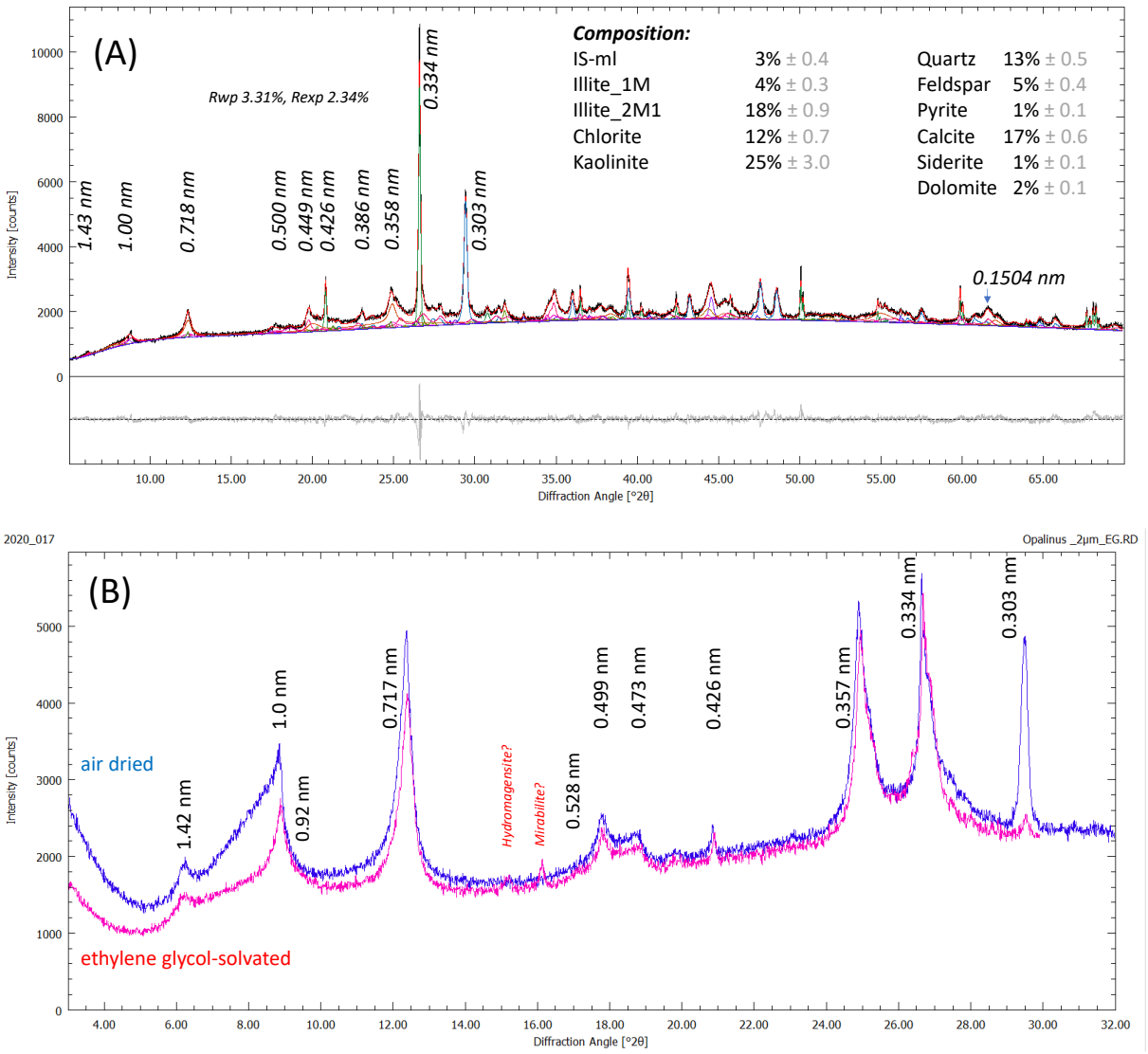

Fig 3.3. *(A) Diffractograms of randomly oriented powder (<40 µm) and oriented mount specimens (< 2 µm) (B) of Opalinus clay and interpretation of phases according to Profex-BGMN refinement and (Rwp and Rexp are fitting parameters of refinement)*

The Sybilla-modelling from oriented mount samples has indicated the presence of difference mixed layer phases including illite, chlorite and kaolinite (Tab 3.3, Fig 3.4).

- The IS R0 GLY (11%) appears at 9.81 Å and 5.04 Å with a distance of (002)/(003) is 8.58°2theta but the percentage of smectitic layer in IS-ml is only 11% and T_{mean} = 24.4 nm.
- The IS R0 GLY (29%) found as small hump at 10.7 Å which shows a low expandability for (001/002)-interferences because of high amount of 1w-smectite, the proportion of each layer as following: %I = 71%, %S-2w =9% and %S-1w =20% and T_{mean} = 12.5 nm.
- Illite (12%) is characterized by d(001) = 10 Å, d(002) = 5 Å and d(003) = 0.33 Å, the T_{mean} = 18 nm
- Chlorite (7%) showed at 14.3 Å, 7.11 Å, 4.74 Å, and 3.55 Å with T_{mean} = 11 nm
- Kaolinite (14%) is found at 7.16 Å and 3.58 Å with T_{mean} = 27 nm
- KS GLY R0 (14%) with 16% smectitic layer and 84% kaolinitic and Tmean = 23.7 appears at 7.48 Å and 3.52 Å where distance between (001/002) and (002/005) = 13.45°2thetha, this result is confirmed a percentage of 17% smectitic layer by Moore and Reynold (1997)

- KSS GLY R0 covers 36% of total clay mineral fraction in this sample with total smectitic layer is 44%, Tmean = 18.5 nm. This phase is characterized by a hump at 12.5 Å, 6.78 Å and 3.35 Å and the distance of (001/002) and (002)/(005) is 13.58 °2θ.

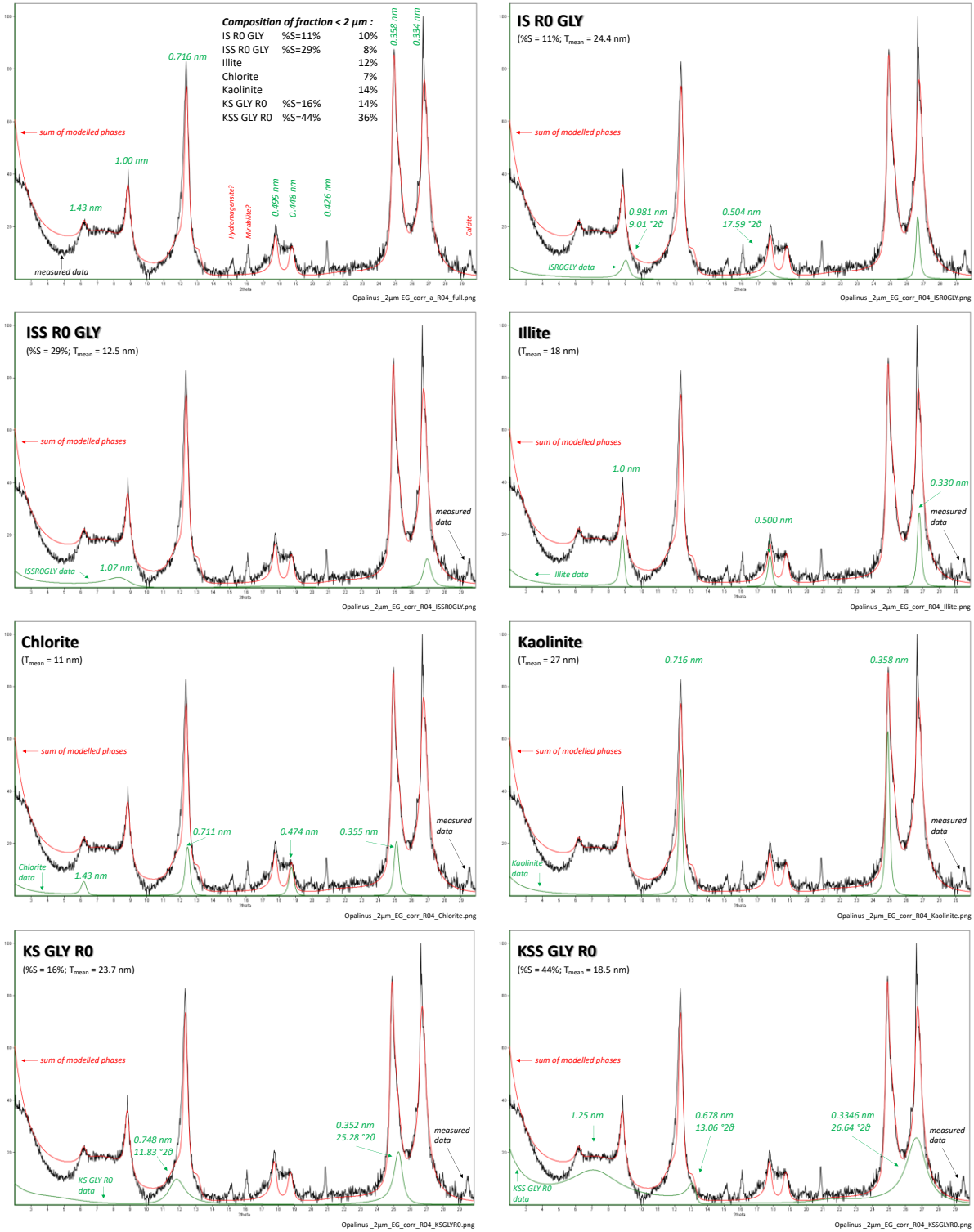

Fig 3.4 *Sybilla modelling of oriented mount specimen (XRD) of Opalinus clay*

3.2.3 Friedland clay

The visual XRD patterns of randomly oriented samples from two powder materials showed the presence of the following minerals: quartz, feldspar (albite, orthoclase) as non-clay minerals, and

kaolinite, chlorite, illite, smectite, and illite-smectite mixed layer phases as clay minerals (Fig. 3.5), with traces of pyrite and anatase (<1 wt.%). The weight percent (wt.%) of each phase was calculated using BGMN-Rietveld refinement:

Powder material (untreated sample, used only for comparison of raw material):

- Illite-smectite mixed layer (IS-ml): 6 wt.%
- Illite (illite 1M and illite 2M1): 57 wt.%
- Chlorite: 2 wt.%
- Kaolinite: 20 wt.%
- Quartz: 13 wt.%
- Feldspars: 2 wt.%

Powder material (initial sample No19, parent material for experiments):

- Ca-smectite: 5 wt.%
- Illite-smectite mixed layer (IS-ml): 14 wt.%
- Illite (illite 1M and illite 2M1): 40 wt.%
- Chlorite: 3 wt.%
- Kaolinite: 16 wt.%
- Quartz: 15 wt.%
- Feldspars: 6 wt.%

XRD measurements with oriented samples, including air-dried and ethylene glycol saturated, were used to characterize the expandable layers. The smectite group of initial material (No19), which included the illite-smectite mixed layer (IS-ml), showed a peak at 12.5 Å under air-dried conditions, which increased to 17.9 Å with a new large reflection at 8.59 Å after ethylene glycol saturation. Illite was identified by a 9.98 Å peak. Chlorite and kaolinite were demonstrated at 7.16 and 7.07 Å, respectively, corresponding to the peaks of chlorite and kaolinite.

Proportions of illitic layers in IS-ml were calculated as described by Moore and Reynolds (1997). This calculation is based on the relationship between the positions of the (001/002) and (002/003) interferences taken from ethylene glycolated specimens. The Friedland clay (initial sample No19) was characterized by illite-smectite mixed layer phases with 39% of smectitic layers (Fig. 3.5).

Validating the Friedland Clay measurements with data from the literature is difficult. The open-cast mining company of the deposit "Siedlungsscholle" has closed and covered the well-known old areas of this deposit and opened a new exploitation field at the east margin. This material is located at the margin of the deposit and was in contact with glacial water during the Pleistocene. For this newly opened Eastfield, no new published data are available. A comparison of published mineralogical results from "Siedlungsscholle", the recent own measurement No19, and a former own measurement from the neighbouring deposit "Burgscholle" (Tab. 3.2) shows a remarkable coincidence of mineral matter between sample No19 (from "Siedlungsscholle" – new field at the east margin of this deposit) and the trade ware of the deposit "Burgscholle."

The clay fraction (<2 µm) was investigated in more detail using Sybilla modelling software, showing the presence of different mixed layer phases of high-charge illite/smectite mixed layer, low-charge beidellite, dioctahedral vermiculite/smectite mixed layer, kaolinite/smectite mixed layer, along with illite, chlorite, and kaolinite (Tab. 3.3).

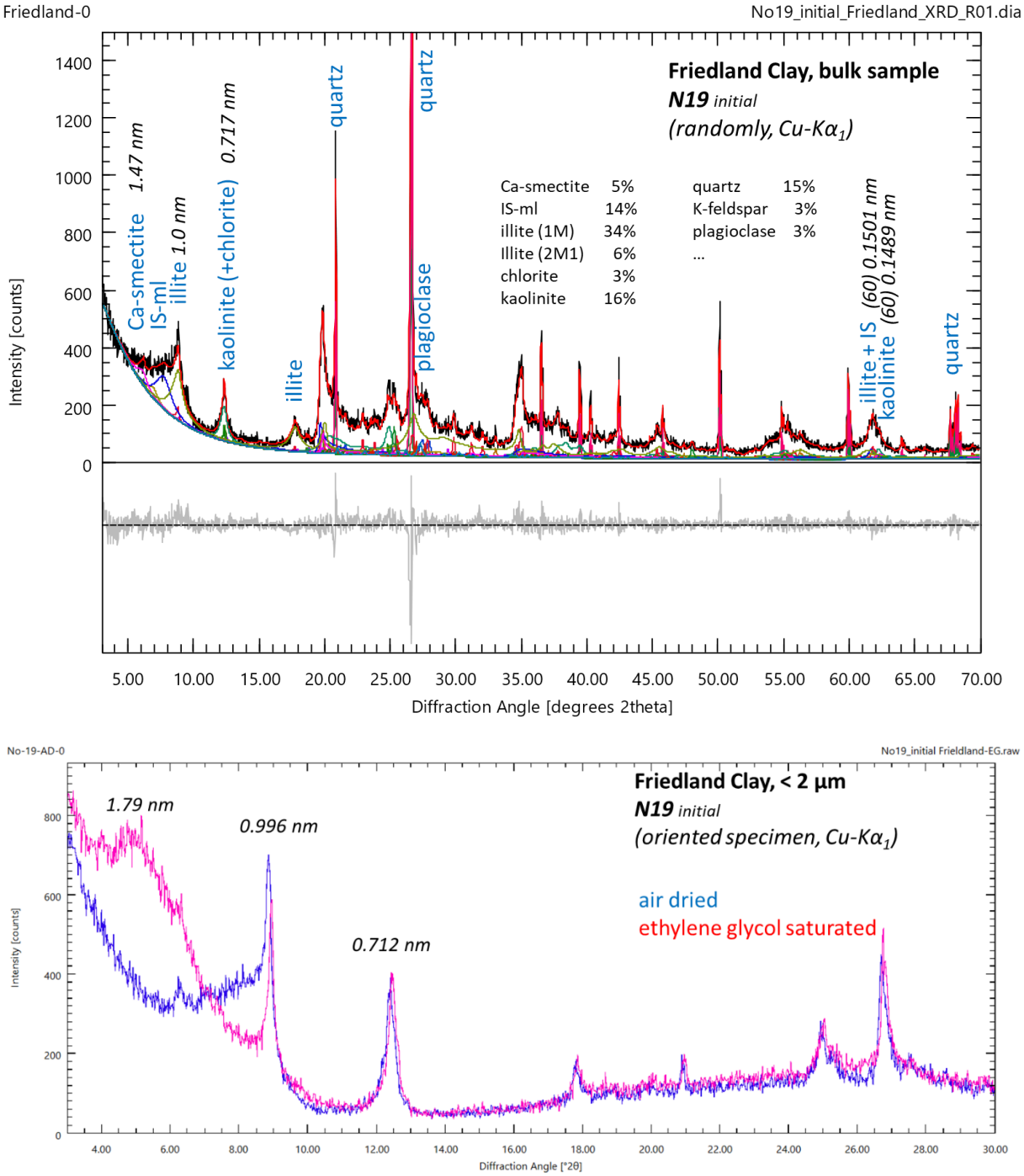

Fig 3.5. *(A) Diffractograms of randomly oriented powder (<40 µm) and oriented mount specimens (< 2 µm) (B) of Friedland clay and interpretation of phases according to Profex-BGMN refinement and (Rwp and Rexp are fitting parameters of refinement)*

- **ISS R0 GLY (54%):** At ~16 Å and 5.2 Å with a distance of (002)/(003) of 7.00°2θ, the percentage of smectitic layer (%S) in IS-ml is 39%.
- **Illite (16%):** Characterized by d(001) = 9.98 Å, d(002) = 5 Å, and d(003) = 0.33 Å.
- **Kaolinite (10%):** Found at 7.16 Å and 3.58 Å.
- **KS GLY R0 (17%):** With 48% smectitic layer and 52% kaolinitic at 8.74 Å and 3.40 Å, where the distance between (001/002) and (002/005) = 15.04°2θ.

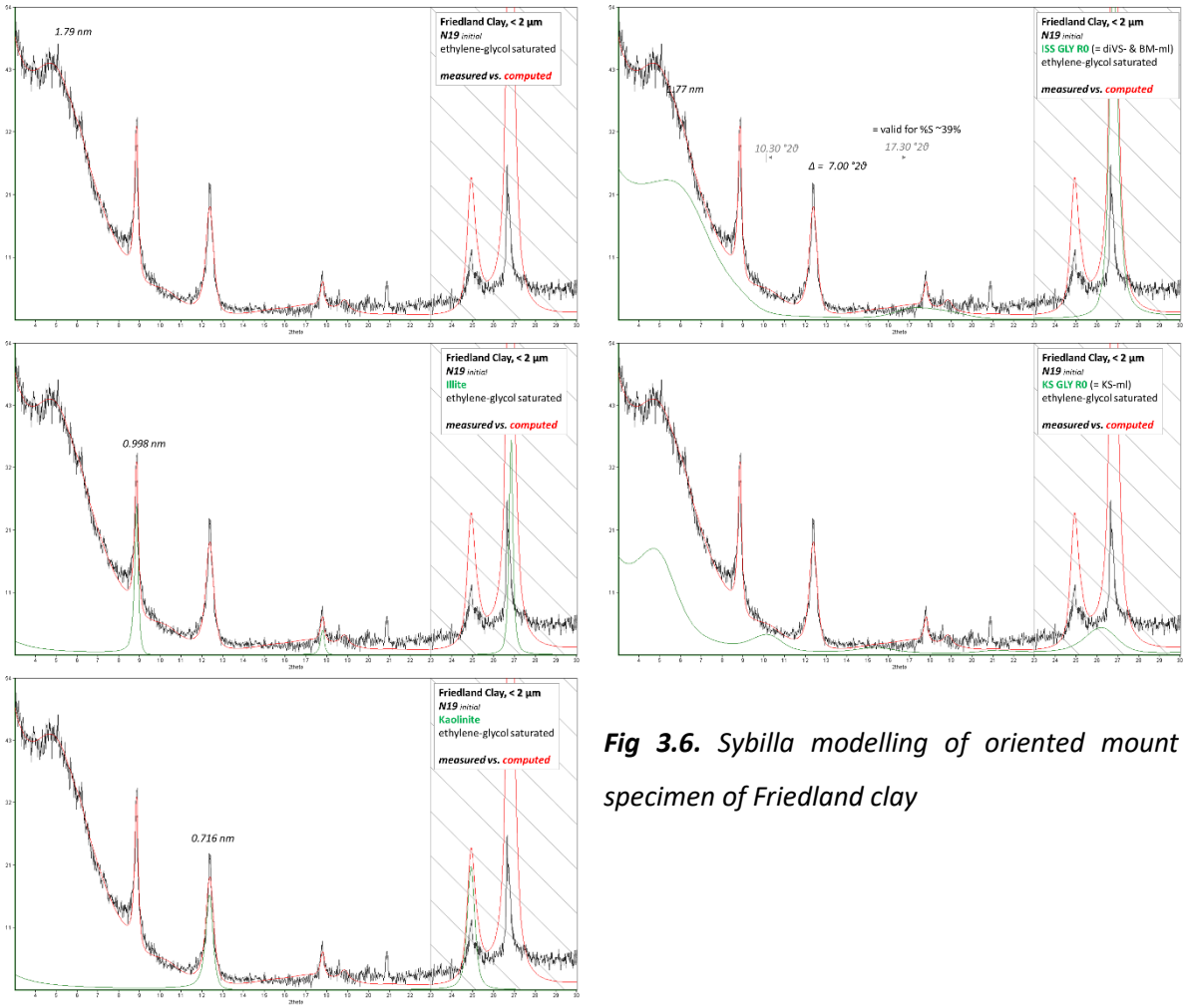

Fig 3.6. *Sybilla modelling of oriented mount specimen of Friedland clay*

3.3 Fourier Transform Infared (FTIR)

3.3.1 B25-bentonite

The FTIR spectroscopic analysis of B25 clay is shown in Fig. 3.7 left. It indicates that smectite is the dominant phase in the clay. The broad adsorption band at 3634 cm^{-1} (AlAlOH) is typical for Al-rich content of smectite (Madejova et al., 1996) and strongly associated with beidellites (Gate, 2005) but also Fe as presences of FeFeOH (3557 cm^{-1} and 3577 cm^{-1}) (Zviagina et al., 2004). The broad band at 3419 cm^{-1} represents the OH-stretching vibration of silanol (Si-OH) groups. These bands originated from the solid and H-O-H stretching oft he water molecules which were absorbend on the solid surface. Moreover, the band at 1635 cm^{-1} assigned to an overtone of the bending vibration of water, which is retained in the matrix.

In the OH-bending area, the broad bands at 1107 cm^{-1} and 1048 cm^{-1} represents the stretching vibrations of Si-O-Si group in tetrahedral sheets of smectite (Farmer and Russel, 1964, Emmerich et al., 1999). The spectral band at 910 cm^{-1} indicated the stretching vibration of AlOHAl and 873 cm^{-1}, 836 cm^{-1} corresponding to the AlOHFe and AlOHMg respectively. The coupled Al-O and Si-O out of plane vibration are assigned to the band at 621 cm^{-1}. The presence of muscovite is shown by different shared bands with smectite and kaolinite as well as quartz but the band at 750 cm^{-1} is typical ones for this phase as mentioned by Velde (1983) and kaolin at 693 cm^{-1} and 3700 cm^{-1}. It is note that, the two shoulders at 929 cm^{-1} in OH-bending region and 3646 cm^{-1} in OH-stretching region indicate the occurrences of beidellite type (Gates, 2005) and a bands at ~693 cm^{-1} shared with quartz is also assigned to Si-O in a ferruginous beidellite (Decarreau et al., 1992), in addition the occurrence of FeMgOH at 3557 and 3577 cm^{-1} suggested a high amount of Fe in smectite structures including beidellite. There were sharp bands at 780 cm^{-1} and 797 cm^{-1}, which confirms the occurrence of quartz. These results are in agreement with previous XRD-data.

3.3.2 Opalinus clay

FTIR scans of Opalinus clay (Fig. 3.7 right) shown strong distinct OH-stretching bands at 3620 cm^{-1}. A Si-O deformation band at 696 cm^{-1} indicated the presence of kaolin (Farmer and Russell, 1964). The tetraheral silica and quartz signals were assigned by Si-O stretching and Si-O vibration at 1111 cm^{-1} and 1038 cm^{-1}, respectively. The intensity of the Si-O vibration was proportional to the intensity of kaolinite bands. In the FTIR spectra, AlAlOH bending band assigned at 911 cm^{-1} which is typical for smectite and IS-ml (Farmer and Russell, 1964). The $AlFe^{3+}OH$ band at 874 cm^{-1} shows a high intensity in comparision with 831 cm^{-1} of AlMgOH band. This is a sign of high content of Fe in octahedral sheet of dioctahedral minerals (e.g. smectite, illite, IS-ml) in Opalinus clay (Craciun, 1984; Gates, 2005). The FT-IR patterns of Opalinus clay show distinct Si-O stretching bands at double peaks of 778 and 798 cm^{-1}, indicating the presence of quartz. Moreover, the presence of calcite and pyrite was found at difference bands of 1428 cm^{-1} (calcite) and 1163 cm^{-1} and 1632 cm^{-1} (pyrite).

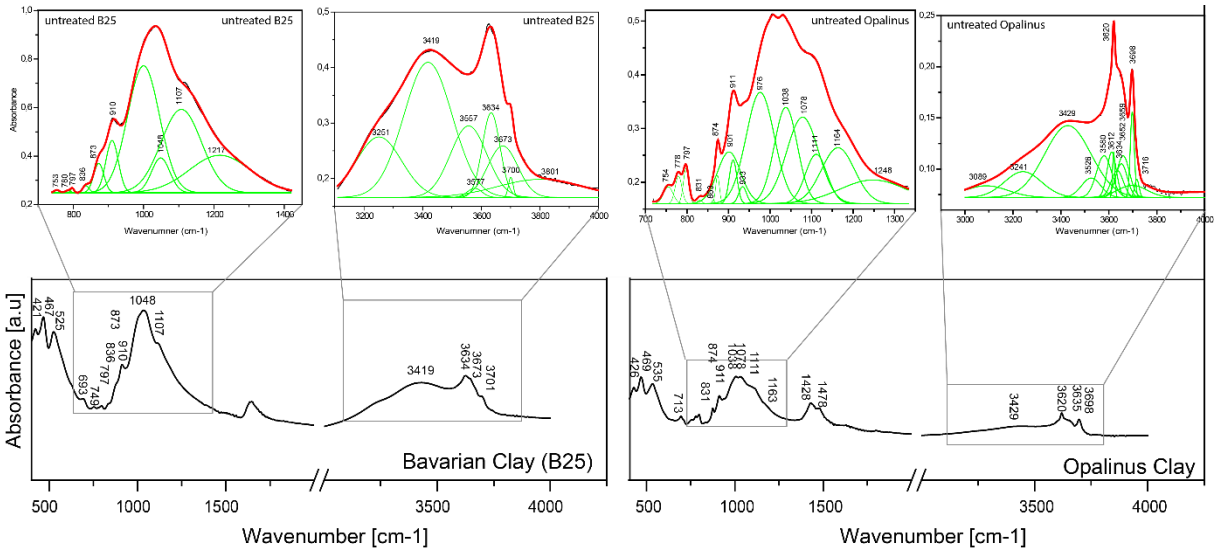

Fig 3.7 *The FTIR-spectra of initial B25 bentonite and Opalinus clay*

3.3.3 Friedland clay

FT-IR scans of Friedland clay (Fig. 3.8) showed strong distinct OH-stretching bands at 3623 cm^{-1}, ~ 3696 cm^{-1}. A Si-O-deformation band at 694 cm^{-1} indicated the presence of kaolinite and a possible absorption band of smectite was present at ~3600 cm^{-1} (Farmer and Russell, 1974). The tetrahedral silica and quartz signals were assigned by Si-O stretching and Si-O vibration at 1028 cm^{-1} and 987 cm^{-1}

respectively. The intensity of the Si-O vibration was proportional to the intensity of kaolinite bands. In FT-IR spectra, Al-OH-Al bending band assigned clearly at 909 cm^{-1} to a typical smectite and kaolinite (Farmer and Russell, 1974). The Al-OH-Fe^{3+} band at 882 cm^{-1} had low intensity reflecting the high Fe content of Friedland clay (Craciun, 1984; Russell and Fraser, 1994; Vantelon et al., 2001; Gates, 2005). Moreover, bending at 829cm^{-1} due to Al-OH-Mg and Al-O vibrations of illite rises to 753 cm^{-1}. An Al-O-Si band was also present (Farmer and Russell, 1974; Russell, 1987). In addition, the FT-IR patterns of Friedland clay show distinct Si-O stretching bands at double peaks of 779 cm^{-1} and 797 cm^{-1}, indicating the presence of quartz (Craciun, 1984).

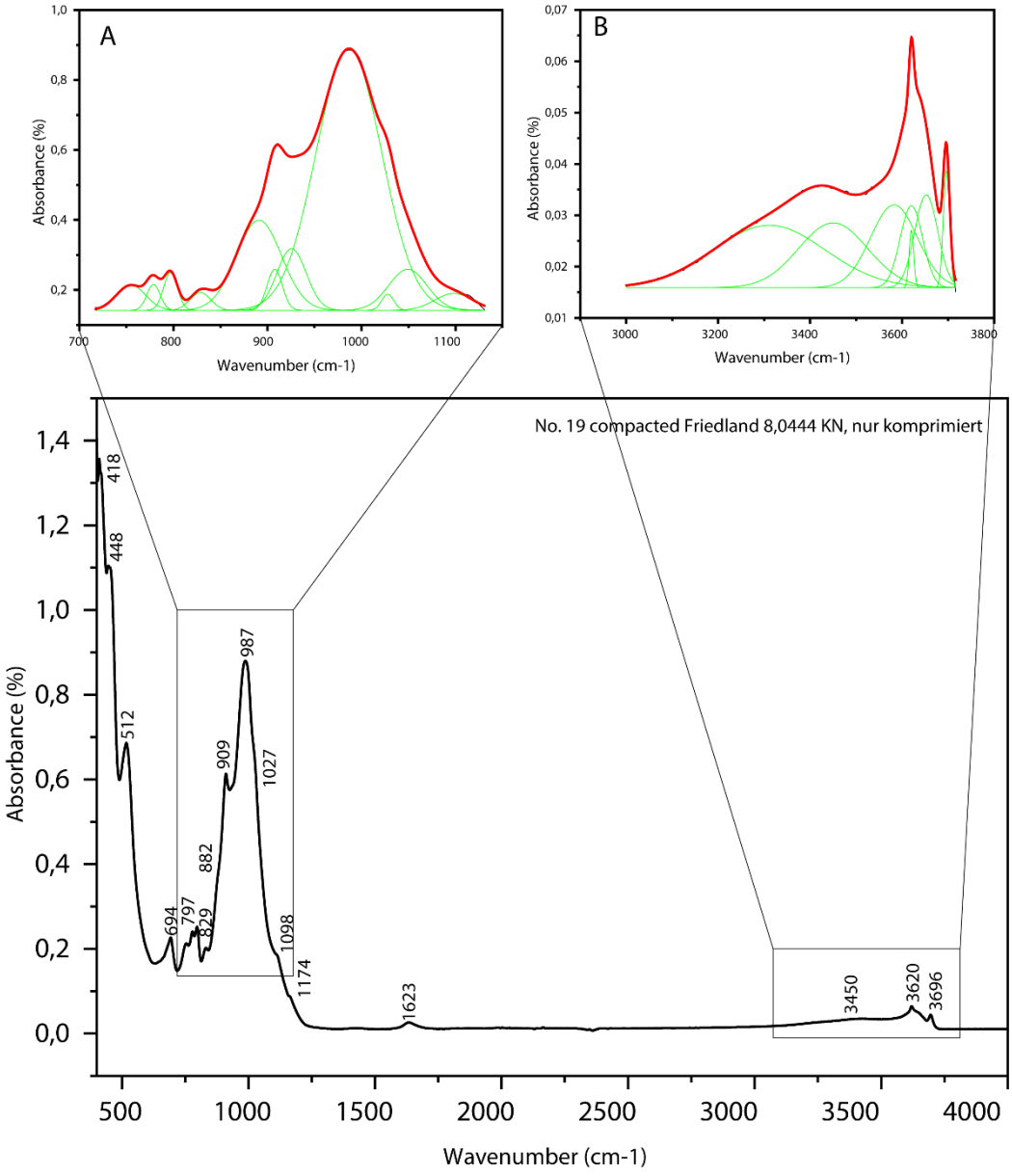

Fig 3.8 *Infrared spectrum of Friedland clay*

3.4 Thermal Analysis (DTA-TG)

Thermal gravimetry (TG) and differential thermal analysis (DTA) techniques were used to determine the elemental and mineralogical composition as well as to understand dehydration and dehydroxylation of the initial materials of B25 bentonite, Opalinus, and Friedland clays. The method additionally allowed to evaluate the temperature at which water is lost as well as the mass lost. The indication of the amount of strongly held water which is normally associated with swelling clays is

provided. The small differences in the temperature at which water loss occurs also support the evidence on the presence of non-swelling and/or mixed layer minerals, as well as impurities in the rocks. Figures 3.9 and 3.10 depict the DTA/TG curve recorded the starting materials of three clays separately. In addition, the changes in the samples upon heating show both endothermic and exothermic peaks at different temperatures due to distinct mineralogical composition of the materials.

Tab 3.4 *The comparison of mass loss between DTA/TG and XRD for all phases and carbonate phases of B25 bentonite and Opalinus clay*

B25 bentonite		***Opalinus clay***	
300-1000°C *(as check for all phases)*		***300-1000°C*** *(as check for all phases)*	
meas.	5.17%	*meas.*	13.90%
XRD-calc.	5.15%	*XRD-calc.*	14.34%
700-1000°C *(as check especially for calcite)*		***700-1000°C*** *(as check especially for calcite+dolomite)*	
meas.	0.06%	*meas.*	6.45%
XRD-calc.	0%	*XRD-calc.*	6.96%

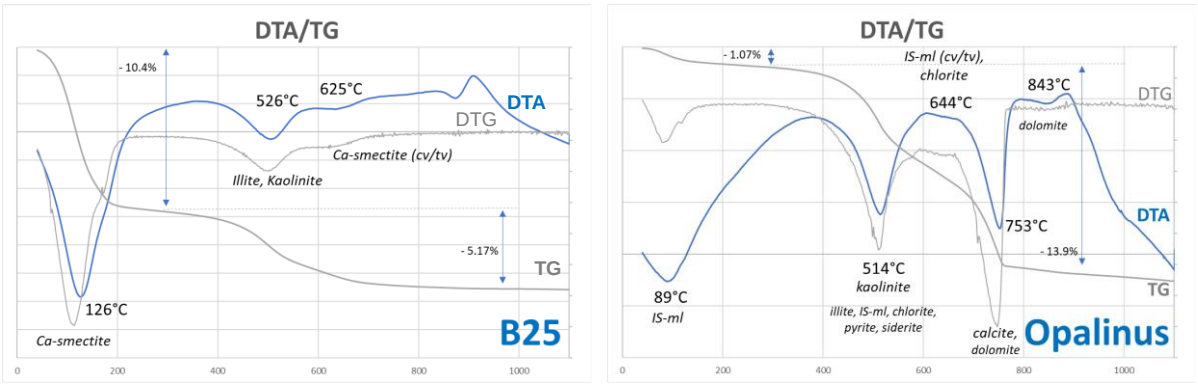

Fig 3.9 *DTA/TG curves of B25 bentonite and Opalinus clay*

3.4.1 B25-bentonite

The B25 bentonite shows a 3 steps of mass loss from room temperature up to 1000 °C. The first step is up to ~ 300 °C, shows the release of water molecules from the surface and interlayer sheet as well as water molecules coordinating exchangeable cations of smectite. High amount of smectite in B25 shows a dominant hydrated phase in bentonite, the mass loss of this step reached up to 10.4%. The second and third steps at the ranges of ~ 300 - ~ 550 °C and 550 – 700 °C, respectively, are related to dehydroxylation of clay minerals as smectite (400-800 °C), kaolinite (450-700 °C) and illite/muscovite (350-600 °C).

The changes in the sample upon heating is additionally interpreted by DTA curves. There are 4 endothermic peaks near 126 °C, 536 °C, 625 °C and nearby 900 °C. The first, most intense endothermic peak shows a shoulder at about 180 °C, which suggests a difference between removal of water molecules from the inner hydration shell of exchangeable cation and from less strongly bound water. Two endothermic peaks, near 526 °C and 625 °C on the DTA curves confirm that the changes observed on the TG curves in the 300 – 700 °C region are due two partly overlapping dehydroxylation processes. According to Brandley and Grim (1951) and Čičel et al. (1992), the endothermic peak near 900 °C is associated with the breakdown of the anhydrous montmorillonite to an „amorphous“ material from which new temperature phases crystallized near 920 °C.

The mass loss of the mineral phases from DTA/TG is cross checked with theoretical mass loss by XRD-results and show a good correlation at 300 – 1000 °C for all phases and 700 – 1000 °C for calcite (Tab 3.4)

3.4.2 Opalinus clay

The Opalinus clay is composed of low amount of smectite (IS-ml) but high amount of illite, chlorite and kaolinite in clay mineral group as shown in XRD-results (tab 3.2). It is responsible for a low mass loss (1.07%) from room temperature up to 1000 °C in the TG-curve of Opalinus clay. It means, aditionally to the dehydration of sample at 89°C, the escape of water molecules (beginning with 118°C – see DTG-signal) from the interlayer space and water molecules coordinating exchangeable cation is mostly absent in 2:1 fixed cation exchange phases (illite, chlorite) and 1:1 clay minerals (kaolinite) in the range up to 300 °C. The peaks in the range of 300 – 500 °C, and 550 – 700 °C are related to dehydroxylation of clay minerals including smectite (400 – 800 °C), kaolinite (450 – 700 °C), illite/muscovite (350 – 600 °C), chlorite (500 – 650 °C). Those steps are represented by 4 endothermic peaks near 89 °C, 514 °C, 644 °C and 843 °C in DTA curve. The first low intense endothermic peak at 118 °C is used to distinguish a removal of water molecules from the inner hydration shell of exchangeable cation in IS-ml from the less strongly bound water (Greene-Kelly, 1957). The two endothermic peaks near 514 and 644 °C on the DTA curves confirm that the changes observed on the TG curves in the region of 300 – 700 °C due to two partly overlapping dehydroxylation processes. Those endothermic peaks are contributed to kaolinite, illite, IS-ml, chlorite, pyrite, and siderite at 514 °C; chlorite, IS-ml (cv/tv) at 644 °C and carbonate of calcite, dolomite at 753 °C and finally 843 °C of dolomite.

The XRD-results of bulk sample have been validated by thermogravimetry (TG). The theoretical mass loss, calculated from XRD-results of bulk sample, was compared with the measured mass loss by TG. The XRD-results of raw Opalinus materials shows a theoretiocal mass loss of 14.34 % compared to the measured mass loss by TG with 13.9 % at 300 – 1000 °C. The content of carbonate phases (calcite + dolomite) is represented by a measured mass loss of 6.45% (by TG-measurement) in the range from 700 – 1000 °C). XRD calculation revealed 6.96% as theoretical mass loss caused by XRD-results for 14% calcite and 1% dolomite (tab 3.4).

3.4.3 Friedland clay

The DTA curve of smectite (Ca-smectite, illite-smectite mixed layer) in Friedland clay is shown in Fig. 3.10. The first endothermic effect observed in the range of 70 – 180 °C corresponds to dehydration of sample and the loss of interlayer water, the second and third correspond to the dehydroxylation what indicated by the mass loss of 1.85% (30 – 300 °C) observed in the TG curve. The TG analyses of other clay minerals phases as kaolinite (1:1 clay minerals), chlorite, illite (2:1 fixed cation exchange phases) show that the evolution of volatiles began at ~400 °C, peaked at ~500 °C and terminated at ~800 °C. These temperatures indicate the dehydroxylation of the clay minerals to the other phases (e.g., kaolinite to metakaolin and final destruction of the metakaolin structure at ~800 °C, illite changed to mullite or cristobalite, decomposition of smectite structure) at ~800 °C. Consequently, the mass loss at the range of 300 – 650 °C is 5.10% and 650 – 1000 °C is 1.16% and total mass loss of Friedland clay at 300 – 1000 °C reached 6.26%.

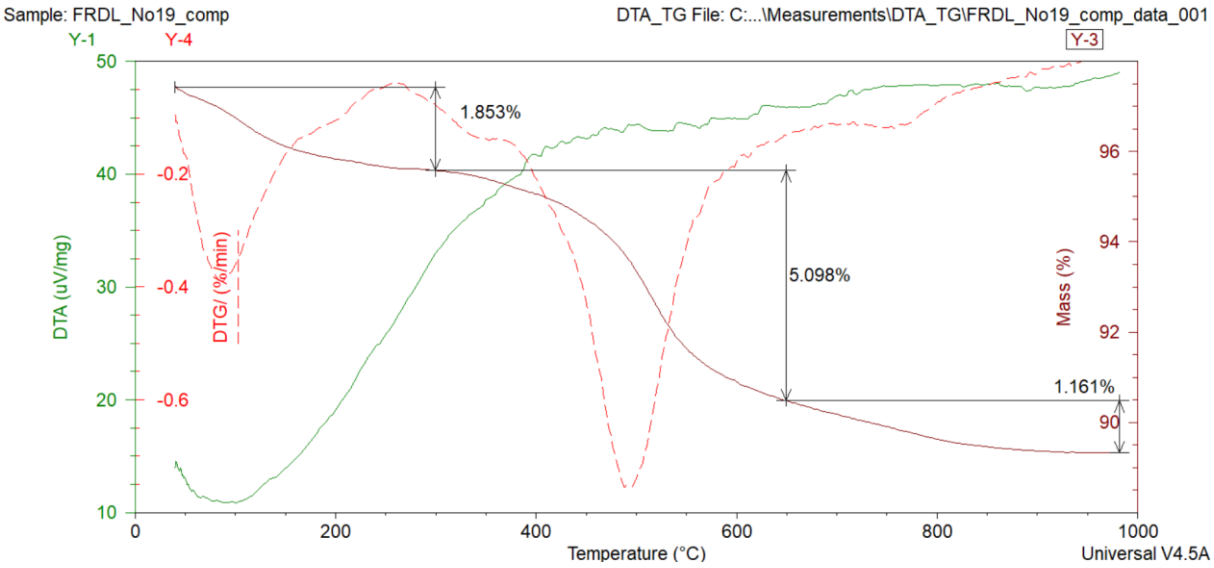

Fig 3.10 *DTA/TG curves of Friedland clay*

3.5 Scanning Electron Microscopy (SEM)

SEM observations were used to detect minerals that were unidentified by other methods (e.g., XRD, FTIR, DTA-TG, TEM-EDX) and to observe the effect of THMC experiments on the stability of clay and clay fabric at a microscopic scale with higher magnifications between 1000x and 3000x. The mineralogical composition was qualitatively identified using energy-dispersive X-ray spectroscopy (EDX) with an acceleration voltage of 15-20 kV. Additionally, the morphology and fabric of the clay were examined to interpret the changes between the compacted initial materials and the reaction products.

3.5.1 B25 bentonite

The photomicrographs in Fig. 3.11 show that the typical structures observed in the initial B25 bentonite are aggregated structures with very dense surfaces. These structures consist of aggregates 10 to 20 µm in diameter, as well as small clay platelets separated by an irregular porous network. Some grains of non-clay minerals are embedded between the clay aggregations or within the clay matrix. It is very common to observe some clay platelets acting as bridges, crossing inter-aggregate pores. The association of large and small aggregate clays shows a laminar structure. These aggregates are limited by large voids (>5 µm). Additionally, they show also an inner-aggregate porosity by voids with 1 – 2 µm as diameter. The presence of large grains such as muscovite, rutile, quartz, and Fe-oxides causes a large fracture system at the borders between the grains and the clay matrix/clay aggregates. Additionally, a laminar structure with thin smectite platelets in a face-to-face contact style is clearly observed, with interparticle pores (<2 µm) apparent. The micropore system develops along the 001-face of smectite platelets from face-to-face contact formations. Based on the morphology and EDX measurements, the dominance of smectite with impurities of non-clay minerals such as quartz, feldspar, Fe-oxides, and rutile is confirmed.

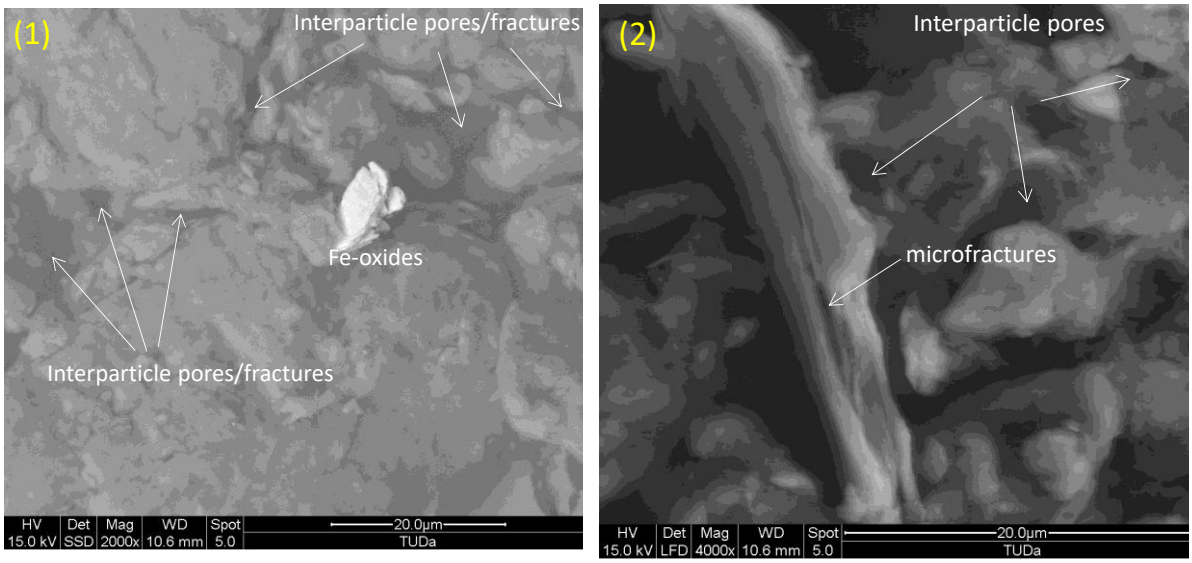

Fig 3.11 *SEM-images of initial compacted B25 bentonite.*

Note: (1) Compacted clay with a lot of linear and irregular shrinkage fractures, interparticles pores/fractures on the dense surface of clay pellet. (2) Loosely compacted clay with a large proportion of smectite causes an abundance of interparticle pores and cavities, likely due to volume reduction when dehydrated after the injection of OPA solution under saturated conditions. Additionally, large, thin, and platy mica particles with a system of linear microfractures between laminar sheets contribute to this phenomenon. The flocculation structure showed the edge-to-face and face-to-face contact style.

3.5.2 Opalinus clay

Electron micrographs of Opalinus clays (Fig. 3.12) show well-developed aggregate and small clay flake structures, with clay bridges acting as connectors in compacted Opalinus clay. The size of clay aggregates is variable (~25 µm), but the clay phases (smectite, illite/smectite) are very fine (1 – 2 µm) and widely distributed as a clay matrix with foliated textures. Non-clay mineral grains of various sizes appear as inclusions and/or embedded in the background of the fine-grained clay matrix, consequently forming abundant inter-particle and inter-aggregate pores. The inter-aggregate pores are angular in form, while inter-particle pores are mainly linear due to the laminar structure of the face-to-face contact style of smectite. The presence of fossils and pyrite, as well as other non-smectite phases, contributes to the widespread distribution of intracrystalline/intergranular macropores, but micropores from intracrystalline/intragranular structures are mostly observed on the crystal/granular surfaces of non-smectite particles. Additionally, linear shrinkage fracture systems are quite abundant in the samples.

In terms of mineralogical composition, SEM-EDX indicates the presence of all minerals detected by XRD. The clay matrix consists of fine-grained illite/smectite, carbonate fossils (shells, diatoms mainly composed of Ca), mica, calcite, quartz, and iron-hydro(oxides) associated with clusters of framboidal pyrite. No recrystallization of smectite to non-swelling clay or conversion processes is observed.

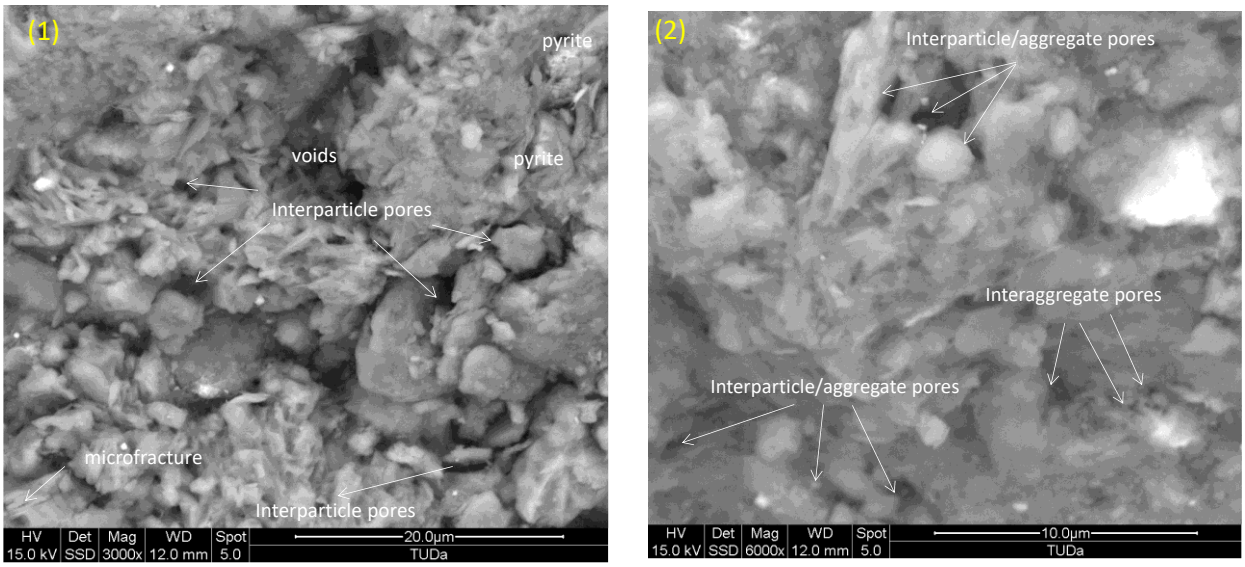

Fig 3.12 *SEM-images of compacted Opalinus*

Note: (1) Aggregation of platy illite-smectite mixed layer, interparticles and inter-aggregation pores and voids are observed with different angular form. The microfractures between sheet of illite-smectite flakes is observed due to the face-to-face and edge-to-face contact style. (2) the interparticle/aggregate pores on the loosely dense clay matrix.

3.5.3 Friedland clay

Under SEM-image observation, the initial Friedland clay (No19) is characterized by aggregated structures with a very dense clay matrix (Fig. 3.13). The small platy flakes of illite-smectite mixed-layer platelets form large aggregations (>25 µm). These are characterized by edge-to-face, face-to-face, and edge-to-edge contact styles, creating a system of pores, cavities, and fractures in different forms. The main component of the illite-smectite mixed layer in the rock shows characteristics of a disordered structure, resulting in lamellar slit and wedge-shaped pore systems.

The distribution of pores and minerals is commonly a combination of micropores between clay minerals and/or interparticle pores between clay minerals and non-clay phases. However, the most abundant are the interparticle pores of the illite-smectite mixed layer. The pore widths range from 2 nm to 10 µm. The shapes of the pores are mostly controlled by the crystal shapes of the lamellar illite-smectite mixed layer and the contact between them. The interaggregate pore fractures (shrinkage and contact surfaces between aggregate-aggregate and clay matrix-aggregate/impurities) are mostly linear and irregular in form, while voids and interparticle/granular/crystalline pores vary from linear to angular, spherical to irregularly polygonal. Intraparticle pores in Friedland clay are not clearly observed in clay minerals but are present in non-clay mineral phases (e.g., pyrite, Fe-oxides).

Fracture types are mainly developed in the illite/smectite mixed layer due to shrinkage and fractures between clay-clay aggregates and clay-impurities aggregates (such as clay and pyrite framboid, clay platelets, and interlayer microfractures). The length of fractures varies from 3 to 12 µm.

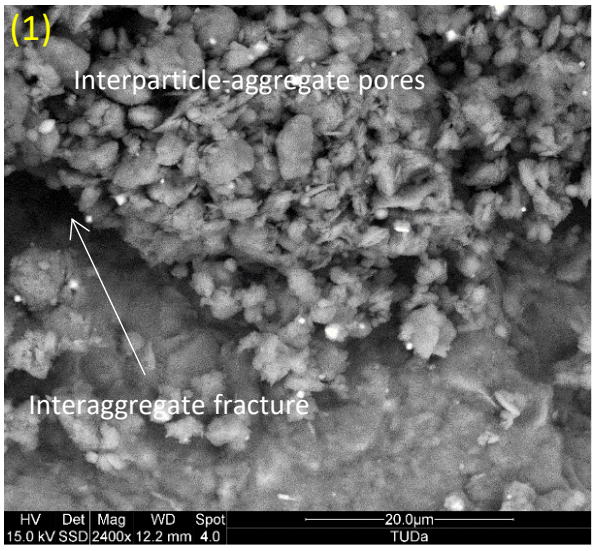

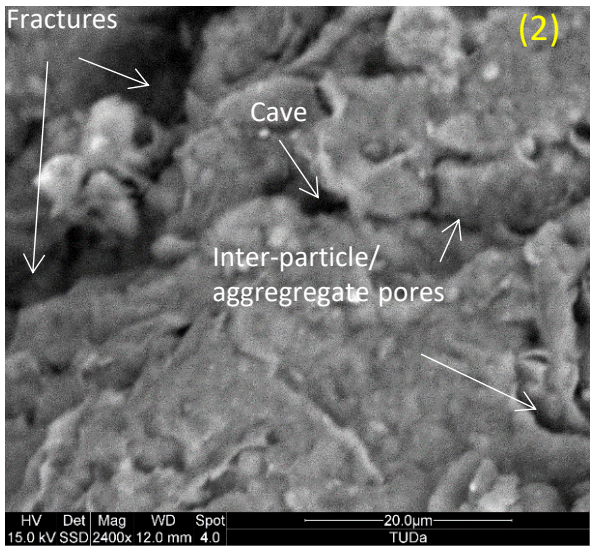

Fig 3.13 *SEM-images of initial Friedland clay*

Note: (1) large aggregate contains platy illite-smectite mixed layer particles. The large system of pores and voids appeared between aggregate of clays but micro interparticle pores are typical observed between illite-smectite platelets. The edge-to-face and face-to-face contact styles are found mainly in the contact between clay particles. (2) large angular fractures and caves (8 – 10 µm in diameter) formed between aggregate of clays but the small and linear fractures are found, too.

3.6 Cation exchange capacity (CEC), specific surface area (SSA) and surface charges

The cation exchange capacity (CEC) and specific surface area (SSA) and surface charge of the three starting materials are showed in (tab. 3.5). Swelling clays are characterized by a high interlayer cation population in the clay structure that releases in a high cation exchange capacity (CEC). The high amount of cation exchange sites is the consequence of the very high surface area of clay and high negative charge on these surfaces.

Barium chloride ($BaCl_2$) and calculation from TEM-EDX were used to determine CEC of two starting materials from Opalinus and B25 bentonite. The results show the smectite rich B25 bentonite is characterized by CEC of 45.15 meq/100 g ($BaCl_2$ method) and 48 meq/100 g (calculation from TEM-EDX) which compares to 56 meq/100 g from Matschiavelli et al (2019) . These different results are reasonable since Matschiavelli shows a higher content of Ca-smectite (55%) in comparison with our B25-material (content of 42% in total of Ca-smectite and IS-ml). Low cation exchange capacity of our bentonite material is also in agreement with low content of Mg as shown in XRF- and TEM-EDX-results (Tab. 1). Moreover, the substitution of Al for Si in tetrahedral sheet from TEM-EDX results and presence of ~750 cm^{-1} absorption band (Fig 3.7 left) are also a reason for this smaller CEC of our bentonite.

Otherwise, the CEC of Opalinus shows very high difference between $BaCl_2$-method (82.36 meq/100 g) and TEM-EDX calculation (52 meq/100 g) as well as Gaucher et al. (2004) as reference data. These authors presented that the CEC from Opalinus changed from 5 – 20.5 meq/100g. TEM-EDX could only support the CEC for clay fraction (< 2µm) which contain high amount of smectite in such fine fraction, it may also the reason for a higher CEC in compare with CEC of Gaucher et al. (2004). Carbonates (calcite, dolomite) can affect the CEC-measurements. Therefore, it is recommended the CEC of Opalinus clay needs to be repeated and cross-checked by additional methods (e.g. copper (II) triethylentetramine).

The CEC of Friedland clays were investigated largely by different authors as well as different methods, (e.g. BaCl2 solution, LiCl solution, ammonium acetate (NH4-Ac) and the copper triethylenetetramine (Cu-trien) methods) for the size fraction >62 µm of Carlson (2004). This author revealed the results in values of 37 cmol(+)/kg, 38 cmol(+)/kg, 35 cmol(+)/kg, and 42 cmol(+)/kg, respectively. It is apparently

lower than our measurement. The smaller grain size (<40 µm) can be attributed to the higher CEC-value due to higher content of clay minerals, especially the presence of Ca-smectite can also be a reason for a higher CEC in compare with the other authors who collected materials in different deposits.

In general, the high swelling clay content but less CEC of B25 and Friedland clay can be explained by the dominance of divalent cations (e.g. Ca and Mg) in the interlayer sheet of smectite rather than monovalent (e.g. Na) exhibited a discernibly lower CEC. Otherwise, the use of $BaCl_2$ as exchangeable cations in the method of Hendershot and Duquitte (1986) has leaded to the overestimation of CEC in Opalinus clay because of dissolution of carbonate phases (e.g. calcite, dolomite and siderite).

The surface charge of all three starting materials showed a negative charge on the surface which are represented to clay minerals, especially smectite group. The Opalinus reached -8.3 µeq/l while B25 and Friedland showed the surface charge values from -13.7 to -19 µeq/l, respectively.

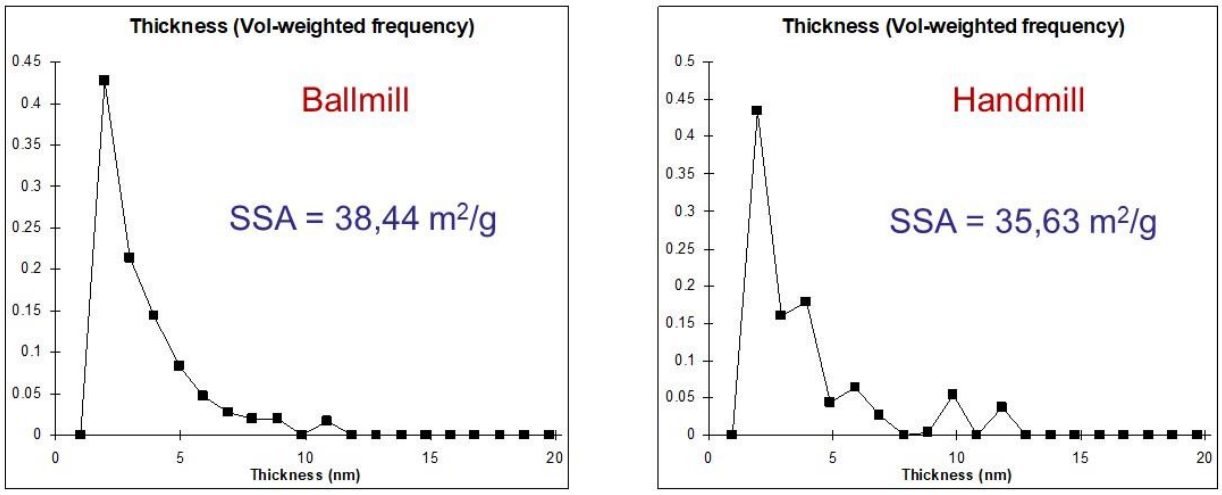

Fig 3.14 *Thickness distribution of grain size from bulk materials of ball mill and hand mill Opalinus clay*

Tab 3.5 *The CEC and BET-specific sureface area of initial B25 bentonite and Opalinus clay*

Sample	CEC (meq/100 g)	SSA (m^2/g)	Surface charge (µeq/l)
B25 Hand mill	45.15	90.39	-13.7
Opalinus Ball mill	88.23	38.44	-
Opalinus Hand mill	82.36	35.63	-8.3
Friedland clay	67.02	42.80	-19.0

The measurements indicated that the highest specific surface area is B25 bentonite that reached 90.39 m^2/g and the lowest ones is Opalinus clay (35.6 – 38.8 m^2/g), Friedland clay stays in the between with the SSA is 42.8 m^2/g. It is not clearly observed the big difference of SSA between hand milled (35.63 m^2/g) and ball milled (38.44 m^2/g) of Opalinus clay. It is compatible with the high amount of smectite and other of bulk materials as observed in XRD-measurement. Furthermore, in order to understand the possibility of mineralogical changes during the grinding of Opalinus claystone to powder, it could effect on the results of permeability experiments, a SSA of two Opalinus starting materials of ball mill

and hand mill was analysed together with calculation of particles thickness from XRD. The results are shown in (Fig 3.14) that indicated a small difference between ball mill and hand mill in both SSA and thickness distribution of grain size. The hand mill materials is less homogenous than ball mill, but the concentration of particles at about 3 – 4 nm are the highest in both which caused a little bit smaller SSA in hand mill material.

3.7 Transmission Electron Microscopy coupled Energy-dispersive X-ray spectroscopy (TEM-EDX)

3.7.1 B25 - bentonite

The fraction < 2 µm of original B25 bentonite sample is mainly composed by dioctahedral vermiculite-smectite mixed layer phases (diVS-ml) and assumed beidellite-montmorillonite interstratifications (B:M ~50:50), abbreviated as BM-ml, and accompanied by montmorillonite and two types of illite. Furthermore, Si-surplus particles (Si, e.g. quartz) were identified in traces in this sample /fig. 3.15/.

	frequency-% *(n = 113 measured particles)*
BM-ml (Cluster1)	35%
diVS-ml (Cluster5)	56%
Montmorillonite (Cluster3)	2%
Illite (Cluster2)	3%
Illite (Cluster4)	2%
Si-surplus	3%

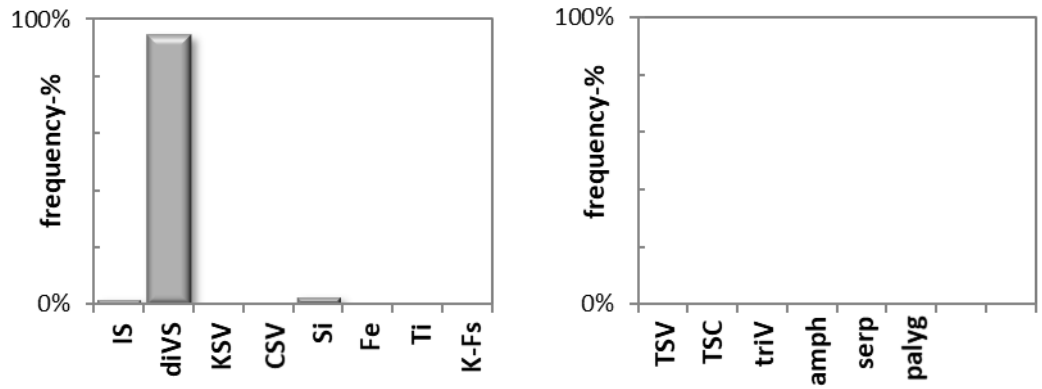

Fig. 3.15. *Distribution of mineral groups in fraction < 2 µm (in frequency-%)*

*Note: **IS** – illite-smectite-mixed layer series in sense of Środon et al. (1992), diVS – dioctahedral vermiculite-smectite illite-smectite-mixed layer series (= charge- and/or K-deficit), **KSV** – kaolinite-smectite-dioctahedral vermiculite-mixed layer series, **CSV** – chlorite-saponite-trioctahedral vermiculite-mixed layer series, **Si** – quartz or particles with Si-surplus, **Fe** – Fe-oxide or Fe-oxyhydroxide, **Ti** – Ti-bearing phases (e.g. rutile, anatase), **K-Fs** – K-feldspar*

Table 3.6. *Summarized chemical composition*

SiO_2	TiO_2	Al_2O_3	Fe_2O_3	MnO	MgO	CaO	Na_2O	K_2O	P_2O_5	Σ	
58.6%	0.0%	22.0%	5.9%		3.0%	1.0%	0.1%	1.1%	0.1%	0.92	measured particles
61.5%	0.5%	21.1%	6.4%	0.1%	4.0%	3.8%	0.4%	2.0%	0.1%	1.00	MAT19 (bulk sample)

All measured clay mineral phases summarized result following mineral formula computed from TEM-EDX-measurement of 110 individual particles:

$$Ca^{2+}_{0.10}\ Mg^{2+}_{0.08}\ Na^{+}_{0.01}\ K^{+}_{0.12}\quad Al^{3+}_{1.27}\ Fe^{3+}_{0.56}\ Mg^{2+}_{0.17}\ Ti^{4+}_{0.00}\ (OH)_2\quad Si^{4+}_{3.70}\ Al^{3+}_{0.30}\ O_{10}$$

SDOM	*± 0.00*	*± 0.00*	*± 0.00*	*± 0.01*	*± 0.01*	*± 0.01*	*± 0.01*	*± 0.00*	*± 0.01*	*± 0.01*

Legend: SDOM - standard deviation of the mean (= the standard deviation divided by the square root of the number of samples)

The interlayer charge is calculated as 0.48 per $(OH)_2$ O_{10} and the octahedral charge as 5.82 per $(OH)_2$ O_{10}. The particles are characterized by a high octahedral Fe-amount.

The summarized chemical composition of all 110 computed particles is compared with chemical data from literature /tab. 3.6/. Such comparison is only limited valid because of different origin of samples and the differences in composition for fraction < 2 µm (the measured sample) and the bulk material (the applied literature data). The chemical composition averaged by measured particles show especially a lower amount of CaO, Na_2O and K_2O as the applied literature data, probably an indication for a higher concentration of feldspars in the bulk sample than in fraction < 2 µm.

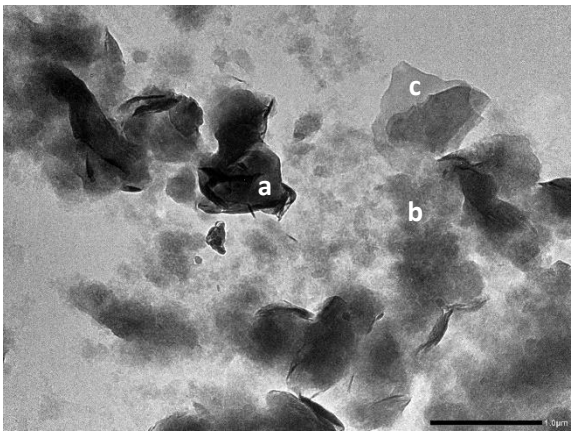

JEM-2100_MAG_X10k_B25-40um_I08.bmp

Magnification: 10k

(a) large (≤ 1 µm) xenomorph film-like platy crystals with folds;
(b) aggregates formed by small (≤ 200 nm) xenomorphous plates;
(c) large (≤ 1 µm) xenomorph plates, homogenous thickness

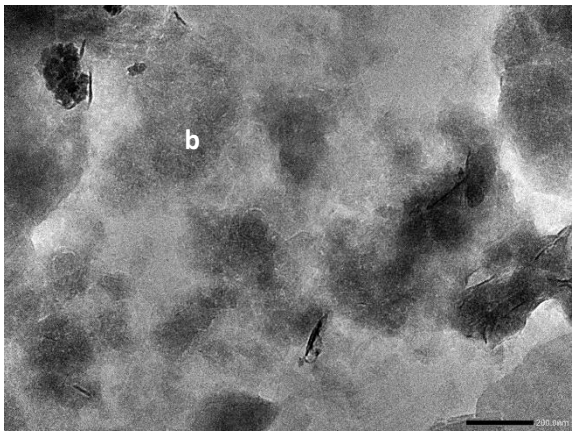

JEM-2100_MAG_X30k_B25-40um_I10.bmp

Magnification: 30k

(b) aggregates formed by small (≤ 200 nm) xenomorphous plates

Fig. 3.16. *Morphology of particles (TEM-micrographs)*

B25 bentonite is characterized by three morphological groups: (i) large (≤ 1 µm) xenomorph film-like platy crystals with folds, (ii) aggregates formed by small (≤ 200 nm) xenomorphous plates and (iii) large (≤ 1 µm) xenomorph plates with homogenous thickness (Fig. 3.16). Thin aggregates formed by small (≤ 200 nm) xenomorphous plates dominate the shapes of particles in the micrographs (Figs. 3.16, 3.17).

The distribution of %S-probability of all measured clay mineral phases (Fig. 3.18) also indicates the occurrence of three groups: (i) montmorillonite (in traces; %S-class = 100%), (ii) as main group a mixture of beidellite-montmorillonite interstratifications and diVS-ml (%S-max of this mixture at 70%) and (iii) illite with K- and charge deficit (%S-class = 0%).

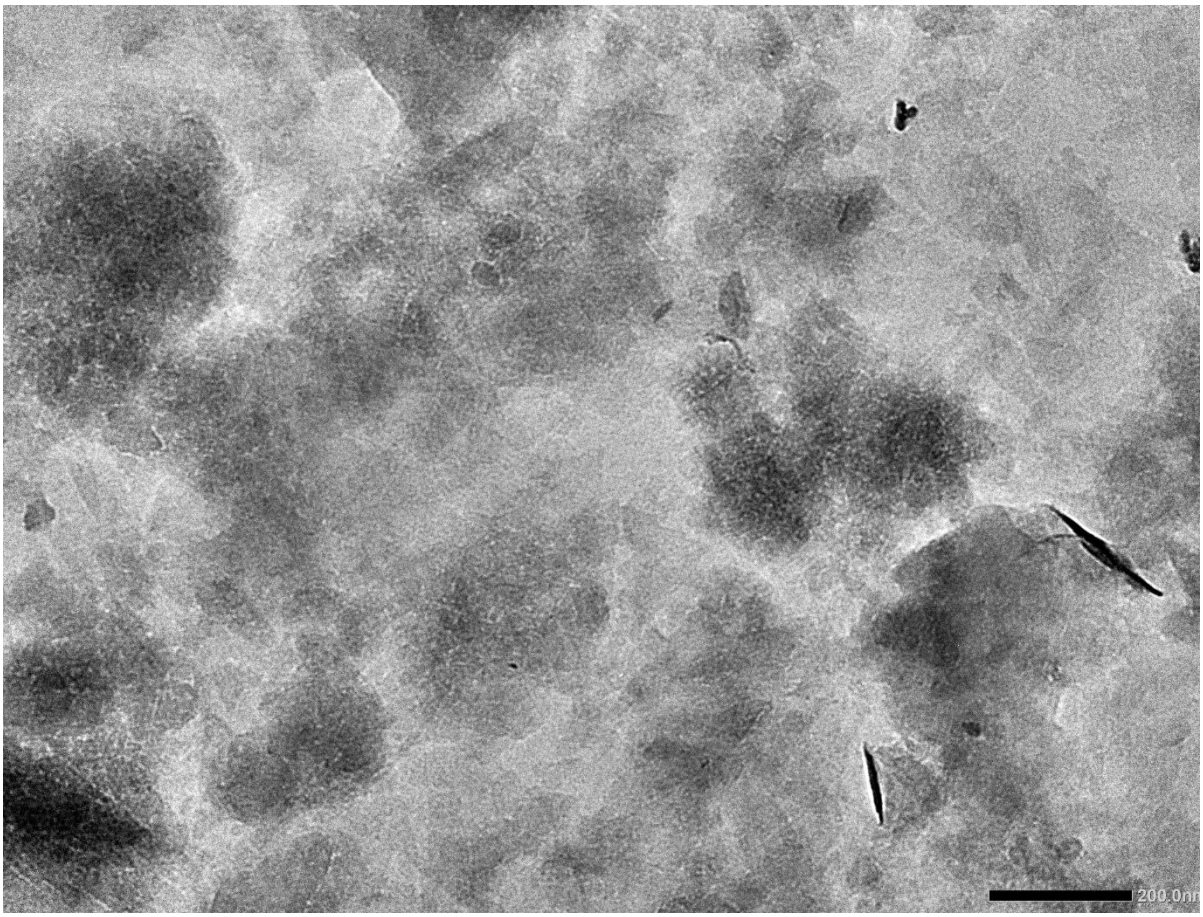

JEM-2100_MAG_X30k_B25-40um-I07.bmp
Magnification: 30k
aggregates formed by small (≤ 200 nm) xenomorphous plates

***Fig. 3.17** Morphology of particles (TEM-micrographs)*

The numerous measured particles by TEM-EDX allow a visualization of distribution of interlayer charges. Considering the TEM-EDX-determined cations Ca^{++}, Mg^{++} and Na^{+} and then computed their ratio as interlayer cations in the mineral formula, Ca^{++}, Mg^{++} and Na^{+} offer to characterize the degree of exchangeable charges in the interlayer space. This charge density of untreated B25 bentonite (< 2 µm) shows only a narrow interval at the maximal frequency-% of charge density at 0.35 per $(OH)_2\ O_{10}$ (fig.3.19). This narrow interval of interlayer charge density caused by exchangeable cations from 0.27 – 0.47 per $(OH)_2\ O_{10}$ represents mainly the BM- and diVS-ml phases. The few measured montmorillonite particles are part of this interval. Also, the measured illite particles (Cluster2) offer only a low number of exchangeable cations and indicating a lower degree of weathering.

Distribution of smectite layers probability (%S)

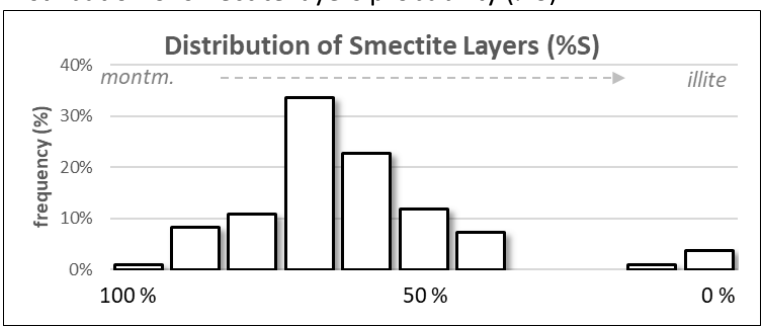

***Description:** The distribution of %S-probability indicates the occurrence of three groups: (i) montmorillonite (in traces), (ii) mixture of beidellite-montmorillonite interstratifications (= assumption) with diVS-ml as well as (iii) illite with K-deficiency.*

***Fig. 3.18a.** Distribution of smectite layers probability (%S)*

Differentiation by relation “Octahedral Mg vs. tetrahedral Si”?

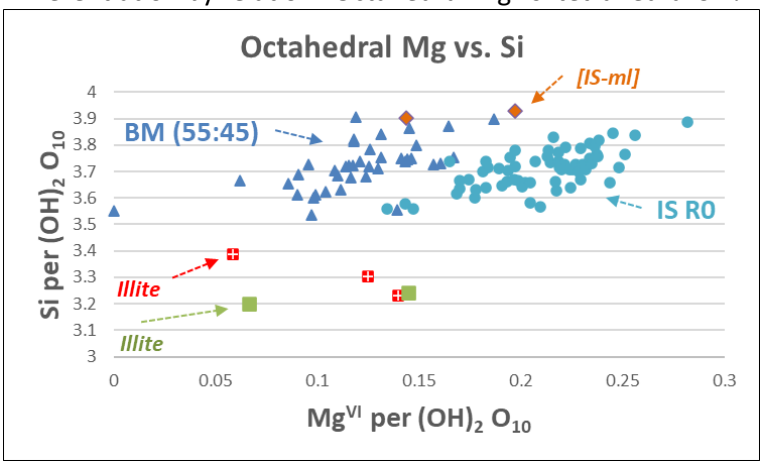

Description: *This diagram indicates the occurrence of two large groups of Mg in relation to tetrahedral Si as result of clustering. Probably, this distribution mirrors 2 phases (I) beidellite-montmorillonite interstratifications (labelled as BM 55:45) and (II) diVS-ml (labeled as IS R0 by Sybilla-processing of XRD-traces of EG-solvated fraction < 2 µm, %Sxrd=55%)*

Fig. 3.18b. *Distribution of octahedral Mg vs. tetrahedral Si [all per $(OH)_2$ O_{10}]*

Distribution of K in relation to tetrahedral Si

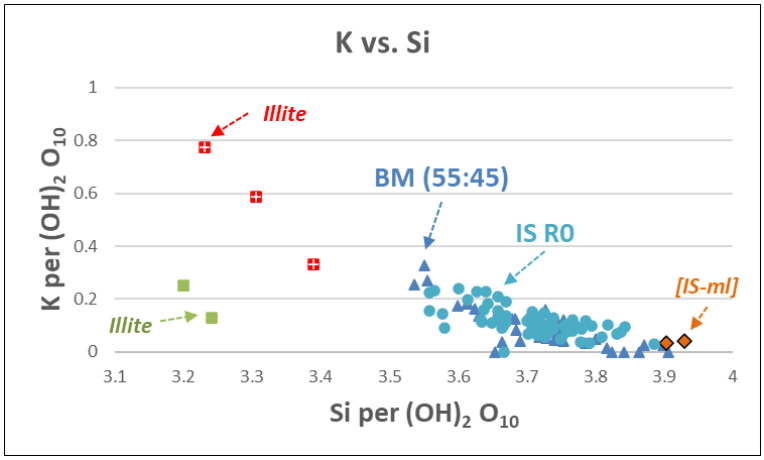

Description: *This diagram visualizes possible particles with a very low K (labelled groups as result of clustering)*

Fig. 3.18c. *Distribution of K in interlayer space vs. tetrahedral Si [all per $(OH)_2$ O_{10}]*

Distribution of charges (exchangeable from interlayer space)

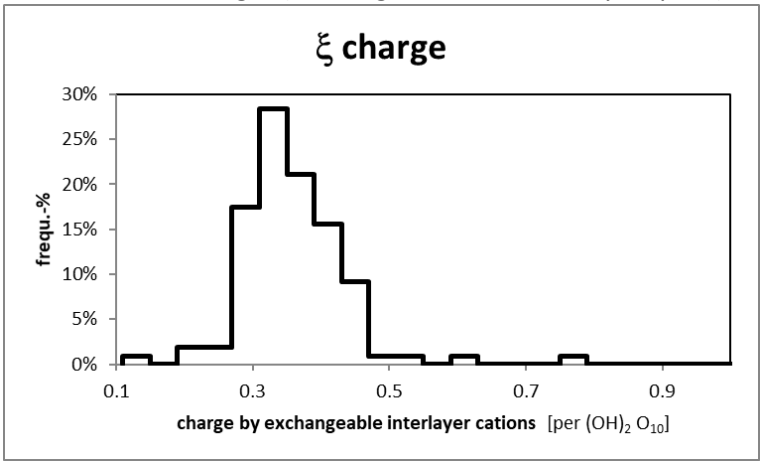

This diagram visualizes the distribution of exchangeable charges in the interlayer space (Ca, Mg, Na) determined and computed by TEM-EDX-data.

Description: *Maximal frequency-% of charge density at 0.35 per $(OH)_2$ O_{10}.*

Fig. 3.19. *Distribution of charges*

Result of Clustering & Comparison with XRD-data (Sybilla-processing)

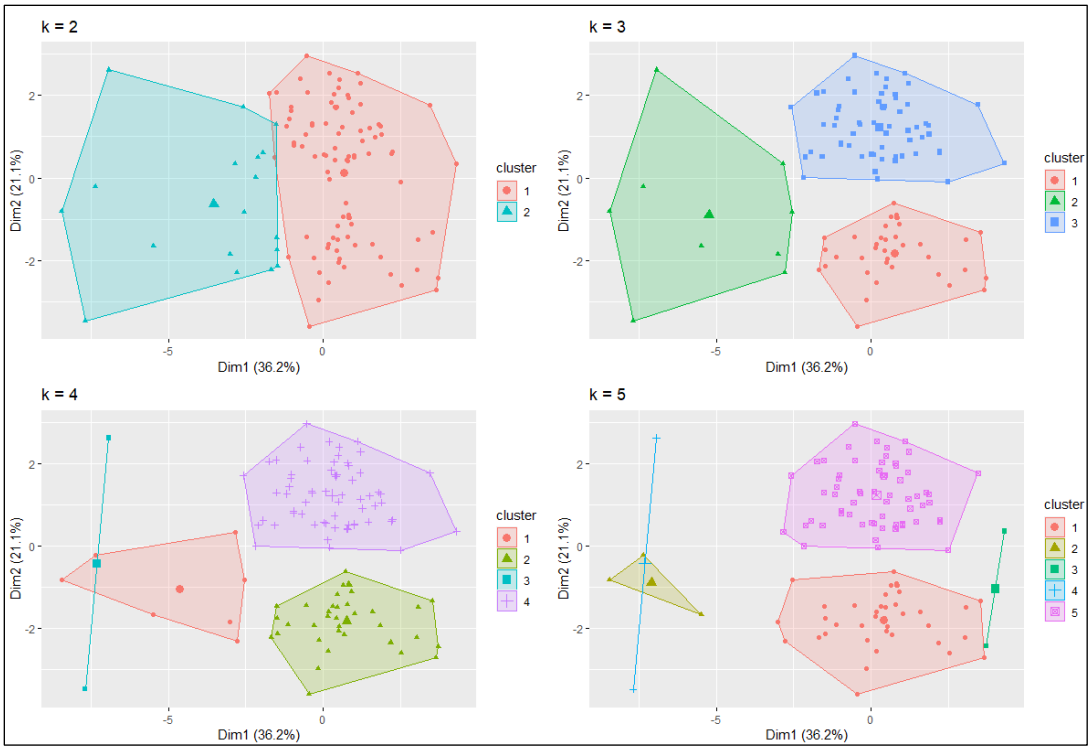

Fig. 3.20. *Clustering of all measured particles for clusters k = 2, k = 3, k = 4 and k = 5 (source for R-coding: https://uc-r.github.io/kmeans_clustering)*

The optimum of clusters was calculated with k = 5 (fig. 3.20). This number of clusters differentiates also clearly illite particles (Cluster2, Cluster4) from smectite-bearing phases (Cluster1, Cluster3, Cluster5) (fig. 21).

		Ca (XII)	Mg (XII)	Na (XII)	K (XII)	Cr3+ (VI)	Al (VI)	Fe3+ (VI)	Mg (VI)	Ti (VI)	Al (IV)	Si (IV)	XII	n_VI	%S
Cluster1	n = 40	0.04	0.11	0.00	0.09	0.00	1.32	0.56	0.12	0.00	0.28	3.72	0.4	2.0	58
Cluster2	n = 3	0.06	0.03	0.03	0.56	0.00	1.55	0.33	0.11	0.01	0.69	3.31	0.8	2.0	10
Cluster3	n = 2	0.11	0.09	0.00	0.04	0.00	1.31	0.46	0.17	0.00	0.08	3.92	0.4	1.9	92
Cluster4	n = 2	0.07	0.28	0.00	0.19	0.00	0.99	0.90	0.11	0.00	0.78	3.22	0.9	2.0	4
Cluster5	n = 63	0.13	0.05	0.01	0.12	0.00	1.22	0.56	0.21	0.00	0.29	3.71	0.5	2.0	56

Fig. 3.21. *Mineral formulae based on TEM-EDX-data summarized following the result of clustering for k=5*

Tab. 3.7 *Comparison of results from TEM-EDX- and XRD-measurements with clustering procedure*

	Sybilla-results	**TEM-EDX-results**	**Notes**
Cluster1	IS R0 (1) *(%S = 99%)*	BM-ml *(%S=100%, %B ~ 55%)*	*XRD: Montmorillonite and beidellite are only to distinguish by Green-Kelly-test (not available here).*
Cluster2	Illite	Illite	*K-deficit, Al(VI)-rich*
Cluster3	IS R0 (1) *(%S = 99%)*	IS-ml *(%S = 92%)*	*high charged Fe-rich Ca,Mg-montmorillonite*
Cluster4	Illite	Illite	*high K-deficit, nearby a Fe-illite*
Cluster5	IS R0 (2) *(%S = 55%)*	diVS-ml *(%S = 56%)*	*high K-deficit, Fe(VI)-rich*

The clustering of TEM-EDX-data offers a good agreement with the recent result of Sybilla-processing of XRD-traces from oriented specimen (tab. 3.7).

IS R0 (1): The X-ray diffraction pattern of the ethylene-glycol saturated oriented specimen shows a full expandability to 1.7 nm and a difference of 5.42°2θ between 2. and 3. order of smectite interferences. This distance is typically for montmorillonite (Moore & Reynolds, 1989). This result of XRD-processing let expect a maximum of particles for %S ~ 90-100% by TEM-EDX-measurements, but the maximum of particles measured by TEM-EDX is to find at %S=70% (fig. 3.18).

Montmorillonite and beidellite have the same behaviour concerning the expandability and they are only to distinguish by XRD using Li like by Greene-Kelly test (Green-Kelly 1952, 1953). So, combination of XRD- and TEM-results (full expandability by XRD and Si ~ 3.72 by TEM-EDX) led conclude the occurrence of 'beidellite-montmorillonite interstratifications', a beidellite-montmorillonite inter-stratification with about 55% beidellite and 45% montmorillonite layers (BM-ml 55:45).

The methodical combination of XRD-processing and TEM-EDX- data (incl. clustering) indicates further sub-groups of identified phases by Sybilla-procedure for illite-smectite mixed layer phases (IS R0 (1)): (i) BM-ml (Cluster1) and (ii) IS-ml (Cluster3) (tab. 3.7).

IS R0 (2): The Sybilla-procedure of XRD-traces (oriented mounts) has shown an occurrence of a second illite-smectite mixed layer phase with a smectite layers probability of %S = 55%. This situation is to find in Cluster5 (%S = 56%) representing a K- and charge deficient and Fe-rich dioctahedral vermiculite-smectite mixed layer phase (diV-ml) (tab. 3.7).

Illite: The Sybilla-procedure of XRD-traces (oriented mounts) draws the occurrence of illite. The clustering of TEM-EDX-data confirmed the Sybilla-results, but it indicates two sub-groups of illite: (i) illite (Cluster2) as K-deficient and Al(VI)-rich illite and (ii) illite (Cluster5) as very high K-deficient and Fe(VI)-rich illite (tab. 3.7).

The Sybilla-processing of XRD-traces (oriented mounts) also supports the existence of kaolinite and kaolinite-smectite mixed layer phases in fine fraction of B25 bentonite. Such phases were not to identify in TEM-EDX-database (a grain size effect?).

Specifics to the identified clay mineral groups

Montmorillonite as part of illite-smectite mixed-layer series *(IS-ml in sense of Środon et al., 1992)*

The term 'illite-smectite mixed layer series in sense of Środon et al. (1992)' describes illite-smectite interstratifications with a normal interlayer charge for illite layers of 0.89 (representing fixed K) and a normal interlayer charge for smectite layers of 0.40 per $(OH)_2\ O_{10}$. This series occurs in B25 bentonite (< 2 µm) in traces as end member of this series: montmorillonite. Only 2 of 110 measured particles belong so to this normal charged group IS-ml in sense of Środon et al. (1992).

Montmorillonite:

$$Ca_{0.11}\ Mg_{0.09}\ Na_{0.00}\ K_{0.04}\quad Al_{1.31}\ Fe^{3+}_{0.46}\ Mg_{0.17}\ Ti_{0.00}\ (OH)_2\quad Si_{3.92}\ Al_{0.08}\ O_{10}$$

Charge: XII = 0.44 VI = 5.64 IV = 15.92 **Σ = 22.00**
Probability of smectite layers (%S): 92%
Probability of illite layers (%I): 8%

Measured particles by TEM-EDX: 2
Result of clustering: Cluster3 (tab. 3.7)

The %S-probability of these particles (%S ~ 92%) indicates the occurrence of montmorillonite. Furthermore, the value for octahedral iron (0.46 per $(OH)_2\ O_{10}$) in the computed mineral formula characterizes this montmorillonite as Fe-rich.

The distribution of %S-probability, specified for normal charged IS-ml, indicates the occurrence only of one group of phases, here with %S mainly at 90% (fig. 3.22).

Distribution of smectite layers probability (%S) in IS-ml *(2 particles only)*

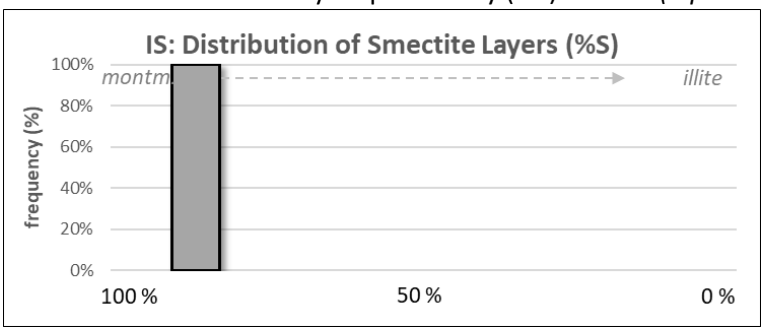

Description: *The distribution of %S-probability indicates also the occurrence of montmorillonite (confirmed as Cluster3).*

Fig. 3.22. *Distribution of smectite layers probability (%S) in IS-ml*

Beidellite-montmorillonite interstratifications (B:M ~50:50)

40 of 110 measured particles belong so to this assumed classification. The dioctahedral character of this group is proofed by X-ray diffraction. The position of the large (060)-interference of smectite is in the random oriented powder specimen at 1.497 Å.

The X-ray diffraction pattern of the ethylene-glycol saturated oriented specimen shows a full expandability to 1.7 nm and a difference of 5.42°2θ between 2. and 3. order of smectite interferences. This distance is typically for montmorillonite (Moore & Reynolds, 1989). This result of XRD-processing let expect a maximum of particles for %S ~ 90-100% by TEM-EDX-measurements, but the maximum of particles measured by TEM-EDX is to find at %S=70% (fig. 3.18).

Montmorillonite and beidellite have the same behaviour concerning the expandability and they are only to distinguish by XRD using Li by means of Greene-Kelly test (Green-Kelly 1952, 1953). So, combination of XRD- and TEM-results (full expandability by XRD and Si ~ 3.69 by TEM-EDX) led conclude the occurrence of 'beidellite-montmorillonite interstratifications', a beidellite-montmorillonite interstratification with about 55% beidellite and 45% montmorillonite layers (BM-ml55:45).

Beidellite-Montmorillonite interstratification (BM ~ 55%:45%) *(Cluster1):*

$$Ca_{0.04}\ Mg_{0.11}\ Na_{0.00}\ K_{0.09}\quad Al_{1.32}\ Fe^{3+}_{0.56}\ Mg_{0.12}\ Ti_{0.00}\ (OH)_2\quad Si_{3.72}\ Al_{0.28}\ O_{10}$$

Charge: XII = 0.40 VI = 5.88 IV = 15.72 **Σ = 22.00**

Measured particles by TEM-EDX: 40
Result of clustering: Cluster1 (tab. 3.7)

Beidellitic structures are characterized by a low octahedral Mg-amount (because of high ratio of octahedral, 3-valent cations). A comparison of octahedral Mg vs. tetrahedral Si indicates the occurrence of two groups for octahedral Mg based on TEM-EDX-data (tab. 3.18b). The group with a lower Mg-ratio should represent the already mentioned BM-ml (55:45) phases (= IS GLY R0_1 with $\%S_{xrd}$ = 99%; see also Cluster1 in (tab. 3.7)) and the other group with a higher Mg-ratio is considered as diVS-ml (= IS GLY R0_2 with $\%S_{xrd}$ = 55%).

Using the results of clustering (see Cluster1 in (tab. 3.7)), the maximum of frequency-% is to find for particles in the Si(IV)-class 3.7 – 3.8 e phuc (fig. 3.32a), representing the mentioned relation 55% mont-morillonite and 55% beidellite as ratio of interstratification. The mineral formulae, summarized in classes of tetrahedral Si, draw for the maximum an Fe-rich BM 55:45 phase with low K, but remarkable amount of Mg in the interlayer space (fig. 3.32b).

Distribution of BM-interstratifications (Cluster1)

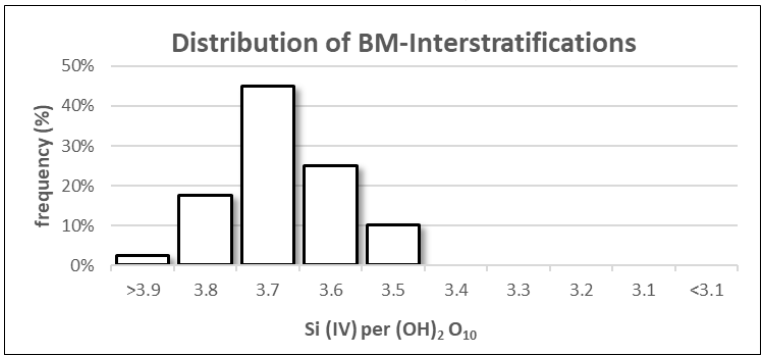

Description: *The distribution of BM-interstratifications (classified as Cluster1) draws a maximum of frequency (%) at tetrahedral Si-value between 3.7 – 3.8 e phuc*

Fig. 3.23a. *Distribution of assumed beidellite-montmorillonite interstratifications*

BM50:50	*particles (abs)*	Ca (XII)	Mg (XII)	Na (XII)	K (XII)	Cr3+ (VI)	Al (VI)	Fe3+ (VI)	Mg (VI)	Ti (VI)	Al (IV)	Si (IV)	XII	n_VI	%S
Si >3.9	n = 1	0.00	0.11	0.00	0.00	0.00	1.32	0.56	0.12	0.00	0.09	3.91	0.2	2.0	90
Si 3.9-3.8	n = 7	0.04	0.11	0.00	0.02	0.00	1.34	0.51	0.14	0.00	0.16	3.84	0.3	2.0	79
Si 3.8-3.7	**n = 18**	**0.05**	**0.11**	**0.00**	**0.08**	**0.00**	**1.28**	**0.59**	**0.13**	**0.00**	**0.26**	**3.74**	**0.4**	**2.0**	**60**
Si 3.7-3.6	n = 10	0.04	0.12	0.00	0.11	0.00	1.36	0.54	0.10	0.00	0.35	3.65	0.4	2.0	48
Si 3.6-3.5	n = 4	0.05	0.08	0.00	0.26	0.00	1.40	0.51	0.08	0.00	0.44	3.56	0.5	2.0	35
Si 3.5-3.4	n = 0														
Si 3.4-3.3	n = 0														
Si 3.3-3.2	n = 0														
Si 3.2-3.1	n = 0														
Si <3.1	n = 0														

Fig. 3.23b. *Computed averaged mineral formulae of phases in the different Si(IV)-classes*

Dioctahedral vermiculite-smectite mixed layer phase (diVS-ml)

The processing of XRD-traces (oriented mounts) by Sybilla-software has drawn the occurrence of two types of IS GLY R0-phases: (i) IS GLY R0 (1) with $\%S_{xrd}$ = 99% above discussed as BM-ml (50:50) and (ii) IS GLY R0 (2) with $S\%_{xrd}$ = 55% (see Cluster5 in (tab. 3.7).

Dioctahedral vermiculite-smectite mixed layer phase (diVS-ml):

$$Ca_{0.13}\ Mg_{0.05}\ Na_{0.01}\ K_{0.12}\quad Al_{1.22}\ Fe^{3+}_{0.56}\ Mg_{0.21}\ Ti_{0.00}\ (OH)_2\quad Si_{3.71}\ Al_{0.29}\ O_{10}$$

Charge: XII = 0.50 VI = 5.79 IV = 15.71 **Σ = 22.00**

Probability of smectite layers (%S): 56%

Probability of illite layers (%I): 44%

Measured particles by TEM-EDX: 63

Result of clustering: Cluster5 (tab. 3.7)

The probability of smectite layers determined by TEM-EDX-data and Sybilla-processing of XRD-traces (oriented mounts) gives similar results: $\%S_{TEM}$ = 56% (fig. 3.24a) and $\%S_{XRD}$ = 55%.

The Rietveld refinement by Profex software (Döbelin & Kleeberg, 2015) draws for octahedral composition of this mixed layer phase in bulk sample: $Al^{3+}_{1.2}$ $Fe^{3+}_{0.60}$ $Mg^{2+}_{0.20}$ per ($(OH)_2$ O_{10}) as best refinement result. This refinement of X-ray diffraction traces confirms additionally the Fe-rich occupation of octahedral layer as determined also by TEM-EDX (fig. 3.24b).

Distribution of smectite layers probability (%S) in diVS-ml (Cluster5)

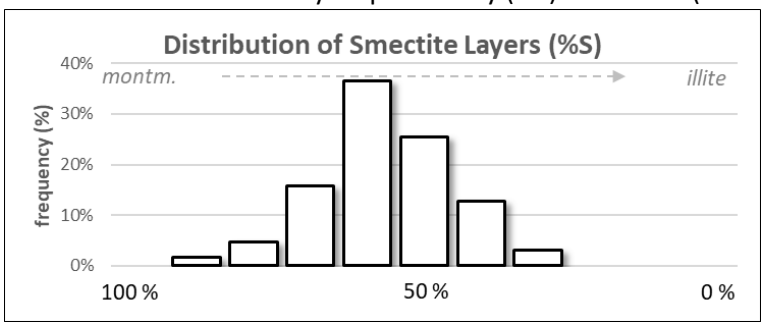

Description: *The distribution of diVS-ml (classified as Cluster5) draws a maximum of frequency (%) for smectite layer probability at 60%*

Fig. 3.24a. *Distribution of smectite layers probability in diVS-ml*

diVS-ml	*particles (abs)*	Ca (XII)	Mg (XII)	Na (XII)	K (XII)	Cr3+ (VI)	Al (VI)	Fe3+ (VI)	Mg (VI)	Ti (VI)	Al (IV)	Si (IV)	XII	n_VI	%S
%S >95%	n = 0														
%S 95-85%	n = 1	0.16	0.02	0.00	0.03	0.00	1.28	0.44	0.28	0.00	0.11	3.89	0.4	2.0	86
%S 85-75%	n = 3	0.10	0.05	0.02	0.08	0.00	1.33	0.43	0.24	0.00	0.16	3.84	0.4	2.0	77
%S 75-65%	n = 10	0.13	0.04	0.02	0.08	0.00	1.24	0.52	0.23	0.00	0.21	3.79	0.4	2.0	68
%S 65-55%	**n = 23**	**0.14**	**0.05**	**0.01**	**0.10**	**0.00**	**1.22**	**0.57**	**0.21**	**0.00**	**0.27**	**3.73**	**0.5**	**2.0**	**59**
%S 55-45%	n = 16	0.14	0.05	0.01	0.13	0.00	1.21	0.58	0.20	0.00	0.34	3.66	0.5	2.0	49
%S 45-35%	n = 8	0.13	0.06	0.02	0.17	0.00	1.19	0.62	0.18	0.00	0.40	3.60	0.6	2.0	41
%S 35-25%	n = 2	0.10	0.08	0.02	0.19	0.00	1.24	0.61	0.14	0.01	0.44	3.56	0.6	2.0	35
%S 25-15%	n = 0														
%S <15%	n = 0														

Fig. 3.24b. *Computed averaged mineral formulae of diVS-ml phases in the different smectite layers probability (%S)-classes*

Illite

The TEM-EDX-based distribution of %S-probability (Fig. 3.18a) indicates three possible groups: (i) the occurrence of montmorillonite with %S ~ 100%, (ii) BM-ml in mixture with diVS-ml (maximum at $Si_{tetrahedral}$ 3.74 per $(OH)_2$ O_{10} and (iii) illite with K- & charge-deficit. The clustering of TEM-EDX-data shows two illite clusters Cluster2 and Cluster4 (tab. 3.7).

Illite *(as end member of diVS-ml series; confirmed as Cluster2):*

$$Ca_{0.06}\ Mg_{0.03}\ Na_{0.03}\ K_{0.56}\quad Al_{1.55}\ Fe^{3+}_{0.33}\ Mg_{0.11}\ Ti_{0.01}\ (OH)_2\quad Si_{3.31}\ Al_{0.69}\ O_{10}$$

Charge: XII = 0.78 VI = 5.91 IV = 15.31 **Σ = 22.00**
Probability of smectite layers (%S): 10%
Probability of illite layers (%I): 90%

Measured particles by TEM-EDX: 3

Illite *(as end member of diVS-ml series; confirmed as Cluster4):*

$$Ca_{0.07}\ Mg_{0.28}\ Na_{0.01}\ K_{0.19}\quad Al_{0.99}\ Fe^{3+}_{0.90}\ Mg_{0.11}\ Ti_{0.00}\ (OH)_2\quad Si_{3.22}\ Al_{0.78}\ O_{10}$$

Charge: XII = 0.89 VI = 5.89 IV = 15.22 **Σ = 22.00**
Probability of smectite layers (%S): 4%
Probability of illite layers (%I): 96%

Measured particles by TEM-EDX: 2

Illite of Cluster2 is characterized by slight K-deficiency and Al-rich octahedral layer. Few smectite layers are not excluded because of Si(IV) = 3.31 e phuc.

Otherwise, illite particles of Cluster4 show a very high K-deficit and very Fe-rich octahedral layer.

The Rietveld refinement by Profex software (Döbelin & Kleeberg, 2015) indicates the occurrence of two polytypes for illite in B25 bentonite: $2M_1$- and 1M-polytype.

Kaolinite-montmorillonite mixed layer phases

The Excel-based procedure (Hoang-Minh et al., 2019) to identify possible clay mineral groups using the TEM-EDX-measurements also includes algorithms to classify kaolinite and kaolinite-montmorillonite mixed layer phases. These algorithms couldn't identify such phases basing on the measured TEM-EDX-data. Even also the clustering gives no indications for the occurrence of kaolinite-bearing phases.

Otherwise, the processing of XRD-traces (oriented mounts) by Sybilla-Software indicated the occurrence of kaolinite-montmorillonite mixed layer phases (KS GLY R1, $\%S_{xrd}$=45%). Such particles should be characterized by a low potassium (because of missing K in kaolinite structure). A visualization of TEM-EDX-measurements in a relation "K vs. Si" shows only two possible measurements (of 108 particles), which could represent phases with a very low potassium ratio in the structure (fig. 3.18c). The mean of particle thickness for KS GLY R1 was computed by Sybilla-software at 11 nm. Probably, this higher thickness is underrepresenting the kaolinite-bearing phases in the TEM-EDX-results in comparison to the finer particles of BM 50:50 in mixture with diVS-ml (T_{mean} ~ 4.4 nm).

Estimation of Specific Dissolution Potential *(in according to Nguyen-Thanh et al., 2014)*

Previous investigations have shown (summarized in Nguyen-Thanh et al., 2014), each bentonite or clay have a specific dissolution potential expressed as loss of smectite layer. The expected specific behaviour of smectite layers is classified using the mineral formula as result of TEM-EDX-measurements. The authors developed different experimental overhead rotation setups to determine the maximal possible loss of smectite layers under pre-defined conditions (fig. 3.25). These different experimental settings should represent different strength of acting forces in mineralogical alteration of original smectite (with water as low energy-level). The previous results with a large series of bentonites and clays allow to predict the expected rate of alteration of smectite layers distinguishing slow-reacting smectite layers (= sleepers), moderate-reacting smectite layers and fast-reacting smectite layers (= sprinters). The limits between these free classes are postulated only: sleepers are smectites with loss of smectite layers lower than Δ%S = 5% and are a sprinter with loss of smectite layers larger than Δ%S = 20%. Negative values for Δ%S mirroring a 'illitization'-like process and positive values represent a smectitization potential.

The modelled values for B25 bentonite (fig. 3.25) let expect mainly a moderate-reacting smectite with a change from the original $Si_{tetrahedral}$ 3.69 in direction to $Si_{tetrahedral}$ 3.60 per $(OH)_2$ O_{10} for the run products (Δ%S = -8%). Otherwise under strong conditions (e.g. higher temperature, high ionic strength, high saline solution), the modelling let assume for B25 bentonite a very fast and nearby complete loss of smectite layers (Δ%S = -96%).

		Specific Dissolution Potential (*)			
B25	**original**	**H2O 20 rpm**	**H2O 60 rpm**	**NaCl 20 rpm**	**NaCl 60 rpm**
Interlayer Type (*)		Ca+Mg	Ca+Mg	Ca+Mg	Na
calculated Δ%S		-8 ± 1	-8 ± 1	-9 ± 1	-96 ± 3
measured $\%S_{initial}$	54				
reaction type					
by modelling*		*moderate*	*moderate*	*moderate*	*sprinter*

Description: *Overhead-rotation systems like H2O 20 rpm serve as indicator for rate of alteration of selected bentonite. Low grade reduction of smectitic layers (Δ%S) indicate a slow reaction of smectite phases (so-called sleeper).*
An opposite behaviour is called as sprinter.

Fig. 3.25. *Specific Dissolution Potential of B25 bentonite, < 2 µm (* in according to Nguyen-Thanh et al., 2014)*

The type of cations in the interlayer space (here type B with Ca + Mg) and the Fe-rich composition of octahedral layer are the driving forces for these estimations.

Following aspect could influence the expected behaviour for B25 bentonite: The alteration mechanisms and the rate of alteration of beidellite are unknown until now.

Finally, only further experiments with the selected bentonite can validate these estimations.

3.7.2 Opalinus clay

The fraction < 2 µm of Opalinus Clay original sample is mainly composed by two different types of dioctahedral vermiculite-smectite mixed layer phases (diVS-ml). Rarely, rutile and quartz were identified in traces in this sample (fig. 3.26).

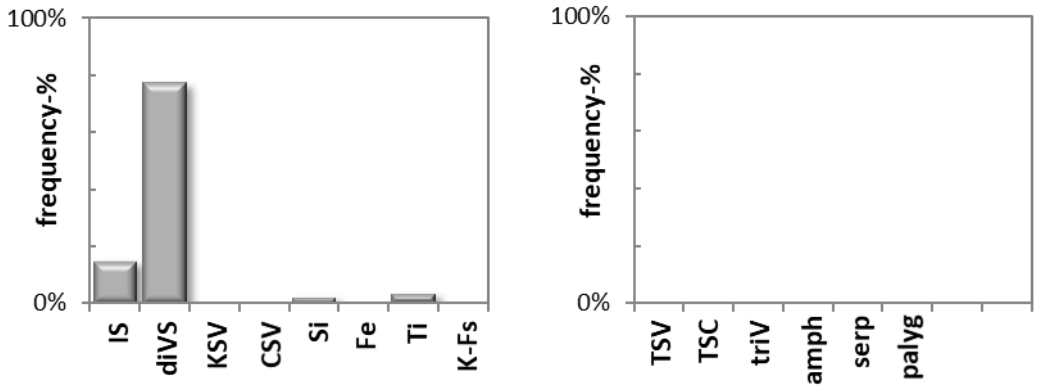

Fig. 3.26. *Distribution of mineral groups in fraction < 2 µm (in frequency-%)*
Legend: ***IS*** *– illite-smectite-mixed layer series in sense of Środon et al. (1992), diVS – dioctahedral vermiculite-smectite illite-smectite-mixed layer series (= charge- and/or K-deficit),* ***KSV*** *– kaolinite-smectite-dioctahedral vermiculite-mixed layer series,* ***CSV*** *– chlorite-saponite-trioctahedral vermiculite-mixed layer series,* ***Si*** *– quartz or particles with Si-surplus,* ***Fe*** *– Fe-oxide or Fe-oxyhydroxide,* ***Ti*** *– Ti-bearing phases (e.g. rutile, anatase),* ***K-Fs*** *– K-feldspar*

The measured and computed particles have shown a calculated CEC-value of 52 meq / 100 g located at surface and in the interlayer space.

	frequency-% *(n = 75 measured particles)*
diVS-ml	92%
Ti-phases	4%
Quartz	3%
Unknown phases	1%

All measured dioctahedral 2:1 clay mineral phases summarized result following mineral formula computed from TEM-EDX-measurement of 70 individual particles:

$$Ca^{2+}_{0.09}\ Mg^{2+}_{0.06}\ Na^{+}_{0.01}\ K^{+}_{0.39}\quad Al^{3+}_{1.40}\ Fe^{3+}_{0.42}\ Mg^{2+}_{0.17}\ Ti^{4+}_{0.01}\ (OH)_2\quad Si^{4+}_{3.46}\ Al^{3+}_{0.54}\ O_{10}$$

SDOM *± 0.01 ± 0.01 ± 0.0 ± 0.02 ± 0.02 ± 0.02 ± 0.01 ± 0.01 ± 0.02 ± 0.02*

Legend: SDOM - standard deviation of the mean (= the standard deviation divided by the square root of the number of samples)

The interlayer charge is calculated as 0.70 per $(OH)_2\ O_{10}$ and the octahedral charge as 5.83 per $(OH)_2\ O_{10}$. The particles are characterized by a high octahedral Fe-amount.

The summarized chemical composition of all 70 computed particles is listed (tab. 3.8).

Table 3.8. *Summarized chemical composition*

SiO_2	TiO_2	Al_2O_3	Fe_2O_3	MnO	MgO	CaO	Na_2O	K_2O	P_2O_5	Σ	
52.7%	0.1%	26.1%	4.3%		2.7%	1.3%	0.0%	3.4%	0.3%	0.91	measured particles
53.1%	1.0%	19.7%	6.2%	<0.1%	2.3%	3.0%	0.6%	2.6%		0.91	GAU03 (SHGN - bulk)

Opalinus Clay original sample is also characterized by two morphological groups: (i) large (≤ 1 µm) xenomorph platy crystals and (ii) aggregates, formed by small (≤ 200 nm) laths with idiomorph ends (fig. 3.27). Aggregates formed by small (≤ 200 nm) laths with idiomorph ends dominate the shapes of particles in the micrographs (fig. 3.27).

Distribution of smectite layers probability (%S)

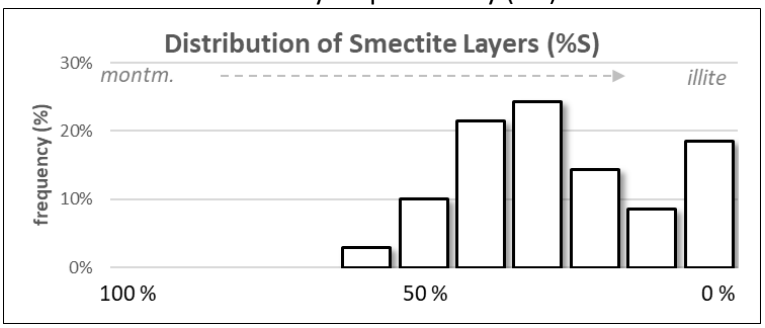

Description: *The distribution of %S-probability indicates two groups: (i) the occurrence of diVS-ml + IS-ml with %S mainly at 30-40% and (ii) illite with K- & charge-deficit.*

Fig. 3.28a. *Distribution of smectite layers probability (%S)*

Differentiation by relation "Octahedral Mg vs. tetrahedral Si"?

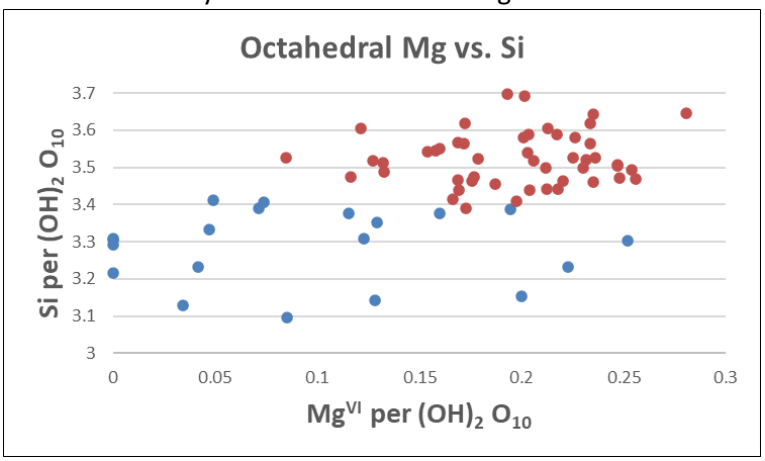

Description: *This diagram doesn't indicate any separation on low and high ratio of Mg in relation to tetrahedral Si (blue dots – Cluster1; red dots – Cluster2). Phases of Cluster2 are mostly characterized by Mg(VI) > 0.1 per $(OH)_2$ O_{10}.*

Fig. 3.28b. *Distribution of octahedral Mg vs. tetrahedral Si [all per $(OH)_2$ O_{10}]*

Distribution of K in relation to tetrahedral Si

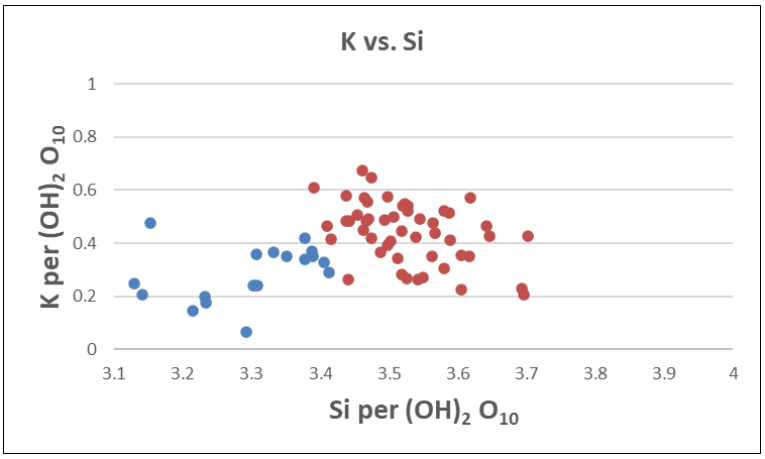

Description: *This diagram indicates a weak separation on low and high ratio of K in relation to tetrahedral Si (blue dots – Cluster1; red dots – Cluster2). Phases of Cluster1 are mostly characterized by K < 0.45 per $(OH)_2$ O_{10}.*

Fig. 3.28c. *Distribution of K in interlayer space vs. tetrahedral Si [all per $(OH)_2$ O_{10}]*

Distribution of charges (exchangeable from interlayer space)

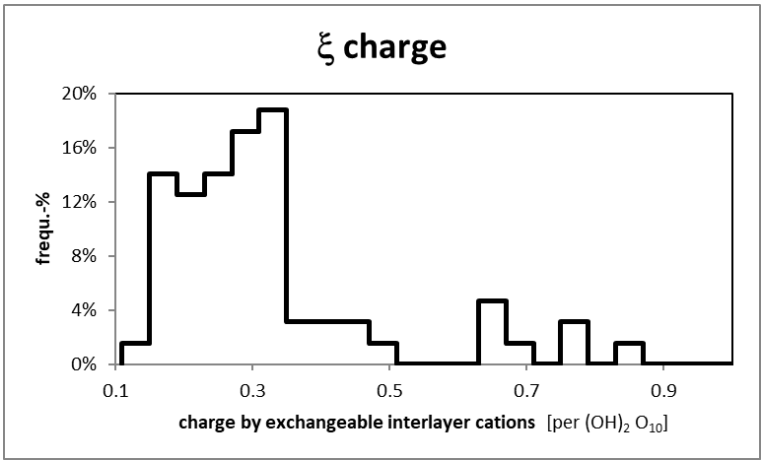

This diagram visualizes the distribution of exchangeable charges in the interlayer space (Ca, Mg, Na) determined and computed by TEM-EDX-data.

Description: *The charge density indicates a broad distribution of exchangeable interlayer cations lower than 0.35 per $(OH)_2$ O_{10}.*

Fig. 3.29. *Distribution of charges*

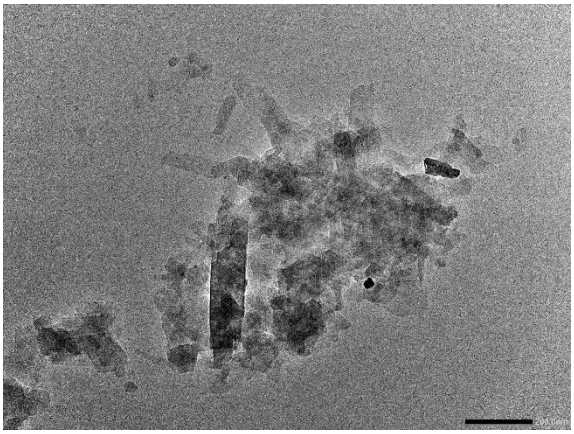

JEM-2100_MAG_X30k_Opalinus-40um-16.9_008.bmp

Magnification: 30k

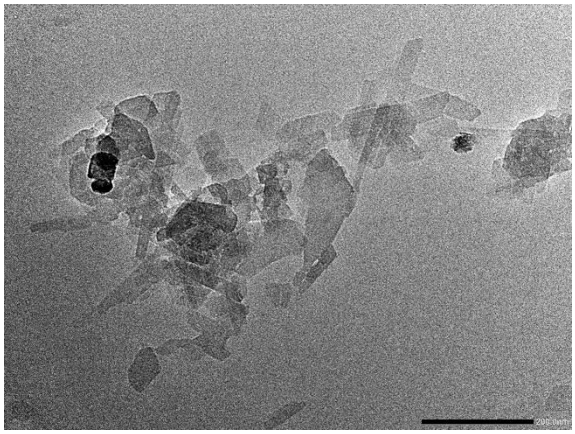

JEM-2100_MAG_X50k_Opalinus-40um-16.9_011.bmp

Magnification: 50k

aggregates composed by slat-shaped crystals (length ~ 200 nm) with idiomorphic ends, commonly parallel or hexagonal intergrowths *(IS-ml and diVS-ml, not to distinguish by morphology of particles)*

Fig. 3.30a. *Morphology of particles (TEM-micrographs)*

The distribution of %S-probability of all measured clay mineral phases (fig. 3.28a) also indicates the occurrence of two groups: (i) diVS-ml with $\%S_{max}$=30-40% and (ii) illite with K-deficiency. A differentiation between

The numerous measured particles by TEM-EDX allow a visualization of distribution of interlayer charges. Considering the TEM-EDX-determined cations Ca^{++}, Mg^{++} and Na^{+} and then computed their ratio as interlayer cations in the mineral formula, Ca^{++}, Mg^{++} and Na^{+} offer to characterize the degree of exchangeable charges in the interlayer space. This charge density of Opalinus Clay original (< 2 µm) shows in this sample a maximal frequency-% of charge density at 0.35 per $(OH)_2$ O_{10} (fig. 3.29). This interval of interlayer charge density caused by exchangeable cations from 0.15 - 0.51 per $(OH)_2$ O_{10} represents mentioned two groups of diVS-ml.

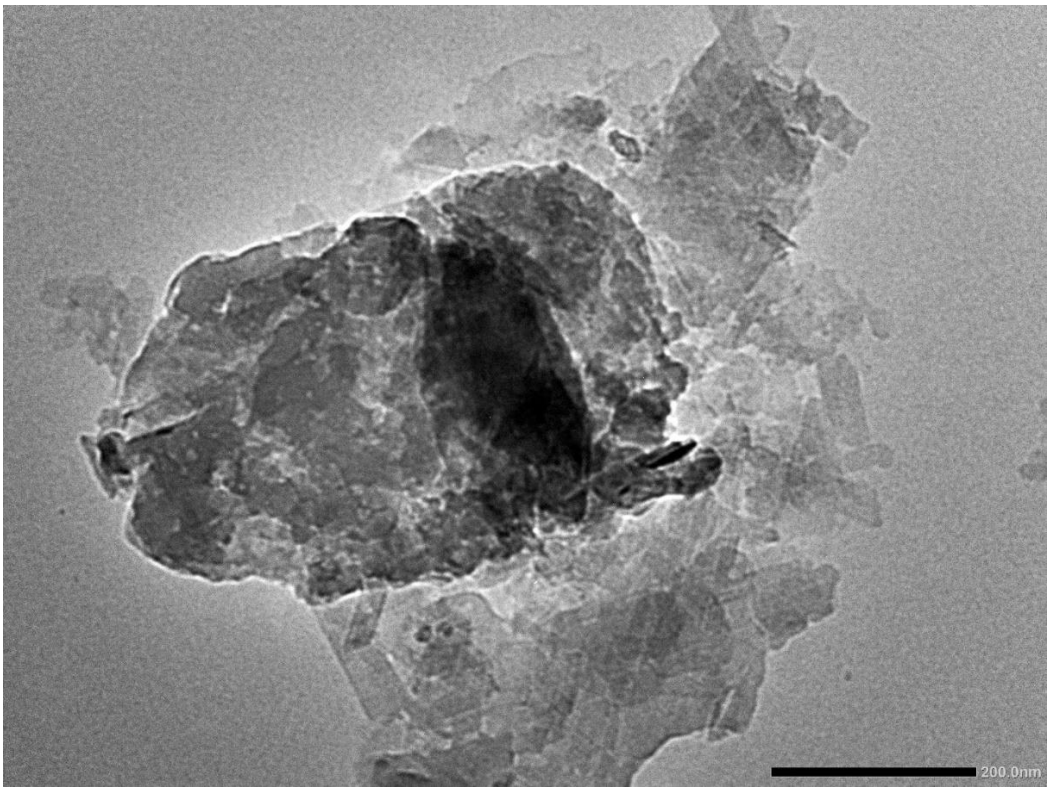

JEM-2100_MAG_X50k_Opalinus-40um-16.9_015.bmp
Magnification: 50k

former idiomorphic platy muscovite weathered into high charged dioctahedral vermiculite-smectite mixed layer phases with K-deficit (%S ~10%, %I ~ 90%)

Fig. 3.30b. *Morphology of particles (TEM-micrographs)*

Result of Clustering

The TEM-EDX-data offers a good agreement with the result of Sybilla-processing of XRD-traces from oriented specimen (tab. 3.9) considering traces of beidellite as further smectite component.

ISS R0: The X-ray diffraction pattern of the ethylene-glycol saturated oriented specimen shows a limited expandability to 1.46 nm. This result of XRD-pattern processing let expect a maximum of particles for %S ~ 50% by TEM-EDX-measurements, but the maximum of particles measured by TEM-EDX is to find at %S = 31%. Using a model for beidellite-montmorillonite-illite-mixed layer phases (BMI-ml) with 3.50, 4.00 and 3.20 as tetrahedral Si-value per $(OH)_2$ O_{10} the calculation of member ratios offers a solution for 10%-layer probability for %B and 40% for %S, if %I is given with 50% [see Cluster2 in (tab. 3.9)].

IS R0 (1): The Sybilla-procedure of XRD-traces (oriented mounts) has shown an occurrence of an illite-smectite mixed layer phase with a smectite layers probability of %S = 11%. This result of XRD-pattern processing is in good agreement with founded maximum of particles for %S ~ 9% by TEM-EDX-measurements (tab. 3.9).

The Sybilla-processing of XRD-traces (oriented mounts) also supports low amount of kaolinite and kaolinite-smectite mixed layer phases in fine fraction of sample.

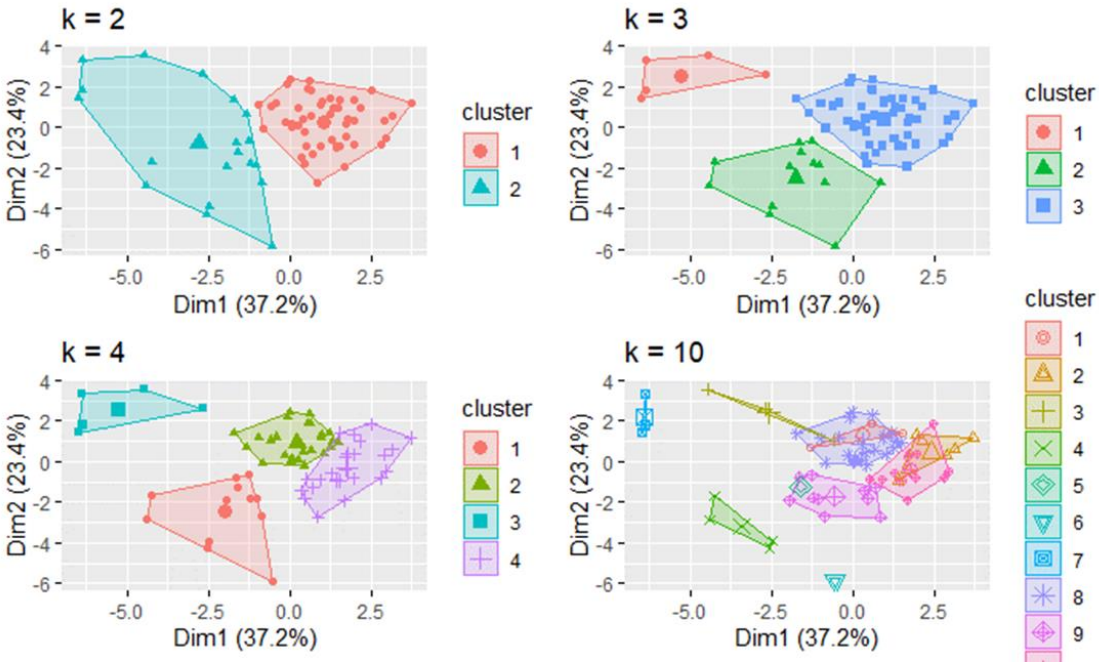

Fig. 3.31. *Clustering of all measured particles for clusters k = 2, k = 3, k = 4 and k = 10 (source for R-coding: https://uc-r.github.io/kmeans_clustering)*

The optimum of TEM-EDX-data-clusters, presented in fig. 3.31, was calculated with k = 2.

Tab. 3.9a *Comparison of results from TEM-EDX- and XRD-measurements*

	Sybilla-results	**TEM-EDX-results**	**Notes**
	Illite	diVS-ml (illite)	*very high K-deficit, low XII-charge deficit, Fe(VI)-rich, low Mg(VI)*
Cluster1	IS R0(1) *(%S = 11%)*	diVS-ml *(%S = 9%)*	*high K-deficit, low XII-charge deficit, Al(VI)- & Fe(VI)-rich*
Cluster2	ISS R0 *(%S = 48%)*	beid. diVS-ml *BMI 10:40:50*	*K-deficit, no XII-charge deficit, Fe(VI)-rich*

Tab. 3.9b. *Mineral formulae based on TEM-EDX-data summarized following the result of clustering for k=2*

		Ca (XII)	Mg (XII)	Na (XII)	K (XII)	Cr3+ (VI)	Al (VI)	Fe3+ (VI)	Mg (VI)	Ti (VI)	Al (IV)	Si (IV)	XII	n_VI	%S
Cluster1	n = 20	0.11	0.12	0.01	0.28	0.00	1.42	0.45	0.10	0.03	0.71	3.29	0.74	2.0	9
Cluster2	n = 50	0.08	0.04	0.00	0.44	0.00	1.39	0.41	0.20	0.00	0.47	3.53	0.68	2.0	31

Dioctahedral vermiculite-smectite mixed layer phase *(Cluster1)*

20 of 70 computed particles belong so to this assumed classification. The dioctahedral character of this group is proofed by X-ray diffraction. The position of the large (060)-interference of smectite is in the random oriented powder specimen at 1.497 Å.

Dioctahedral vermiculite-smectite mixed layer phase *(Cluster1)*

$$Ca_{0.11}\ Mg_{0.12}\ Na_{0.01}\ K_{0.28}\quad Al_{1.42}\ Fe^{3+}_{0.45}\ Mg_{0.10}\ Ti_{0.03}\ (OH)_2\quad Si_{3.29}\ Al_{0.71}\ O_{10}$$

Charge: XII = 0.74 VI = 5.97 IV = 15.29 **Σ = 22.00**
Measured particles by TEM-EDX: 20
Probability of smectite layers (%S): 9%
Probability of illite layers (%I): 91%
Result of clustering: Cluster1 (tab 3.9)

A comparison of octahedral Mg vs. tetrahedral Si doesn't indicate any differentiation for octahedral Mg in comparison to Cluster2 based on TEM-EDX-data (fig. 2.28b). Particles of Cluster1 contain commonly Mg(VI) < 0.25 per $(OH)_2$ O_{10} in octahedral layer. Also, a separation on low and high K in relation to Si is not to identify between Cluster1 and Cluster2 (fig. 28c). Phases of Cluster1 are mostly characterized by K < 0.45 per $(OH)_2$ O_{10}.

The mineral formulae, summarized in classes of %S, draws for the maximum an Al- & Fe-rich diVS-ml with a low Mg(VI) as well as low amount of K in the interlayer space (tab 3.10).

Tab. 3.10. *Computed averaged mineral formulae of diVS-ml phases in the different smectite layers probability (%S)-classes*

diVS-ml	*particles (abs)*	**Ca (XII)**	**Mg (XII)**	**Na (XII)**	**K (XII)**	**Cr3+ (VI)**	**Al (VI)**	**Fe3+ (VI)**	**Mg (VI)**	**Ti (VI)**	**Al (IV)**	**Si (IV)**	**XII**	**n_VI**	**%S**
%S >95%	n = 0														
%S 95-85%	n = 0														
%S 85-75%	n = 0														
%S 75-65%	n = 0														
%S 65-55%	n = 0														
%S 55-45%	n = 0														
%S 45-35%	n = 0														
%S 35-25%	n = 0														
%S 25-15%	n = 6	0.09	0.09	0.01	0.35	0.00	1.49	0.40	0.11	0.00	0.61	3.39	0.72	2.0	17
%S <15%	**n = 14**	**0.13**	**0.13**	**0.01**	**0.25**	**0.00**	**1.39**	**0.48**	**0.09**	**0.04**	**0.76**	**3.24**	**0.76**	**2.0**	**6**

Dioctahedral vermiculite-smectite mixed layer phase *(beid. diVS-ml, Cluster2)*

$$Ca_{0.08}\ Mg_{0.04}\ Na_{0.00}\ K_{0.44}\quad Al_{1.39}\ Fe^{3+}_{0.41}\ Mg_{0.20}\ Ti_{0.00}\ (OH)_2\quad Si_{3.53}\ Al_{0.47}\ O_{10}$$

Charge: XII = 0.68 VI = 5.79 IV = 15.53 **Σ = 22.00**
Probability of smectite layers (%S): 50%
Probability of illite layers (%I): 50%
Measured particles by TEM-EDX: 50
Result of clustering: Cluster2 (tab. 3.9)

A comparison of octahedral Mg vs. tetrahedral Si doesn't indicate any differentiation for octahedral Mg in comparison to Cluster1 based on TEM-EDX-data (fig. 3.28b). Particles of Cluster2 contain commonly Mg(VI) > 0.1 per $(OH)_2$ O_{10} in octahedral layer.

The mineral formulae, summarized in classes of %S, draws for the maximum an Al- & Fe-rich diVS-ml as well as reduced amount of K in the interlayer space (tab 3.11).

Tab. 3.11. *Computed averaged mineral formulae of diVS-ml phases in the different smectite layers probability (%S)-classes*

beid. diVS-ml *particles (abs)*	**Ca (XII)**	**Mg (XII)**	**Na (XII)**	**K (XII)**	**Cr3+ (VI)**	**Al (VI)**	**Fe3+ (VI)**	**Mg (VI)**	**Ti (VI)**	**Al (IV)**	**Si (IV)**	**XII**	**n_VI**	**%S**
%S >95% n = 0														
%S 95-85% n = 0														
%S 85-75% n = 0														
%S 75-65% n = 0														
%S 65-55% n = 0														
%S 55-45% n = 5	0.10	0.02	0.00	0.35	0.00	1.35	0.41	0.23	0.00	0.32	3.68	0.58	2.0	51
%S 45-35% n = 11	0.07	0.04	0.01	0.41	0.00	1.39	0.40	0.20	0.00	0.41	3.59	0.64	2.0	39
%S 35-25% n = 20	**0.08**	**0.04**	**0.01**	**0.44**	**0.00**	**1.44**	**0.37**	**0.19**	**0.00**	**0.49**	**3.51**	**0.68**	**2.0**	**30**
%S 25-15% n = 14	0.08	0.05	0.00	0.50	0.00	1.32	0.47	0.20	0.00	0.56	3.44	0.76	2.0	22
%S <15% n = 0														

Kaolinite-montmorillonite mixed layer phases

The Excel-based procedure (Hoang-Minh et al., 2019) to identify possible clay mineral groups using the TEM-EDX-measurements also includes algorithms to classify kaolinite and kaolinite-montmorillonite mixed layer phases. These algorithms couldn't compute no such phases basing on the measured TEM-EDX-data. Such particles have shown small hexagonal plates typically for kaolinite-bearing phases.

Estimation of Specific Dissolution Potential *(in according to Nguyen-Thanh et al., 2014)*

Previous investigations have shown (summarized in Nguyen-Thanh et al., 2014), each bentonite or clay have a specific dissolution potential expressed as loss of smectite layer. The expected specific behaviour of smectite layers is classified using the mineral formula as result of TEM-EDX-measurements. The authors developed different experimental overhead rotation setups to determine the maximal possible loss of smectite layers under pre-defined conditions. These different experimental settings should represent different strengths of acting forces in mineralogical alteration of original smectite (with water as low energy-level). The previous results with a large series of bentonites and clays allow to predict the expected rate of alteration of smectite layers distinguishing slow-reacting smectite layers (= sleepers), moderate-reacting smectite layers and fast-reacting smectite layers (= sprinters). The limits between these classes are postulated only: sleepers are smectites with loss of smectite layers lower than Δ%S = 5% and are a sprinter with loss of smectite layers larger than Δ%S = 20%. Negative values for Δ%S mirroring a 'illitization'-like process and positive values represent a smectitization potential.

The modelled values for Opalinus Clay (fig. 3.32) let expect mainly a slow-reacting smectite with a change from the original %S-value = 24% to 23% for the run products (Δ%S = -1%). Otherwise under strong conditions (e.g. higher temperature, high ionic strength, high saline solution), the modelling let assume for Opalinus Clay a very fast and nearby complete loss of smectite layers (Δ%S = -103%).

The type of cations in the interlayer space (here type B with Ca + Mg) and the Fe-rich composition of octahedral layer are the driving forces for these estimations.

Few aspects could influence the expected behaviour for Opalinus Clay:

1. The occurrence of pyrite let expect a higher degree of dissolution and so a higher loss of smectite layers than modelled.
2. Mixed layer phases offer a Si-buffer. Dissolved Si can again be precipitated in the alteration process as new-precipitated smectite layer. The key parameter is the grade of migration of dissolved Si far from the reaction site during the reaction. A fast transport of dissolved Si away from the reaction site is causing an 'illitization' and a slow transport away from the reaction site is offering partially a smectitization.

Finally, only further experiments with the selected clay can validate these estimations.

		Specific Dissolution Potential (*)			
Opalinus	**$\%S_{initial}$**	**H2O 20 rpm**	**H2O 60 rpm**	**NaCl 20 rpm**	**NaCl 60 rpm**
Interlayer Type (*)		Ca+Mg	Ca+Mg	Ca+Mg	Na
calculated Δ%S		1 ± 2	1 ± 2	1 ± 3	-103 ± 3
measured $\%S_{initial}$	24				
reaction type					
by modelling*		*sleeper*	*sleeper*	*sleeper*	*sprinter*

Description: *Overhead-rotation systems like H2O 20 rpm serve as indicator for rate of alteration of selected bentonite. Low grade reduction of smectitic layers (Δ%S) indicate a slow reaction of smectite phases (so-called sleeper). An opposite behaviour is called as sprinter*

Fig 3.32. *Specific Dissolution Potential of Opalinus Clay, < 2 µm (* in according to Nguyen-Thanh et al., 2014)*

3.7.3 Friedland clay

The fraction < 2 µm of Friedland Clay N10 sample is mainly composed by beidellite-montmorillonite-illite mixed layer phases (BMI-ml) and beidellitic dioctahedral vermiculite-smectite mixed layer phases (beid. diVS-ml). Furthermore, kaolinite and kaolinite-smectite-ml phases (with computed KSV =

60:25:15), chlorite-smectite-vermiculite mixed layer phases, Si-surplus particles (Si, e.g. quartz) and rutile were identified in traces in this sample (fig. 3.33).

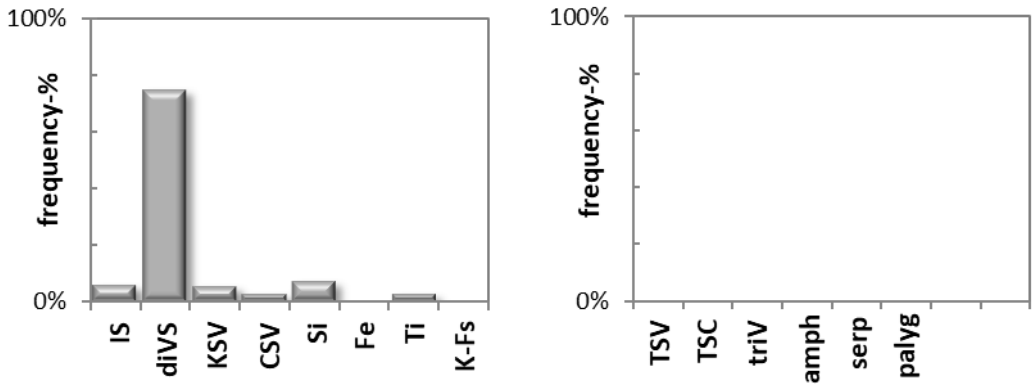

Fig. 3.33. *Distribution of mineral groups in fraction < 2 µm (in frequency-%)*

Legend: ***IS*** *– illite-smectite-mixed layer series in sense of Środon et al. (1992), diVS – dioctahedral vermiculite-smectite illite-smectite-mixed layer series (= charge- and/or K-deficit),* ***KSV*** *– kaolinite-smectite-dioctahedral vermiculite-mixed layer series,* ***CSV*** *– chlorite-saponite-trioctahedral vermiculite-mixed layer series,* ***Si*** *– quartz or particles with Si-surplus,* ***Fe*** *– Fe-oxide or Fe-oxyhydroxide,* ***Ti*** *– Ti-bearing phases (e.g. rutile, anatase),* ***K-Fs*** *– K-feldspar*

The measured and computed particles have shown a calculated CEC-value of 32 meq / 100 g located at surface and in the interlayer space.

	frequency-% *(n = 152 measured particles)*
BMI-ml	53%
beid. diVS-ml	28%
Kaolinite & KSV-ml	5%
CSV-ml	3%
Si-surplus	7%
Ti-phases	3%
Unknown	1%

All measured dioctahedral 2:1 clay mineral phases summarized result following mineral formula computed from TEM-EDX-measurement of 123 individual particles:

$$Ca^{2+}_{0.02}\ Mg^{2+}_{0.09}\ Na^{+}_{0.01}\ K^{+}_{0.35}\quad Al^{3+}_{1.36}\ Fe^{3+}_{0.52}\ Mg^{2+}_{0.10}\ Ti^{4+}_{0.02}\ (OH)_2\quad Si^{4+}_{3.49}\ Al^{3+}_{0.51}\ O_{10}$$

SDOM *± 0.00 ± 0.00 ± 0.00 ± 0.01 ± 0.02 ± 0.01 ± 0.01 ± 0.00 ± 0.01 ± 0.01*

Legend: SDOM - standard deviation of the mean (= the standard deviation divided by the square root of the number of samples)

Table 3.12. *Summarized chemical composition*

SiO_2	TiO_2	Al_2O_3	Fe_2O_3	MnO	MgO	CaO	Na_2O	K_2O	P_2O_5	Σ	
59.4%	0.3%	28.1%	5.9%		2.5%	0.3%	0.1%	3.3%	0.1%	1.00	measured particles of original Friedland Clay

The interlayer charge is calculated as 0.58 per $(OH)_2\ O_{10}$ and the octahedral charge as 5.93 per $(OH)_2\ O_{10}$. The particles are characterized by a high octahedral Fe-amount.

The summarized chemical composition of all 123 computed particles is listed (tab. 3.12).

Friedland Clay, Siedlungsscholle, East-field is characterized by two morphological groups: (i) large (≤ 1 µm) xenomorph platy crystals and (ii) aggregates, partially with folds, formed by small (≤ 100 nm) xenomorphous plates (fig. 3.34). Aggregates formed by small (≤ 100 nm) xenomorphous plates dominate the shapes of particles in the micrographs (fig. 3.34).

The distribution of %S-probability of all measured clay mineral phases (fig. 3.35a) also indicates the occurrence of two groups: (i) BMI- and beidellitic diVS-ml phases incl. illite with K-deficiency as well as (ii) montmorillonite (rare).

The numerous measured particles by TEM-EDX allow a visualization of distribution of interlayer charges. Considering the TEM-EDX-determined cations Ca^{++}, Mg^{++} and Na^{+} and then computed their ratio as interlayer cations in the mineral formula, Ca^{++}, Mg^{++} and Na^{+} offer to characterize the degree of exchangeable charges in the interlayer space. This charge density of Friedland Clay (< 2 µm) shows in this sample a broad interval with two maximal frequency-% of charge density at 0.15 and 0.23 per $(OH)_2$ O_{10} (fig. 3.37). This broad interval of interlayer charge density caused by exchangeable cations from 0.10 - 0.43 per $(OH)_2$ O_{10} represents mainly IS-ml (lowest peak at 0.15 per $(OH)_2$ O_{10}) and the diVS-ml phases with the other higher peak at 0.23 per $(OH)_2$ O_{10}.

The TEM-EDX-data offers a good agreement with the result of Sybilla-processing of XRD-traces from oriented specimen, but only under consideration of the option beidellite (tab. 3.13).

IS R0 (1): The X-ray diffraction pattern of the ethylene-glycol saturated oriented specimen shows a nearby full expandability to 1.67 nm and a difference of 5.68°2θ between 2. and 3. order of smectite interferences. This distance is typically for a probability of smectite layers (%S) of 80% (Moore & Reynolds, 1989). This result of XRD-processing let expect a maximum of particles for %S ~ 80% by TEM-EDX-measurements, but the maximum of particles measured by TEM-EDX is to find at %S=40% (fig. 3.35a). Using a model for beidellite-montmorillonite-illite-mixed layer phases (BMI-ml) with 3.50, 4.00 and 3.20 as tetrahedral Si-value per $(OH)_2$ O_{10} the calculation of member ratios offers a solution for 60%-layer probability for %B and 20% for %S, if %I is given with 20% (see Cluster2 in tab. 3.13).

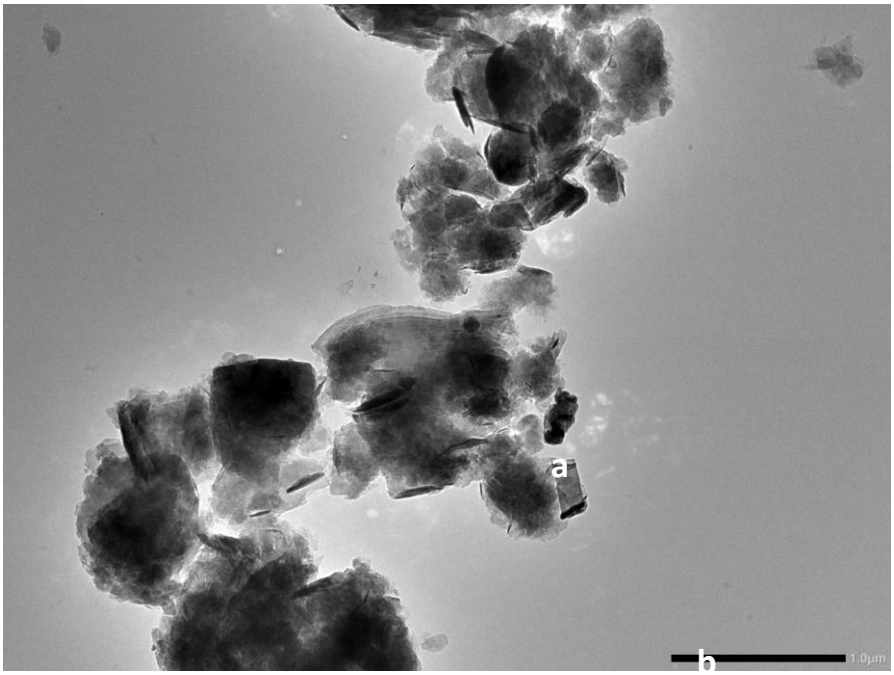

JEM-2100_MAG_X10k_007_AISZ-5ML.bmp

Magnification: 10k

(a) large (≤ 1 µm) xenomorph platy crystals;
(b) aggregates, partially with folds, formed by small (≤ 100 nm) xenomorph plates

Fig. 3.34. *Morphology of particles (TEM-micrographs)*

Distribution of smectite layers probability (%S)

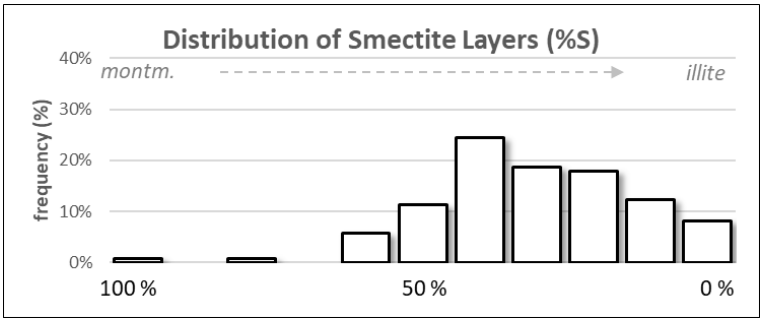

Description: *The distribution of %S-probability indicates the occurrence of two groups: (i) BMI- and beidellitic diVS-ml phases incl. illite with K-deficiency as well as (ii) montmorillonite (rare).*

Fig. 3.35a. *Distribution of smectite layers probability (%S)*

Differentiation by relation "Octahedral Mg vs. tetrahedral Si"?

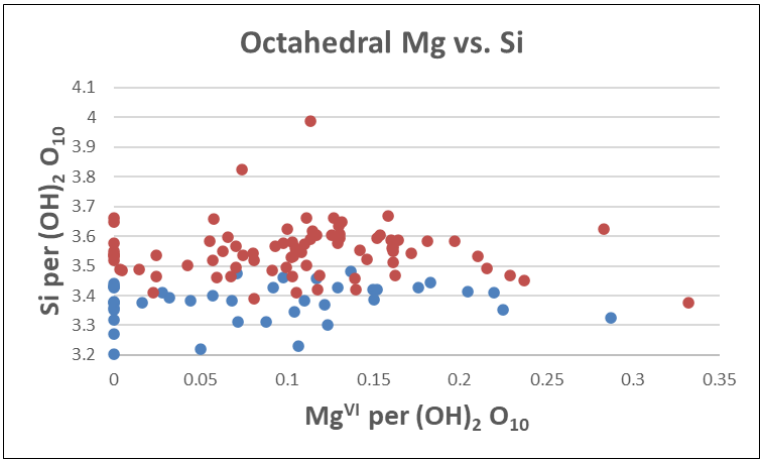

Description: *This diagram doesn't indicate any trend of Mg in relation to tetrahedral Si, also not between BMI-ml phases of cluster2 (red dots) and beidellitic diVS-ml phases of cluster1 (blue dots).*

Fig. 3.35b. *Distribution of octahedral Mg vs. tetrahedral Si [all per $(OH)_2$ O_{10}]*

Distribution of K in relation to tetrahedral Si

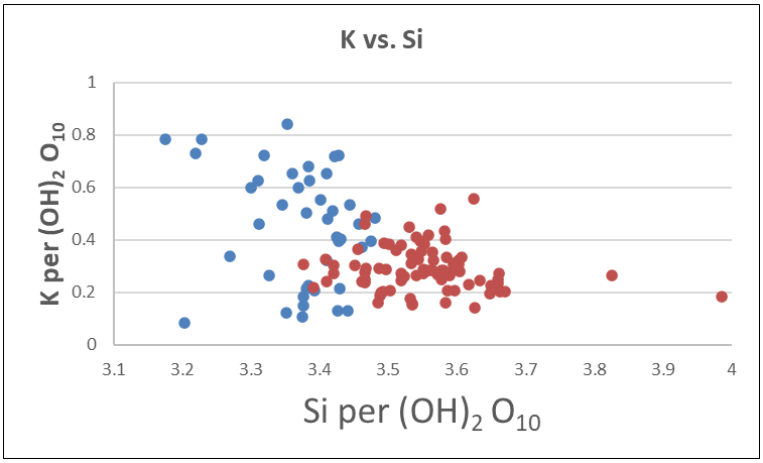

Description: *This diagram visualizes a trend to higher K-values in beidellitic diVS-ml / cluster1 (blue dots) than in beidellite-montmorillonite-illite-ml phases / cluster2 (red dots).*

Fig. 3.36. *Distribution of K in interlayer space vs. tetrahedral Si [all per $(OH)_2$ O_{10}]*

Distribution of charges (exchangeable from interlayer space)

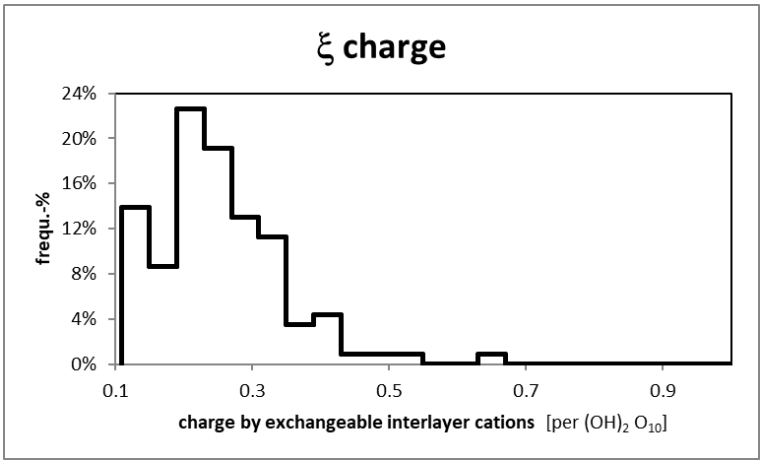

This diagram visualizes the distribution of exchangeable charges in the interlayer space (Ca, Mg, Na) determined and computed by TEM-EDX-data.

Description: *Bimodal distribution of charge density with (i) first maximal frequency-% at 0.15 per $(OH)_2$ O_{10} (mica) as well as (ii) at 0.23 per $(OH)_2$ O_{10} as second maximal frequency-%*

Fig. 3.37. *Distribution of charges*

Result of Clustering

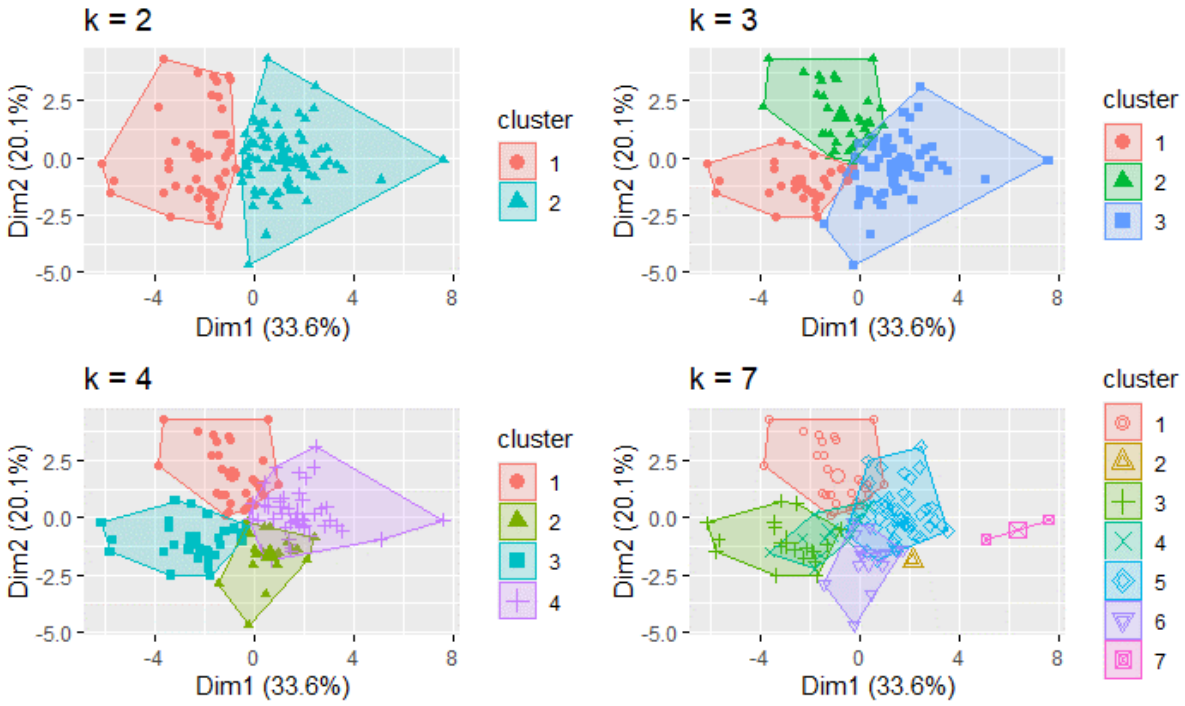

Fig. 3.38. *Clustering of all measured particles for clusters k = 2, k = 3, k = 4 and k = 7 (source for R-coding: https://uc-r.github.io/kmeans_clustering)*

The optimum of TEM-EDX-data-clusters (fig. 3.38) was calculated with k = 2 (here applied) and k=7.

		Ca (XII)	Mg (XII)	Na (XII)	K (XII)	Cr3+ (VI)	Al (VI)	Fe3+ (VI)	Mg (VI)	Ti (VI)	Al (IV)	Si (IV)	XII	n_VI	%S
Cluster1	n = 42	0.01	0.08	0.01	0.45	0.00	1.50	0.40	0.08	0.03	0.63	3.37	0.65	2.0	15
Cluster2	n = 81	0.02	0.10	0.00	0.29	0.00	1.30	0.58	0.11	0.02	0.45	3.55	0.54	2.0	34

Tab. 3.13a. *Mineral formulae based on TEM-EDX-data summarized following the result of clustering for k=2*

Tab. 3.13b. *Comparison of results from TEM-EDX- and XRD-measurements*

	Sybilla-results	TEM-EDX-results	Notes
	Illite	beid. diVS-ml (illite)	*high K-deficit, low XII-charge deficit, Al(VI)-rich, Fe(VI)-rich*
Cluster1	IS R0(2) *(%S = 25%)*	beid. diVS-ml, without illite *(BMI 05:15:75)*	*high K-deficit, charge deficit, Al(VI)-rich, Fe(VI)-rich*

Cluster2	IS R0(1) *(%S = 82%)*	BMI ~60:20:20	*XRD: Montmorillonite and beidellite is only to distinguish by Green-Kelly-test (not available here).*
	Kaolinite + KS GL R0		*in traces only*

IS R0 (2): The Sybilla-procedure of XRD-traces (oriented mounts) has shown an occurrence of a second illite-smectite mixed layer phase with a smectite layers probability of %S = 25%. This situation is to find also by TEM-EDX ($\%S_{TEM}$ = 15%). Using a model for beidellite-montmorillonite-illite-mixed layer phases (BMI-ml) with 3.50, 4.00 and 3.20 as tetrahedral Si-value per $(OH)_2\ O_{10}$ the calculation of member ratios offers a solution for 5%-layer probability for %B and 20% for %S, if %I is given with 75% (see Cluster2 in tab. 3.13a,b)]. That means, few parts of smectite layers are formed as beidellite in these phases. These phases represent remarkable K-amounts and slight charge deficit and Al- & Fe-rich, beidellitic dioctahedral vermiculite-smectite mixed layer phase (beid. diVS-ml) (tab. 3.13a,b).

The Sybilla-processing of XRD-traces (oriented mounts) also supports the existence of kaolinite and kaolinite-smectite mixed layer phases in fine fraction of sample. The mineral formula was to compute for only 3 particles of KSV-ml phases (average: %K 60%, %S 26%, %V 14%).

Specifics to the identified clay mineral groups

Beidellite-montmorillonite-illite-ml (BMI-ml 60:20:20) *(Cluster2)*

81 of 123 computed particles belong so to this assumed classification. The dioctahedral character of this group is proofed by X-ray diffraction. The position of the large (060)-interference of smectite is in the random oriented powder specimen at 1.497 Å.

Montmorillonite and beidellite have the same behaviour concerning the expandability and they are only to distinguish by XRD using Li by means of Greene-Kelly test (Greene-Kelly 1952, 1953). So, combination of XRD- and TEM-results (full expandability by XRD and Si ~ 3.55 by TEM-EDX) led conclude the occurrence of beidellite (fig. 3.39).

Beidellite-montmorillonite-illite-ml *(BMI 60:20:20)*

$$Ca_{0.02}\ Mg_{0.10}\ Na_{0.00}\ K_{0.29}\quad Al_{1.30}\ Fe^{3+}_{0.58}\ Mg_{0.11}\ Ti_{0.02}\ (OH)_2\quad Si_{3.55}\ Al_{0.45}\ O_{10}$$

Charge: XII = 0.54 VI = 5.91 IV = 15.45 **Σ = 22.00**
Measured particles by TEM-EDX: 81
Result of clustering: Cluster2 (tab. 3.13)

In this sample, beidellite is characterized by a low octahedral Mg-amount (because of high ratio of octahedral, 3-valent cations). A comparison of octahedral Mg vs. tetrahedral Si doesn't indicate any differentiation for octahedral Mg based on TEM-EDX-data [fig. 3.35b]. Particles of Cluster2 contain full interval of Mg(VI) from 0.0 to 0.3 per $(OH)_2\ O_{10}$ in octahedral layer. Particles of Cluster2 show also a trend to lower K in interlayer space than particles of Cluster1 (fig. 3.36),

Using the results of TEM-EDX data processing (see cluster2 in tab. 3.13), the maximum of frequency-% is to find for particles at 3.5-3.6e phuc (fig. 3.39). The mineral formulae, summarized in classes of %S, draws for the maximum an Fe-rich BMI-ml with low Mg(VI), but remarkable amount of K in the interlayer space (tab. 3.14).

Distribution of beidellite-montmorillonite-illite-ml phases (BMI-ml)

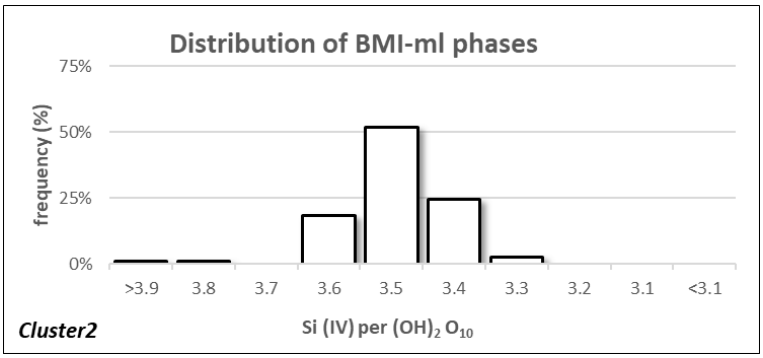

Description: *The distribution of BMI-ml phases (cluster2) draws a maximum of frequency (%) at tetrahedral Si-value between 3.5 – 3.6 e phuc.*

Fig. 3.39. *Distribution of smectite layer probability (%S) in diVS-ml*

Tab. 3.14. *Computed averaged mineral formulae of phases in the different Si(IV)-classes*

BMI 60:20:20?	*particles (abs)*	Ca (XII)	Mg (XII)	Na (XII)	K (XII)	Cr3+ (VI)	Al (VI)	Fe3+ (VI)	Mg (VI)	Ti (VI)	Al (IV)	Si (IV)	XII	n_VI	%S
Si >3.9	n = 1	0.03	0.06	0.00	0.18	0.00	1.32	0.48	0.11	0.00	0.01	3.99	0.37	1.9	106
Si 3.9-3.8	n = 1	0.02	0.10	0.00	0.27	0.00	1.32	0.52	0.07	0.00	0.17	3.83	0.52	1.9	75
Si 3.8-3.7	n = 0														
Si 3.7-3.6	n = 15	0.02	0.08	0.00	0.27	0.00	1.28	0.60	0.12	0.00	0.36	3.64	0.47	2.0	45
Si 3.6-3.5	**n = 42**	**0.02**	**0.08**	**0.01**	**0.31**	**0.00**	**1.32**	**0.57**	**0.10**	**0.02**	**0.45**	**3.55**	**0.52**	**2.0**	**34**
Si 3.5-3.4	n = 20	0.03	0.13	0.00	0.29	0.00	1.28	0.60	0.10	0.02	0.54	3.46	0.62	2.0	24
Si 3.4-3.3	n = 2	0.03	0.20	0.00	0.26	0.00	1.00	0.69	0.21	0.10	0.62	3.38	0.72	2.0	16
Si 3.3-3.2	n = 0														
Si 3.2-3.1	n = 0														
Si <3.1	n = 0														

Beidellitic dioctahedral vermiculite-smectite mixed layer phase (Cluster1)

(beid. diVS-ml, %S = 25%, without illite)

$$Ca_{0.02}\ Mg_{0.09}\ Na_{0.01}\ K_{0.40}\ \ Al_{1.50}\ Fe^{3+}_{0.40}\ Mg_{0.08}\ Ti_{0.02}\ (OH)_2\ \ Si_{3.42}\ Al_{0.58}\ O_{10}$$

Charge: XII = 0.62 VI = 5.96 IV = 15.42 **Σ = 22.00**

Probability of smectite layers (%S): 25%

Probability of illite layers (%I): 75%

Measured particles by TEM-EDX: 27

Illite as part of beid. diVS-ml series

$$Ca_{0.01}\ Mg_{0.07}\ Na_{0.01}\ K_{0.54}\ \ Al_{1.49}\ Fe^{3+}_{0.39}\ Mg_{0.08}\ Ti_{0.05}\ (OH)_2\ \ Si_{3.30}\ Al_{0.70}\ O_{10}$$

Charge: XII = 0.72 VI = 5.99 IV = 15.30 **Σ = 22.00**

Probability of smectite layers (%S): 9%

Probability of illite layers (%I): 91%

Measured particles by TEM-EDX: 15

Kaolinite-montmorillonite mixed layer phases

The Excel-based procedure (Hoang-Minh et al., 2019) to identify possible clay mineral groups using the TEM-EDX-measurements also includes algorithms to classify kaolinite and kaolinite-montmorillonite mixed layer phases. These algorithms could identify such phases basing on the measured TEM-EDX-data for only 3 particles. Such particles have shown small hexagonal plates typically for kaolinite-bearing phases.

References

Bossart, P.J., 2008, Mont terri rock laboratory project: programme 1996 to 2007 and results. Federal Office of Topography Swisstopo.

Bradley, W.F. and R.E. Grim, 1951, High temperature thermal effects of clay and related materials. American Mineralogist, 36(3-4): p. 182-201.

Breidung, K. P., 2002, Verwahrung von Kali- und Steinsalzbergwerken einschließlich langzeitsicherer Schachtabdichtungen. Kali und Salz, 2, p. 28–39.

Carlson, L., 2004. Bentonite Mineralogy. Part 1: Methods of investigation – a Literature review. Part 2: Mineralogical research of selected bentonites. Posiva Oy, Olkiluoto. p. 78.

Čičel, B., et al.,1992. Mineralogical composition and distribution of Si, Al, Fe, Mg and Cain the fine fractions of some Czech and Slovak bentonite. Geol. Carpathica, Ser. Clays, 43(1): p. 3-7.

Crâciun, C., 1984. Influence of the Fe3+ –for – Al3+ Octahedral Substitutions on the IR Spectra of Montmorillonite Minerals. Spectroscopy Letters, 17(10): p. 579-590.

Decarreau, A., O. Grauby, and S. Petit, 1992, The actual distribution of octahedral cations in 2:1 clay minerals: Results from clay synthesis. Applied Clay Science, 7(1): p. 147-167.

Döbelin, N., Kleeberg, R. (2015). Journal of Applied Crystallography 48, 1573-1580. DOI: 10.1107/S1600576715014685

Farmer, V.t. and J. Russell, 1964, The infra-red spectra of layer silicates. Spectrochimica acta, 20(7): p. 1149-1173.

Gates, W.P., 2005. Infrared Spectroscopy and the Chemistry of Dioctahedral Smectites, in The Application of Vibrational Spectroscopy to Clay Minerals and Layered Double Hydroxides, J.T. Kloprogge, Editor. 2005, Clay Minerals Society. p. 0.

Gaucher, E., A. Fernández, and H.N. Waber, 2003. Rock and Mineral Characterisation of the Opalinus Clay Formation. p. 281-303.

Greene-Kelly, R., 1955. Dehydration of the montmorillonite minerals. Mineralogical magazine and journal of the Mineralogical Society, 30(228): p. 604-615.

Hendershot, W.H. and M. Duquette, 1986. A Simple Barium Chloride Method for Determining Cation Exchange Capacity and Exchangeable Cations. Soil Science Society of America Journal, 50(3): p. 605-608.

Hoang-Minh, T., 2006. Characterization of clays and clay minerals in industrial application: substitution non-natural additives by clays in UV protection. Dissertation, Universtiy of Greifswald.

Karnland, O., S. Olsson, and U. Nilsson, 2006. Mineralogy and sealing properties of various bentonites and smectite-rich clay materials. Svensk Kärnbränslehantering AB (SKB). p. 70.

Kasbohm, J., 2003. Zur Langzeitstabilität von Na-Montmorillonit in hochsalinaren Lösungen. Habilitationsschrift, Universität Greifswald.

Laurich, B., Fourrière, A., Gräsle, W., 2019. LT-A Experiment: How fracture wetting leads to closure. Mont Terri Project, Technical Note 2020-29, October 2019.

Madejová, J., et al., 1996. Preparation and infrared spectroscopic characterization of reduced-charge montmorillonite with various Li contents. Clay Minerals, 31(2): p. 233-241.

Matschiavelli N, Kluge S, Podlech C, Standhaft D, Grathoff G, Ikeda-Ohno A, Warr LN, Chukharkina A, Arnold T, Cherkouk A. (2019). The Year-Long Development of Microorganisms in Uncompacted Bavarian Bentonite Slurries at 30 and 60 °C. Environ Sci Technol. 53(17),10514-10524. DOI: 10.1021/acs.est.9b02670.

Meleshyn A, Hinze M, Middelhoff M, Friedenberg L, Jantschik K, 2024, Thermische Integrität von Ton und Tonsteinen - Experiment und gekoppelte THMC-Simulationen (THMC-Sim): Gesellschaft für Anlagen- und Reaktorsicherheit, Braunschweig

Nagra, 2002, Project Opalinus Clay: Synthesis of the Geological Research Results – Feasibility of Disposing Spent Fuel Elements, Vitrified High-Level Radioactive as Well as Long-Lived Intermediate-Level Waste. National Cooperative for the Disposal of Radioactive Waste (Nagra): Wettingen, Switzerland.

Pearson, F., et al., 2003. Mont Terri Project - Geochemistry of Water in the Opalinus Clay Formation at the Mont Terri Rock Laboratory.

Sitz, P., Gruner, M., Rumphorst, K., 2003. Bentonitdichtelemente für langzeitsichere Schachtverschlüsse im Salinar. Kali und Salz 3, p. 6-13.

Taut, T., Kleeberg, R., Bergmann, J., 1998. The new Seifert Rietveld program BGMN and its application to quantitative phase analysis. Mater. Struct. 5, 57–64.

Ufer, K., et al., 2008. Quantitative phase analysis of bentonites by the rietveld method. Clays and Clay Minerals, 56(2): p. 272-282.

Vantelon, D., et al., 2001. Fe, Mg and Al distribution in the octahedral sheet of montmorillonites. An infrared study in the OH- bending region. Clay Minerals, 36(3): p. 369-379.

Velde, B., 1983. Infrared OH-stretch bands in potassic micas, talcs and saponites; influence of electronic configuration and site of charge compensation. American Mineralogist, 68(11-12): p. 1169-1173.

Zandanel, A., et al., 2002. Impacts of Crystalline Host Rock on Repository Barrier Materials at 250 °C: Hydrothermal Co-Alteration of Wyoming Bentonite and Steel in the Presence of Grimsel Granodiorite. Minerals, 12, DOI: 10.3390/min12121556.

Zviagina, B.B., et al., 2004. Interpretation of infrared spectra of dioctahedral smectites in the region of OH-stretching vibrations. Clays and Clay Minerals, 52(4): p. 399-410.

Part II. REACTION PRODUCTS

Introduction

It is expected a phase-analytical characterization of clay mineral phases in treated B25 bentonite, Opalinus Clay and Friedland Clay by X-ray diffraction (XRD) of bulk samples as powder specimen and for fraction < 2 µm as oriented specimen, by thermogravimetry of bulk sample (TG) and by transmission electron microscopy (TEM) for fraction < 2 µm. The treatment itself was carried out by GRS gGmbH in Braunschweig. The sample bodies were percolated by adapted Opalinus solution under different temperatures (35°C, 60°C, 100°C, 125°C, 150°C) and time intervals.

Specifically, for B25 bentonite: After the experiment, mostly three samples were investigated from each sample body – material from top position, from central part and from the bottom. The flow direction during the percolation was from the bottom to the top of the clay specimens.

Methodology, results, and graphs of measurements are summarized in separated supplements for all samples. These four supplements also contain the description of each applied method.

About selected mineralogical terms used in this report

Smectite (in senso of international classification)

→ ***Smectite*** (approached in this report)
- → montmorillonite
- → beidellite
- → beidellite-montmorillonite intergrowth (BM)
- …

→ ***Mixed-layer phases*** (approached in this report)
- → illite-smectite interstratification (IS-ml)*
  - →beidellite-montmorillonite-illite interstratification (BMI-ml)
- → kaolinite-smectite-dioctahedral vermiculite interstratification (KSV-ml)
- ...

* *term „IS-ml": extended approach in senso of Środon et al., 1992*
- *→normal charged:*
  - *illite-smectite interstratification (IS-ml)*
- *→K- and/or charge deficit:*
  - *dioctahedral vermiculite-smectite interstratification (diVS-ml)*

The phase-analytical differential diagnostics of clay mineral matter, applied for this report, offer a more detailed view and discussion even to smectite-bearing intergrowths and interstratifications. The mineralogical terms applied in this report are presented and summarized here considering the framework of international classification for clay minerals.

Pure smectite minerals (e.g. montmorillonite, beidellite etc.) and smectite-bearing mixed-layer phases are summarized as members of term SMECTITE in senso of international classification of clay minerals. In result of investigation of B25 bentonite the connected occurrence of montmorillonite and beidellite was concluded. The distribution of these two smectite minerals in the measured particles is not clear: (i) vertically in *c*-axis as interstratification (= layer-by-layer) or (ii) horizontally in *ab*-axes more as intergrowth. In this report the term intergrowth is used so far only beidellite and montmorillonite which are members of measured particles.

Summary "Smectite behaviour"

Tab. I. *Overview about different smectite behaviour in all three sample-series*
(in direction of rising thermal load in experiments)

	B25 Bentonite	Friedland Clay	Opalinus Clay
Sum effect, mirrored by all dioctahedral particles (unclassified), measured by TEM			
tetrahedral Si	slight decreasing *(fig. 9)*	± constant *(at Si = 3.49 e phfu) (fig. 19)*	orig. vs treated: decreas. treatm.: ± constant *(at Si = 3.25 ± 0.05 e phfu) (fig. 26)*
Ca-smectite			
ratio in bulk sample	main phase *(tab. 1)*	minor phase, trace *(tab. 7)*	
smectite species	beidellite > montm. *((tab. 3))*	beidellite >> montm. *(tab. 9)*	
mass-% development	slight reduction *(from 35% to 25%) (fig. 2)*	± constant *(at 5% - 6%) (fig. 12)*	
%S-development	± constant *(at %S=70-100%) (tab. 3)*	± constant *(at %S=100%, available only ≤60°C) (tab. 9, fig. 14)*	
diVS-ml			
ratio in bulk sample	minor phase *(tab. 1)*	minor phase *(tab. 7)*	minor phase, trace *(tab. 13)*
smectite species	montm. >> beidellite *(tab. 4)*	montm. >> beidellite *(tab. 10)*	montm. >>> beidellite *(tab. 15)*
mass-% development	± stable *(variable 5% - 15%) (fig. 4)*	± stable *(variable 13%-16%) (fig. 12)*	%S=50%: destroyed %S=20%: no trend *(mass-% at 30% ±10%) (fig. 21)*
%S-development	reduction *(from 55% to 20%) (fig. 5)*	rising *(from 25% to 52%) (fig. 14)*	%S=50%: destroyed %S=20%: rising *(from 11% to 26%) (fig. 22)*
KS-ml			
ratio in bulk phase	minor phase *(tab. 1)*	minor phase *(tab. 7)*	minor phase *(tab. 13)*
smectite species	not to determine	not to determine	not to determine
mass-% development	rising *(< 2 µm: 25% → 45%) (fig. 7)*	± stable *(< 2 µm: variable at 10 %) (fig. 16)*	slight decreasing *(< 2 µm: 47% → 32%) (fig. 24)*
%S-development	rising *(< 2 µm: 45% → 70%) (fig. 8)*	± constant *(< 2 µm: ~50%) (fig. 17)*	± stable *(< 2 µm: at 40% ±8%) (fig. 25)*

Smectite is the main responsible mineralogical phase, which determines the swelling behaviour of clays and bentonites. In B25 bentonite and Friedland Clay, smectite is distributed in three different groups of smectite-bearing phases (Ca-smectite, diVS-ml, KS-ml), in Opalinus Clay only in two groups (diVS-ml, KS-ml). Each group has shown a specific behaviour during the experiments (tab. I).

The role played by the KS-ml phases shown is largely unclear. The analytical evidence is mostly only a result of the modelling of X-ray diffractograms (oriented specimen) and indirect evaluation of thermogravimetry in comparison to powder X-ray diffractometry.

In summary, in the experiments with increasing thermal load, sample B25 shows a slight 'illitization'. In contrast, the Friedland and Opalinus samples reveal largely stable, unchanged conditions.

1. Mineral matter in B25 bentonite

Tab. 1. *Mineral matter of B25 bentonite (bulk sample)*

Sample	Ca-Smectite	diVS-ml	Illite (1M)	Illite (2M1)	Kaolinite + KS-ml	Σ clay	Quartz	K-feldspar	Plagioclase	Anhydrite	Cerussite	Analcime	Diaspore	Rutile + Anatase	Calcite	Natrolite	Σ total
B25 original	32%	10%	15%	17%	14%	*86%*	10%	2%	2%								*100%*
35°C, 93.6h, OPA																	
No4_T	37%	6%	10%	10%	7%	70%	12%	2%	12%	<1%		1%		1%	2%		*101%*
No4_C	34%	4%	18%	10%	7%	73%	13%	2%	9%	1%		<1%		<1%	2%		*97%*
No4_B	35%	5%	10%	10%	12%	72%	14%	3%	7%	1%		<1%		<1%	1%		*100%*
35°C, 285h, OPA.0.7 MPa																	
No23	28%	15%	8%	11%	15%	77%	14%	3%	4%	1%		<1%		<1%	1%		*100%*
60°C, 454h, OPA																	
No5_T	28%	3%	9%	10%	9%	60%	26%	3%	9%	1%				1%	2%		*100%*
No5_C	35%	3%	10%	10%	11%	69%	16%	2%	7%	2%		<1%	2%	1%	2%		*98%*
No5_B	28%	5%	22%	8%	6%	68%	16%	2%	8%	2%		<1%		1%	*1%		*100%*
100°C, 110h, OPA																	
No0_T	25%	11%	10%	10%	11%	66%	13%	4%	11%	2%	<1%	<1%		1%	*2%		*99%*
No0_C	26%	9%	14%	7%	13%	69%	9%	3%	12%	2%		<1%	2%	<1%	*2%	<1%	*100%*
No0_B	24%	12%	14%	7%	24%	80%	11%	2%	2%	1%	<1%	<1%		1%	<1%	2%	*100%*
100°C, 35d, OPA																	
No2_T	24%	12%	11%	10%	12%	68%	9%	3%	13%	2%		1%	<1%	1%	*2%	<1%	*100%*
No2_C	24%	15%	14%	9%	12%	74%	11%	2%	7%	1%		<1%	<1%	1%	*1%	<1%	*96%*
No2_B	30%	10%	9%	13%	14%	74%	10%	1%	8%	1%		<1%		<1%	1%	2%	*100%*
125°C, 98.6h, OPA																	
No15	31%	6%	20%	7%	12%	76%	11%	2%	5%	1%		1%	<1%	<1%	2%	2%	*100%*
150°C, 4d, OPA																	
No3_T	26%	14%	9%	9%	12%	70%	9%	3%	11%	1%		1%		<1%	*2%	<1%	*99%*
No3_C	21%	14%	13%	6%	12%	65%	8%	5%	12%	2%		<1%		1%	3%	<1%	*98%*
No3_B	20%	17%	7%	9%	13%	66%	10%	4%	14%	1%		1%		1%	2%	<1%	*99%*

Legend: *Ca-Smectite – beidellite/montmorillonite-intergrowth; diVS-ml – IS-ml with K- and/or charge deficiency; * – including indications by TG for additional amount of amorphous calcium carbonate; standard deviation, absolute – see Supplement "XRD, powder"*

Smectite is mainly to find in B25 bentonite as beidellite-rich Ca-smectite and furthermore as mont-morillonite in illite-smectite mixed layer phases with K- and/or charge deficiency (diVS-ml) and in kaolinite-smectite mixed layer phases. Further minor phases are illite, kaolinite, quartz, and feldspar. Compaction of bentonite material and the percolation and heating processes during the experiments cause traces of zeolites (analcime, natrolite), sulfates (anhydrite), carbonates (calcite – crystalline and probably also as amorphous calcite carbonate; cerussite), rutile, anatase as well as hydroxides (diaspore) (tab. 1). Generally, limit of detection of this applied Rietveld method is about 2 %. The here mentioned phases (tab. 1) with such low amount show in the samples their main peak not covered by possible sub-peaks of other verified phases.

A comparison of XRD-results with mass loss data from thermogravimetry measurements indicates the occurrence of an additional amorph phase, especially for samples from experiments at 60°C and 100°C. In these samples, the additional mass loss is mainly to find in temperature interval higher than 650°C in TG-measurement. This situation let assume amorph calcium carbonate (ACC) with 1-2% in marked samples (tab. 1).

Tab. 2. *B25 bentonite (original) composition – own measurement in comparison with literature*

	B25 bentonite			
	own results	Ufer et al., 2008	Kaufhold et al., 2012	Matschiavelli et al., 2019
Ca-smectite	32%	43.2%	61%	55%
diVS-ml	10%			
Illite_1M	15%			
Illite_2M1	17%	16.6%	17%	15%
Chlorite				
Kaolinite	14%	21.9%	4%	12%
Σ clay	***86%***	***82%***	***82%***	***82%***
Quartz	10%	13.2%	13%	10%
Orthoclase	2%	1.7%	5%	
Albite	2%	3.5%		3%
Pyrite				
Calcite				1%
Siderite				
Dolomite				4%
Rutile				1%
Gypsum				
Σ total	***100%***	***100%***	***100%***	***100%***

calculated DTA/TG-signal basing on XRD-results

mass loss 300-650°C	*XRD_calc*	*XRD_calc*	*XRD_calc*	*XRD_calc*	*mass loss (%)*
smectite (beidellite)	0.72%	0.98%	1.38%	1.24%	4.52
diVS-ml	0.43%				4.55
kaolinite	1.89%	3.04%	0.56%	1.67%	13.90
illite 1M	0.64%				4.41
mass loss 650-1000°C					
smectite (montm.)	0.76%	1.02%	1.45%	1.30%	4.74
illite 2M1	0.74%	0.73%	0.75%	0.66%	4.41
calcite				0.44%	44.00
dolomite				1.96%	48.99
					measured by TG
mass loss 300-650°C (%)	3.69%	4.02%	1.93%	2.91%	***3.72%***
mass loss 650-1000°C (%)	1.49%	1.76%	2.20%	4.36%	***1.47%***
mass loss 300-1000°C (%)	**5.18%**	**5.78%**	**4.13%**	**7.28%**	**5.19%**

Legend: *Ca-smectite – 50:50 beidellite-montmorillonite intergrowth; mass loss (%) – theoretical mass loss (in %) in thermo-gravimetry for 100% of certain phase used as basis unit to calculate the XRD_calc values for each by XRD detected phase*

Validation of B25 bentonite composition

The measured composition of original and uncompacted B25 bentonite is in a good agreement (tab. 2) with already published data from literature (Ufer et al, 2008; Kaufhold et al., 2012; Matschiavelli et al., 2019). Differences between here presented own measurements and literature references are to recognize in the amount of kaolinite, in listing of illite (1M) and summarizing of Ca-smectite and diVS-ml as total Ca-smectite in literature. Thermogravimetric investigations of B25 bentonite support the here reported results of kaolinite amount (tab. 2).

Generally, the here reported compositions of untreated and treated bentonite were verified by combination of following methods:

- TEM-EDX results, cross-checked by oriented specimen (XRD) after Sybilla-modelling of probability of smectite layers, also offer indications to the occurrence of beidellite

- XRD of powder samples (bulk) has been cross-checked by thermogravimetry using the mass loss to verify especially the XRD-results to kaolinite, indications to kaolinite-smectite mixed layer phases, and carbonates (see example: tab. 2).

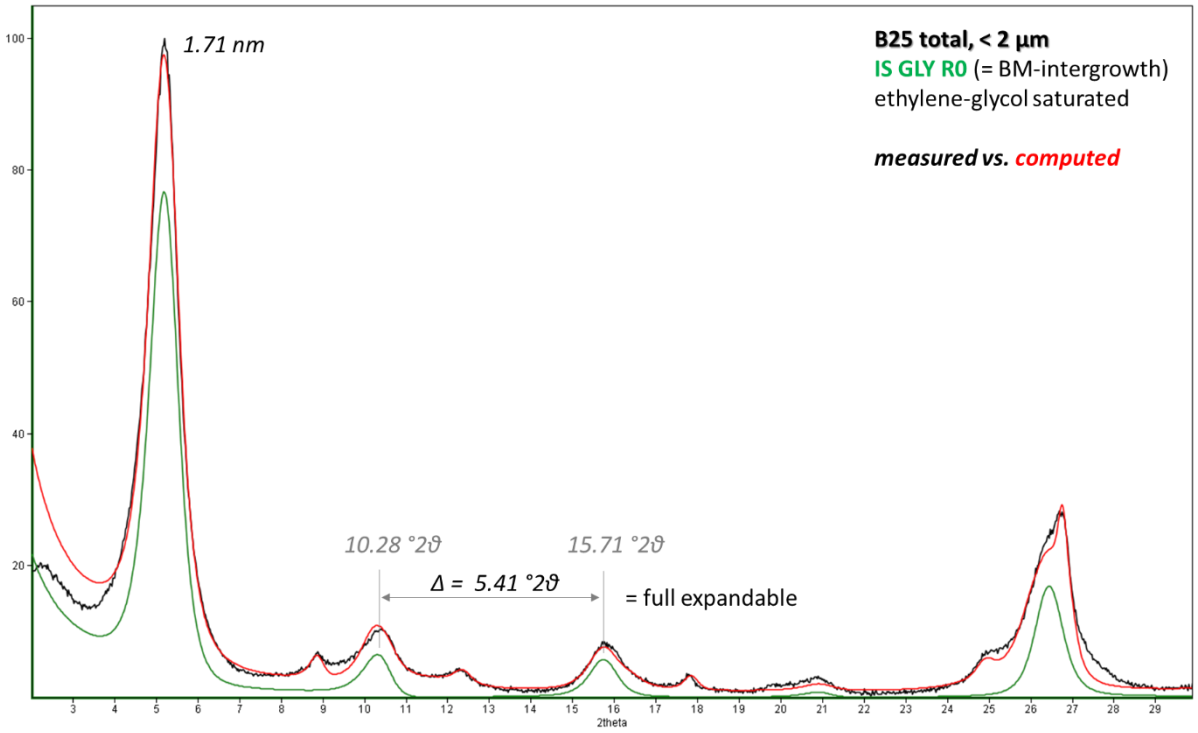

Fig. 1. *B25, original (< 2 µm) - X-ray diffraction pattern of the ethylene-glycol saturated oriented* ***specimen*** *(with computing of Ca-smectite by Sybilla-software – green line)*

Beidellite-rich Ca-Smectite

Identification by XRD: The X-ray diffraction pattern of the ethylene-glycol saturated oriented specimen shows a full expandability to 1.7 nm and a difference at 5.4° 2θ between 2. and 3. order of smectite interferences (fig. 1). This distance is typically for montmorillonite (Moore & Reynolds, 1989). An exception from this situation is drawn only by two samples (No 23 – 35°C, 0.7 MPa: %S = 80%; No 15 – 125°C: %S = 60%). Air dried oriented specimen show a (001)-interference at 1.41-1.56 nm and indicate a dominating Ca, Mg-occupation of interlayer space. Only sample No 15 (125°C) lets record this XRD-peak at 1.26 nm. This development could pronounce in this sample an interlayer occupation by mono-valent cations like Na or smectite with 1-water layer is under pressing the more typical 2-water layers.

Mineral formula by TEM-EDX and clustering: The full expandability of ethylene-glycol saturated oriented specimen let assume Si-values close to 4 per $(OH)_2$ O_{10} in computation of mineral formula basing on TEM-EDX-analyses but calculated were values between 3.47 - 3.78 e phuc. This situation is considered as intergrowth between beidellite (Si ~ 3.5), montmorillonite (Si ~ 4) and sometimes also in interstratification with illite (Si ~ 3.2).

Tab. 3. *Structural formulae for Ca-smectite B25 samples with estimation of beidellite-ratio*

		phase (low illite)		mineral formula (clustering of TEM-EDX-results)										%S (XRD-oriented)	mass-% (XRD-oriented)
				Ca	Mg	Na	K	Al	Fe^{3+}	Mg	Ti	Al	Si		
Original	B25_40µm	BMI	55:45:00	0.04	0.11	0.00	0.09	1.32	0.56	0.12	0.00	0.28	3.72	99%	47%
Orig., compacted	B25_repeat	BMI	70:30:00	0.16	0.04	0.02	0.11	1.18	0.59	0.21	0.02	0.35	3.65		
OPA, 35°C	No4_T	BMI	100:00:00	0.08	0.12	0.01	0.14	1.00	0.92	0.08	0.01	0.50	3.50	100%	67%
	No4_C	BMI	100:00:00	0.15	0.06	0.05	0.21	0.95	0.88	0.15	0.01	0.53	3.47	100%	53%
	No4_B	BMI	80:20:00	0.17	0.01	0.00	0.07	1.02	0.83	0.22	0.00	0.41	3.59	100%	41%
OPA, 35°C, inj.	No23	BMI	35:45:20	0.11	0.08	0.00	0.09	1.24	0.59	0.17	0.01	0.31	3.69	82%	50%
OPA, 60°C	No5_T	BMI	65:35:00	0.05	0.12	0.00	0.09	1.28	0.60	0.11	0.01	0.33	3.67	100%	41%
	No5_C	BMI	65:35:00	0.07	0.11	0.00	0.05	1.12	0.77	0.10	0.01	0.33	3.67	} 100%	32%
		BMI	100:00:00	0.07	0.14	0.00	0.12	0.97	0.96	0.06	0.01	0.49	3.51		
	No5_B	BMI	85:15:00	0.08	0.00	0.22	0.33	0.96	0.74	0.30	0.01	0.42	3.58	100%	39%
OPA, 100°C	No0_T	BMI	55:45:00	0.08	0.09	0.00	0.06	1.27	0.58	0.14	0.01	0.28	3.72	99%	58%
	No0_C	BMI	50:45:05	0.12	0.08	0.00	0.07	1.24	0.57	0.18	0.01	0.29	3.71	94%	28%
	No0_B	BMI	70:30:00	0.18	0.04	0.01	0.10	1.18	0.60	0.22	0.01	0.34	3.66	100%	28%
OPA, 100°C	No2_T	BMI	70:30:00	0.09	0.10	0.00	0.11	1.24	0.61	0.15	0.00	0.34	3.66	} 100%	25%
		BMI	75:25:00	0.28	0.00	0.02	0.10	1.13	0.56	0.29	0.01	0.38	3.62		
	No2_C	BMI	65:35:00	0.10	0.07	0.01	0.12	1.23	0.59	0.17	0.01	0.33	3.67	100%	21%
	No2_B	BMI	45:55:00	0.15	0.05	0.00	0.03	1.26	0.52	0.22	0.00	0.22	3.78	⎡	
		BMI	65:35:00	0.12	0.08	0.00	0.11	1.21	0.61	0.17	0.01	0.34	3.66	⎢	
		BMI	70:30:00	0.19	0.03	0.02	0.12	1.16	0.60	0.23	0.01	0.36	3.64	⎢ 100%	11%
		BMI	90:10:00	0.11	0.10	0.00	0.13	1.37	0.53	0.09	0.01	0.46	3.54	⎢	
		BMI	95:05:00	0.13	0.00	0.00	0.09	1.36	0.58	0.14	0.01	0.47	3.53	⎣	
OPA, 125°C	No15														
OPA, 150°C	No3_T	BMI	70:30:00	0.11	0.09	0.00	0.11	1.22	0.60	0.17	0.01	0.35	3.65	100%	26%
	No3_C	BMI	70:30:00	0.15	0.06	0.00	0.11	1.20	0.60	0.20	0.01	0.35	3.65	100%	38%
	No3_B	BMI	75:25:00	0.15	0.06	0.00	0.11	1.22	0.59	0.18	0.01	0.37	3.63	100%	40%

Legend: *BMI – beidellite-montmorillonite-illite; %S – probability of smectite layer; mass-% - result of Sybilla-modelling (oriented XRD) of fraction < 2 µm*

Beidellite-ratio in Ca-smectite is dominating in all samples. A BMI-ratio at 70:30:00 is commonly to observe. Samples No 23 (35°C) with a BMI-ratio of 35:40:20 and No 15 (125°C) without beidellite-dominated smectite (tab. 3) are again the only exceptions. The untreated Ca, Mg-smectite is characterized by high octahedral Fe^{3+} (0.56 per $(OH)_2$ O_{10}). This value is rising in all experimental samples, especially for reactions products of experiments at 35°C and 60°C (e.g. sample No4_T: 0.92 per $(OH)_2$ O_{10}). The calculated structural formulae (tab. 3) show variable tetrahedral Si-values (from 3.47 – 3.78 e phuc), but the full expandability is stable nearby in all samples.

Further indications for beidellite by FTIR: The FTIR spectroscopic analysis of B25 clay indicates that smectite is the dominant phase in this bentonite. The broad adsorption band at 3634 cm^{-1} (AlAlOH) is typical for Al-rich content of smectite (Madejova et al., 1996) and strongly associated with beidellites (Gate, 2005). Also, Fe is high present as FeFeOH (3557 cm^{-1} and 3577 cm^{-1}) (Zviagina et al., 2004). The two shoulders at 929 cm^{-1} in OH-bending region and 3646 cm^{-1} in OH-stretching region indicate the occurrence of beidellite (Gates, 2005). A band at ~693 cm^{-1} shared with quartz is also assigned to Si-O in a ferruginous beidellite (Decarreau et al., 1992).

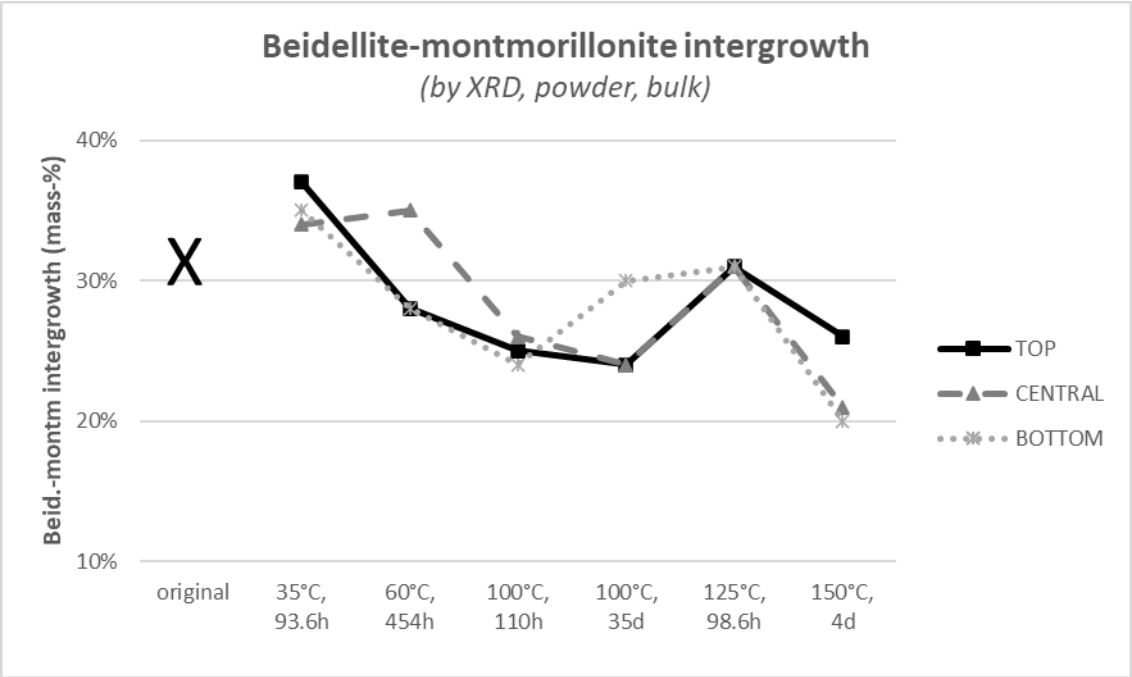

Fig. 2. *Mass distribution of Ca-smectite in bulk samples of B25 bentonite*
Note: *Sample No 15 (125°C) is only a single sample (without separation in top, central and bottom)*

Development of mass-distribution: Ca-smectite shows a trend to a slight mass reduction with increasing thermal load (fig. 2) from 35% in direction to 25%.

Special development in sample No15 (and partially also in sample No2_B): Sample No15 contains in the bulk material 31% Ca-smectite (proofed by XRD powder- & TG-measurements and Profex-processing). So, a remarkable amount of Ca-smectite with %S=100% should occur in fraction < 2 µm of sample No15. But XRD of oriented specimen for fraction < 2 µm of No15 shows only 10 % with %S = 60% (and further diVS-ml with 24% at %S=28%) (tab. 5). The data of oriented XRD are in good agreement with TEM & clustering. That means now, sample No15 has not in fraction < 2 µm the expected full expandable smectite, but 31% Ca-smectite in bulk powder sample. This situation between composition of bulk sample and material < 2 µm let assume that Ca-smectite is underwent a further process in this temperature level of experiments (125°C). In HTMC-experiments, smectite aggregates can filled by precipitated Si, which was dissolved before from smectite particles. In case of a low Si-dissolution rate, dissolved Si is transported away by flow of solution. In case of an increased Si-dissolution rate, the amount of dissolved Si is too high for the transport alone by flow of solution. The result of that is filling of smectite aggregates by precipitated Si-gel. Theses aggregates are “glued”. The grain size separation of bulk material into fraction < 2 µm by sedimentation (for XRD-measurement on oriented specimen) is not involving now the larger smectites aggregates solidified by before dissolved Si. So, such smectite aggregates occur only in a reduced amount or are missing (like in sample No15) than in fraction < 2 µm.

A similar development of reduced amount of full expandable smectite could be observed in sample No2_B (100°C). This sample is characterized by 30 % Ca-smectite in bulk material (tab. 1) and only 11% full expandable phases in fraction < 2 µm (tab. 5).

How is it possible to verify this assumed process? The bulk material is to separate in few fractions and each fraction is to measure by XRD (randomly oriented) related to distribution of Ca-smectite. An enrichment of Ca-smectite in fractions larger 2 µm should be to expect.

Dioctahedral Vermiculite-Smectite Mixed-Layer (diVS-ml)

Identification by XRD: The X-ray diffraction pattern of the ethylene-glycol saturated oriented specimen draw a further group of swelling. The difference between 2. and 3. order of smectite interferences is variable representing smectite layer probabilities (%S) between 8 - 60% ($\%S_{mean}$ = 30-35%) (tab. 4). The smectite layer probability (%S) of uncompacted original B25 bentonite is to find at %S = 55% (fig. 3).

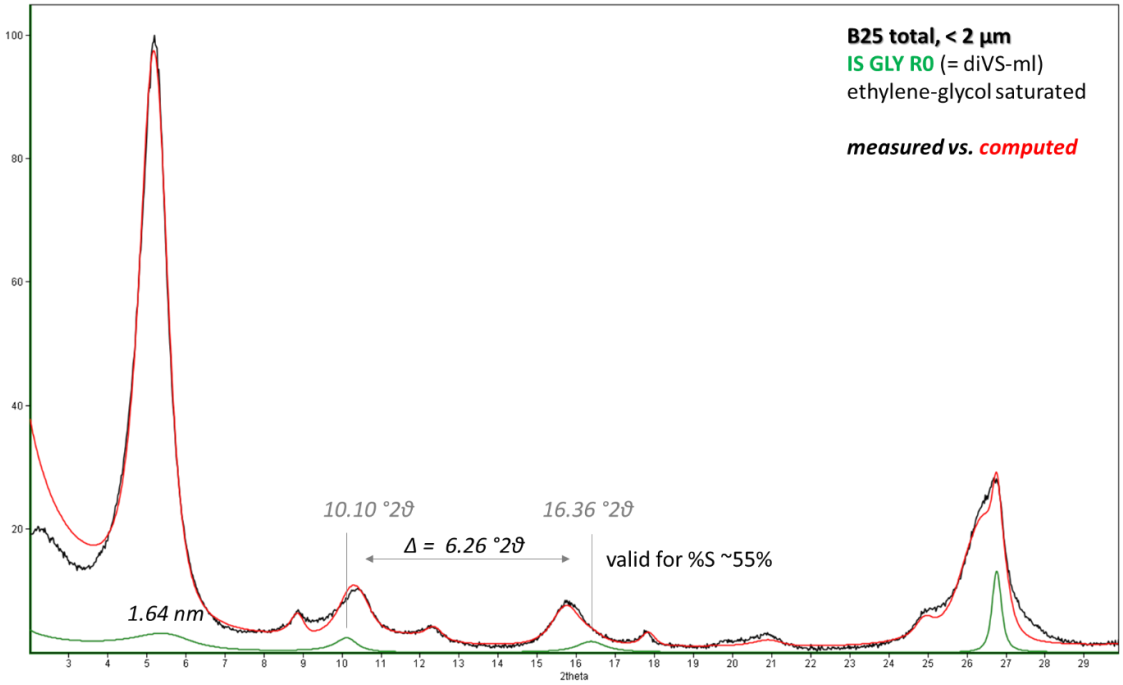

Fig. 3. *B25, original (< 2 µm) - X-ray diffraction pattern of the ethylene-glycol saturated oriented specimen (with computing of diVS-ml by Sybilla-software – green line)*

Tab. 4. *Structural formulae for diVS-ml phases in B25 samples with estimation of beidellite-ratio*

		phase (high illite)		mineral formula (clustering of TEM-EDX-results)										%S (XRD-oriented)	mass-% (XRD-oriented)
				Ca	Mg	Na	K	Al	Fe^{3+}	Mg	Ti	Al	Si		
Original	B25_40µm	BMI	00:55:45	0.13	0.05	0.01	0.12	1.22	0.56	0.21	0.00	0.29	3.71	55%	16%
Orig., compacted	B25_repea	BMI	00:25:75	0.11	0.06	0.01	0.29	1.35	0.50	0.14	0.01	0.51	3.49		
OPA, 35°C	No4_T	BMI	00:30:70	0.03	0.01	0.05	0.62	1.10	0.66	0.22	0.02	0.54	3.46	30%	11%
	No4_C	BMI	10:30:60	0.13	0.05	0.26	0.35	0.77	0.77	0.44	0.01	0.54	3.46	38%	19%
	No4_B	BMI	10:30:60	0.15	0.09	0.00	0.16	0.95	0.92	0.12	0.01	0.55	3.45	38%	15%
OPA, 35°C	No23	BMI	00:40:60	0.32	0.00	0.00	0.14	1.03	0.56	0.40	0.01	0.41	3.59	45%	13%
		BMI	20:25:55	0.13	0.03	0.04	0.35	1.35	0.46	0.20	0.01	0.54	3.46		
OPA, 60°C	No5_T	BMI	05:35:60	0.05	0.13	0.00	0.29	1.24	0.63	0.11	0.02	0.56	3.44	33%	14%
	No5_C	BMI	20:20:60	0.05	0.10	0.00	0.34	1.18	0.72	0.08	0.02	0.58	3.42	39%	18%
	No5_B	BMI	40:15:45	0.13	0.00	0.22	0.38	0.84	0.85	0.30	0.01	0.57	3.43	55%	17%
OPA, 100°C	No0_T	BMI	00:35:65	0.09	0.11	0.00	0.16	1.18	0.67	0.14	0.02	0.43	3.57	30%	8%
	No0_C	BMI	00:30:70	0.10	0.10	0.00	0.17	1.30	0.57	0.12	0.01	0.46	3.54	30%	13%
	No0_B	BMI	00:25:75	0.22	0.04	0.02	0.19	1.12	0.63	0.24	0.01	0.51	3.49	25%	19%
OPA, 100°C	No2_T	BMI	00:25:75	0.12	0.05	0.01	0.34	1.39	0.45	0.17	0.00	0.52	3.48	20%	20%
	No2_C	BMI	00:25:75	0.08	0.10	0.01	0.26	1.27	0.59	0.13	0.02	0.53	3.47	23%	11%
	No2_B	BMI	00:30:70	0.18	0.02	0.01	0.27	1.23	0.53	0.21	0.03	0.49	3.51	8%	23%
OPA, 125°C	No15	BMI	05:55:40	0.15	0.05	0.03	0.11	1.19	0.60	0.21	0.01	0.35	3.65	60%	10%
		BMI	00:25:75	0.11	0.07	0.03	0.28	1.26	0.55	0.16	0.03	0.54	3.46	28%	24%
OPA, 150°C	No3_T	BMI	00:25:75	0.10	0.16	0.00	0.11	1.06	0.85	0.08	0.00	0.53	3.47	22%	11%
	No3_C	BMI	00:25:75	0.10	0.07	0.00	0.31	1.37	0.47	0.14	0.02	0.52	3.48	22%	10%
	No3_B	BMI	00:30:70	0.31	0.01	0.00	0.15	1.08	0.60	0.31	0.01	0.46	3.54	27%	9%

Legend: *BMI – beidellite-montmorillonite-illite; %S – probability of smectite layer*

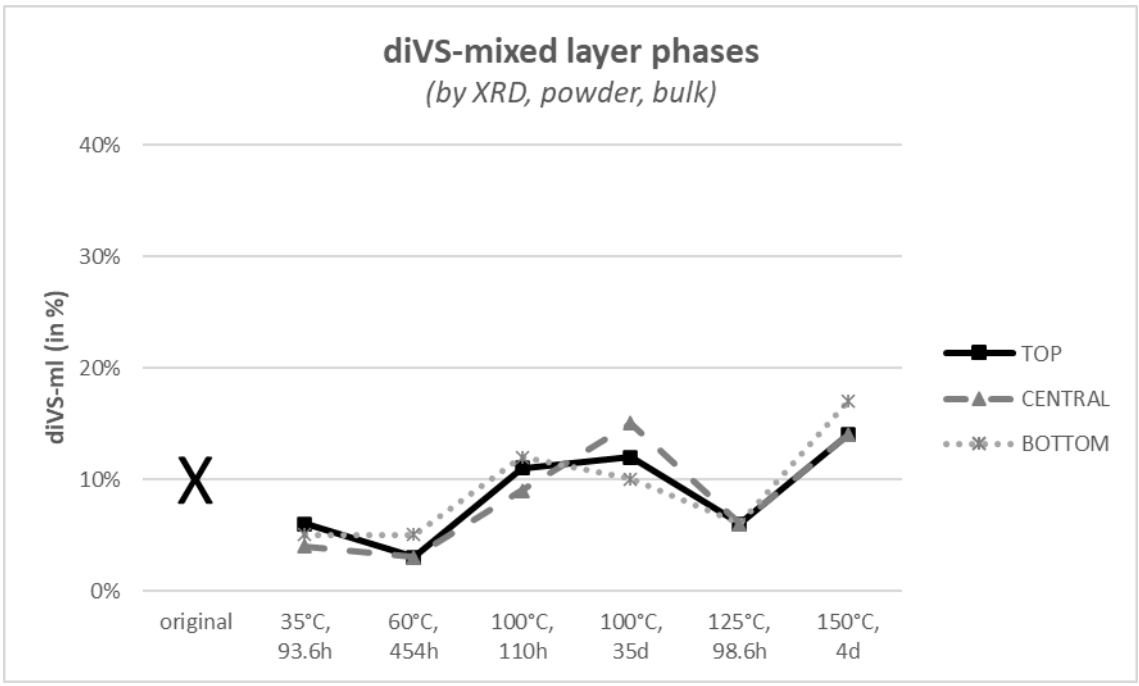

Fig. 4. *Mass distribution of diVS-ml in bulk samples of B25 bentonite*
Note: *Sample No 15 (125°C) is only a single sample (without separation in top, central and bottom)*

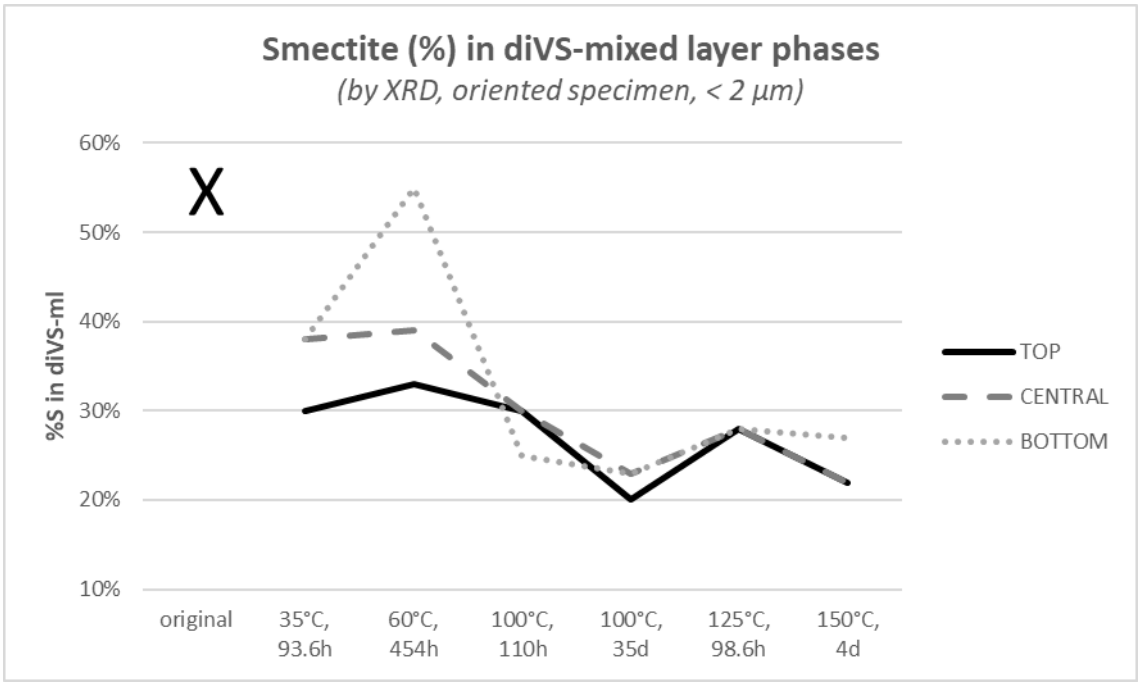

Fig. 5. *Smectite layer probability of diVS-ml in fraction < 2 µm of B25 bentonite*
Note: *Sample No 15 (125°C) is only a single sample (without separation in top, central and bottom)*

Tab. 5. *Mineral matter of B25 bentonite (< 2 µm) – oriented specimen*

Sample	Beidellite-Montm. intergrowth	diVS-ml	Illite	Kaolinite	Kaolinite-Smectite-ml *(KS GL R1)*	Kaolinite-Smectite-ml *(KS GL R0)*	*Σ total*
B25 original	47% *(%S = 99%)*	16% *(%S = 55%)*	9%	5%	23% *(%S = 45%)*		*100%*
35°C, 93.6h, OPA							
No4_T	67% *(%S = 100%)*	11% *(%S = 30%)*	10%	5%		7% *(%S = 58%)*	*100%*
No4_C	53% *(%S = 100%)*	19% *(%S = 38%)*	6%	2%		21% *(%S = 65%)*	*101%*
No4_B	41% *(%S = 100%)*	15% *(%S = 38%)*	11%	6%		27% *(%S = 62%)*	*100%*
35°C, 285h, OPA, 0.7 MPa							
No23	50% *(%S = 82%)*	13% *(%S = 45%)*	10%	6%		22% *(%S = 57%)*	*101%*
60°C, 454h, OPA							
No5_T	41% *(%S = 100%)*	14% *(%S = 33%)*	8%	5%		31% *(%S = 61%)*	*99%*
No5_C	32% *(%S = 100%)*	18% *(%S = 39%)*	8%	6%		37% *(%S = 65%)*	*101%*
No5_B	39% *(%S = 100%)*	17% *(%S = 55%)*	13%	8%		23% *(%S = 65%)*	*100%*
100°C, 110h, OPA							
No0_T	58% *(%S = 99%)*	8% *(%S = 30%)*	20%	3%	12% *(%S = 45%)*		*101%*
No0_C	28% *(%S = 94%)*	13% *(%S = 30%)*	4%	7%	44% *(%S = 75%)*	4% *(%S = 48%)*	*100%*
No0_B	28% *(%S = 100%)*	19% *(%S = 25%)*	9%	8%	11% *(%S = 76%)*	25% *(%S = 58%)*	*100%*
100°C, 35d, OPA							
No2_T	25% *(%S = 100%)*	20% *(%S = 20%)*	2%	7%	37% *(%S = 79%)*	8% *(%S = 48%)*	*99%*
No2_C	21% *(%S = 100%)*	11% *(%S = 23%)*	3%	7%	47% *(%S = 78%)*	12% *(%S = 48%)*	*101%*
No2_B	11% *(%S = 100%)*	8% *(%S = 23%)*	11%	10%	51% *(%S = 75%)*	12% *(%S = 48%)*	*101%*
125°C, 98.6h, OPA							
No15	10% *(%S = 60%)*	24% *(%S = 28%)*	14%	18%	34% *(%S = 75%)*		*100%*
150°C, 4d, OPA							
No3_T	26% *(%S = 100%)*	11% *(%S = 22%)*	5%	6%	39% *(%S = 74%)*	13% *(%S = 48%)*	*100%*
No3_C	38% *(%S = 100%)*	10% *(%S = 22%)*	4%	6%	27% *(%S = 76%)*	16% *(%S = 48%)*	*101%*
No3_B	40% *(%S = 100%)*	9% *(%S = 27%)*	3%	5%	30% *(%S = 78%)*	13% *(%S = 48%)*	*100%*

Legend: *diVS-ml – IS-ml with K- and/or charge deficiency; %S – probability of smectite layers*

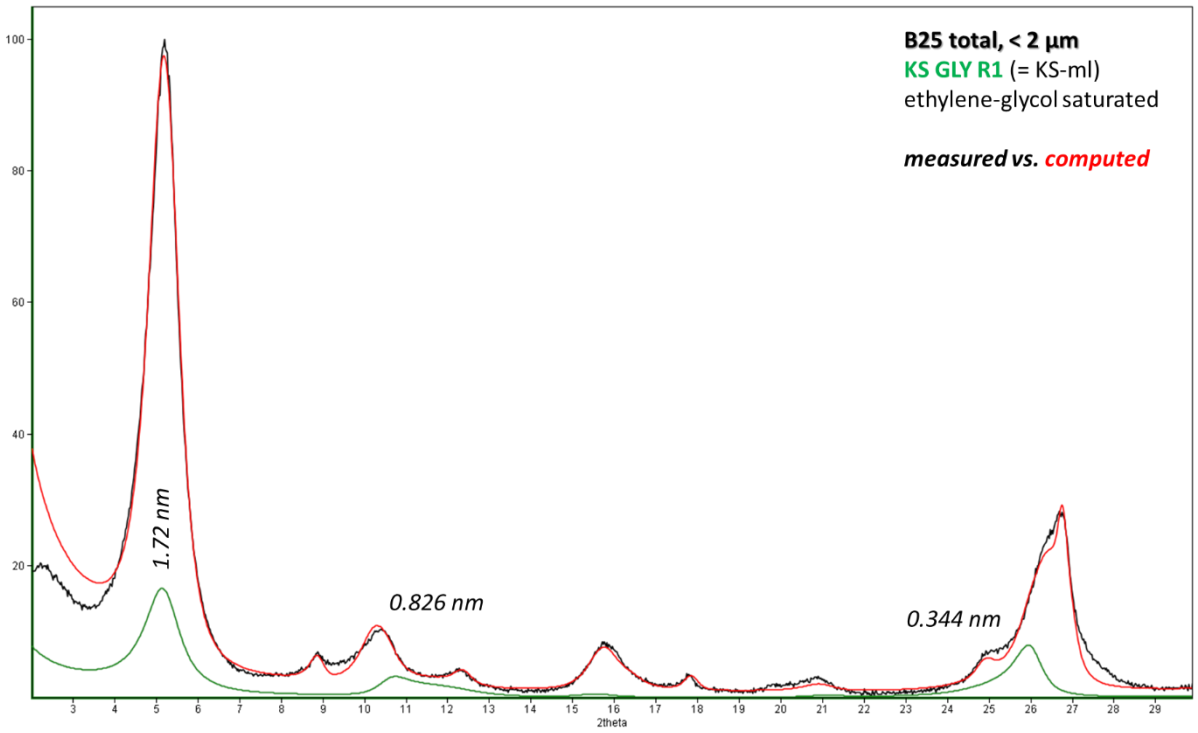

Fig. 6. *B25, original (< 2 µm) - X-ray diffraction pattern of the ethylene-glycol saturated oriented specimen (with computing of KS-ml by Sybilla-software – green line)*

Mineral formula by TEM-EDX and clustering: The cross-checking between phases with limited expandability using ethylene-glycol saturated oriented specimen and TEM-EDX-data (incl. clustering) shows illite-smectite mixed layer phase with K- and charge deficiency. For these phases, montmorillonite is the dominating smectite component. Beidellite occurs in diVS-ml only in few samples in traces (only exception: sample No 5_B with BMI 40:15:45) (tab. 4). That means, reduced tetrahedral Si-values after experiments are linked with reduced swelling properties by a higher illite layer probability (%I).

Development of mass-distribution: diVS-ml phases show with increasing thermal load a slight variable mass distribution close to the original composition (fig. 4).

Development of expandability: diVS-ml phases in B25 bentonite draw with increasing thermal load a remarkable reduction of smectite layer probability from %S=55% (original B25) to close to 20% (150°C) (fig. 5).

Kaolinite-Smectite Mixed-Layer (KS-ml)

Identification by XRD: The occurrence of kaolinite-smectite mixed layer is mainly indicated by modelling of XRD-pattern of oriented specimen using Sybilla-software (developed by Chevron Inc.: Aplin et al., 2006) (tab. 5; fig. 6). Few particles, measured by TEM-EDX, indicated KS-ml phases, but it was not possible to calculate a valid structural formula.

Development of mass-distribution: KS-ml phases in fraction < 2 µm show as trend with increasing thermal load a rising ratio to the original composition (fig. 7).

Development of expandability: KS-ml phases in B25 bentonite (< 2 µm) draw with increasing thermal load a rising smectite layer probability from %S=45% (original B25) to close to 70% (150°C) (fig. 8).

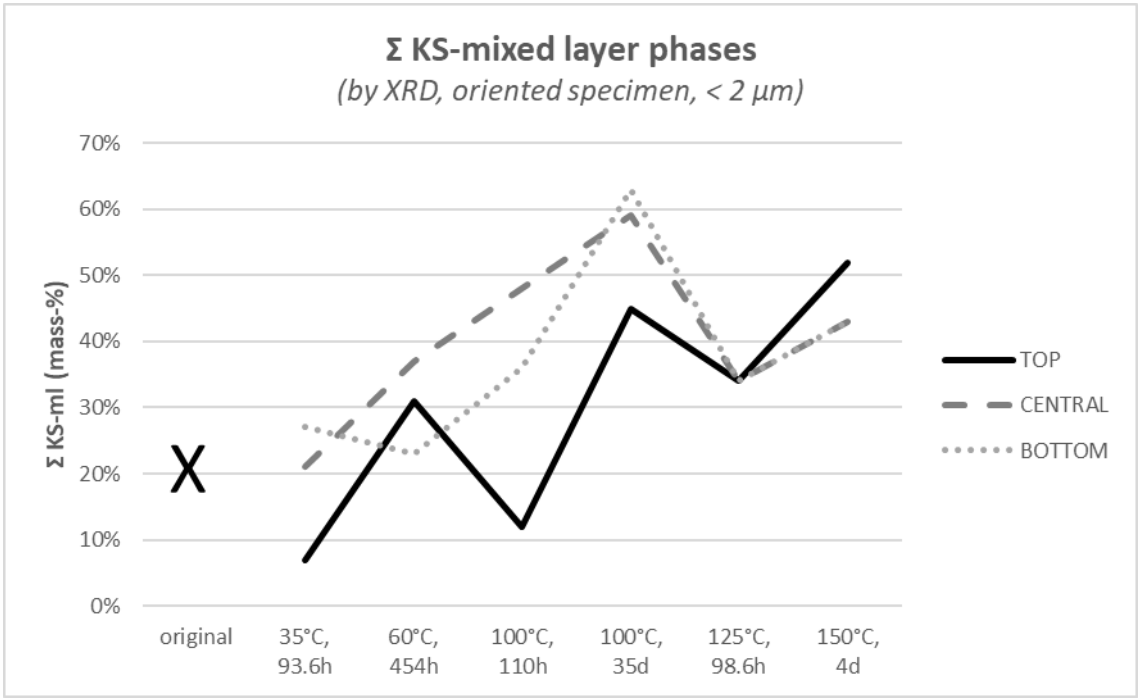

Fig. 7. *Mass distribution of KS-ml in samples of B25 bentonite (< 2 µm)*
Note: *Sample No 15 (125°C) is only a single sample (without separation in top, central and bottom)*

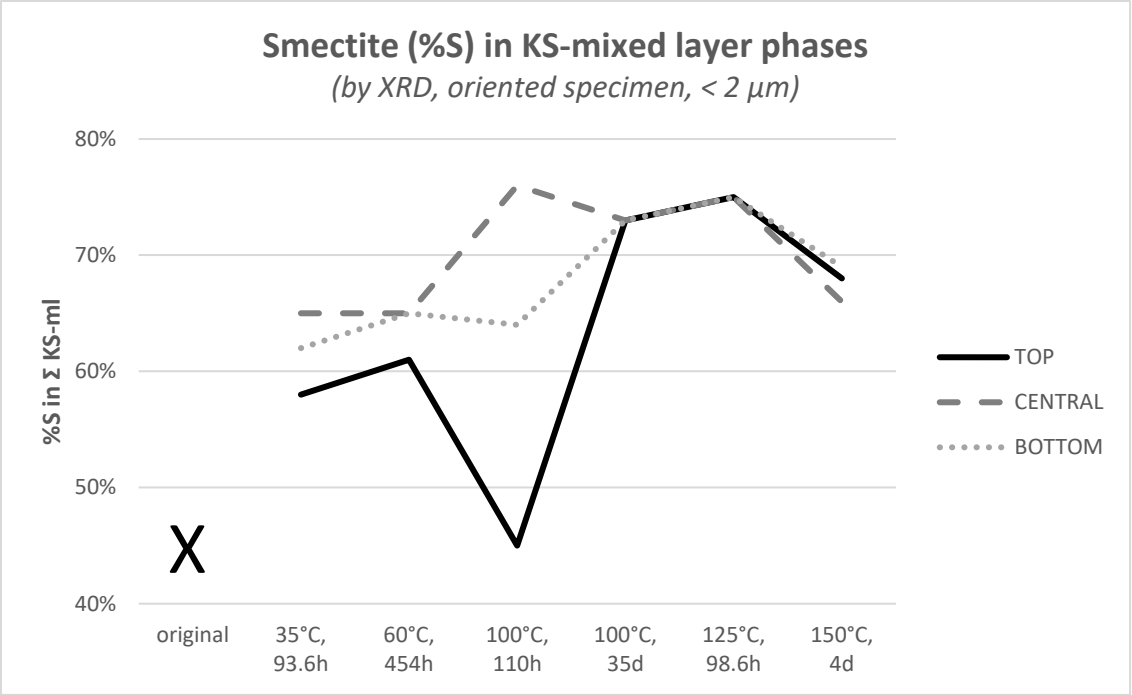

Fig. 8. *Smectite layer probability of KS-ml in fraction < 2 µm of B25 bentonite*
Note: *Sample No 15 (125°C) is only a single sample (without separation in top, central and bottom)*

Smectite-behaviour in experiments

Smectite is the main responsible mineralogical phase, which determines the swelling behaviour of bentonite. In B25 bentonite, smectite is distributed in three different groups of phases (Ca-smectite, diVS-ml, KS-ml). Each group has shown a specific behaviour during the experiments (tab. 6).

Tab. 6. *B25 – Overview about different smectite behaviour*

	role of phase in bulk sample	smectite species	mass-% development	%S-development	assumptions to expandab.
Ca-smectite	main phase *(tab. 1)*	beidellite > montm. *(tab. 3)*	slight reduction *(from 35% to 25%) (fig. 2)*	± constant *(at %S=70-100%) (tab. 3)*	slight impact for reduction
diVS-ml	minor phase *(tab. 1)*	montm. >> beidellite *(tab. 4)*	± stable *(variable 5% - 15%) (fig. 4)*	reduction *(from 55% to 20%) (fig. 5)*	slight impact for reduction
KS-ml	minor phase *(tab. 1)*	not to determine	rising *(< 2 µm: 25% → 45%) (fig. 7)*	rising *(< 2 µm: 45% → 70%) (fig. 8)*	increasing

(in direction of rising thermal load in experiments)

The summarizing impact of Ca-smectite together with diVS-ml on expandability is mirrored by TEM-EDX-measurements (fig. 9). The original material shows the highest tetrahedral Si-value per $(OH)_2\ O_{10}$ with Si = 3.72. The first Si-downfall at 35°C is caused by the beidellitization of Ca-smectite (tab. 3) (see BMI at 100:00:00). The expandability should be not limited at 35°C.

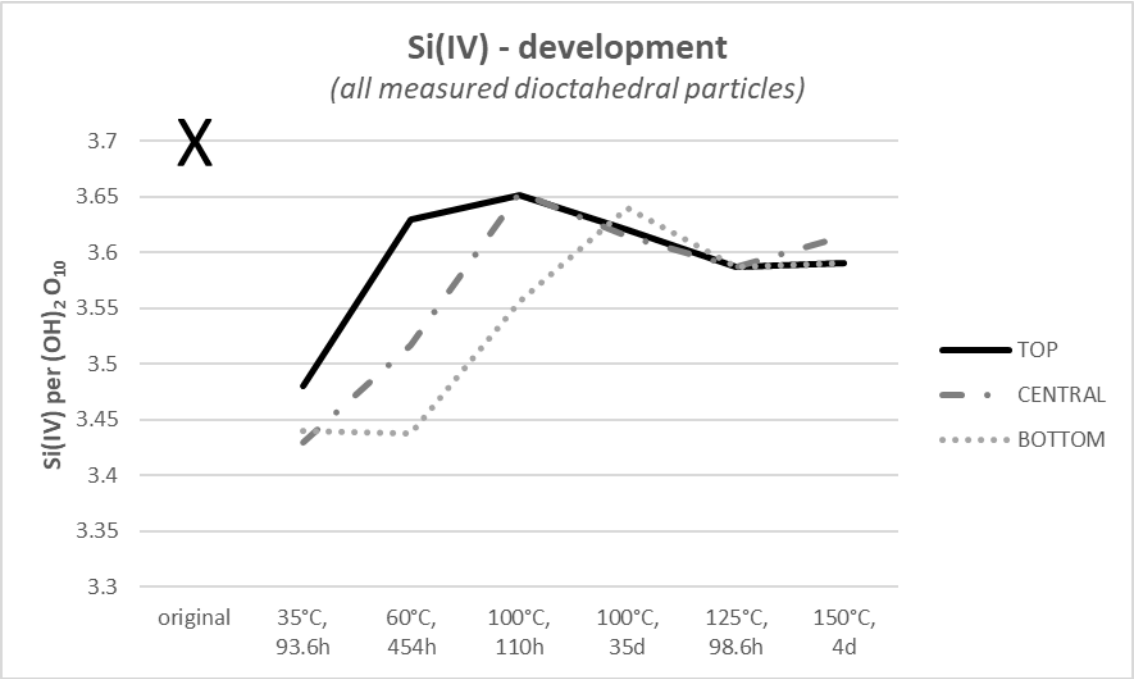

Fig. 9. *Behaviour of tetrahedral Si per $(OH)_2$ O_{10} in fraction < 2 µm of B25 bentonite*
Note: *Sample No 15 (125°C) is only a single sample (without separation in top, central and bottom); KS-ml not included here*

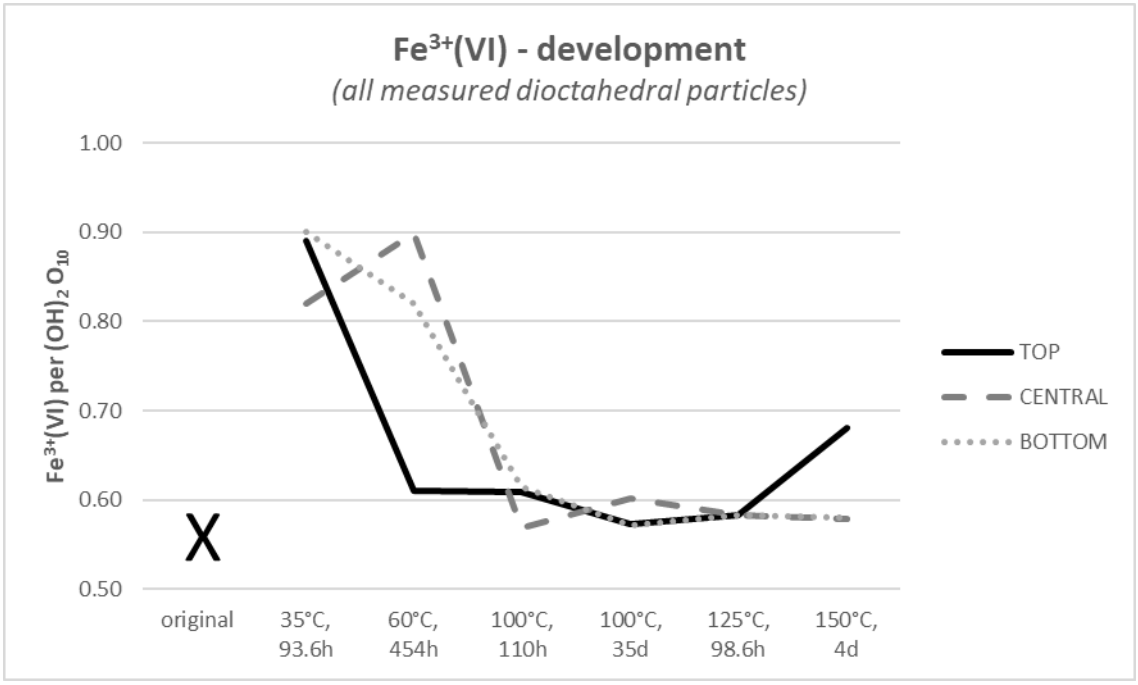

Fig. 10. *Development of octahedral Fe^{3+} per $(OH)_2$ O_{10} in fraction < 2 µm of B25 bentonite*
Note: *Sample No 15 (125°C) is only a single sample (without separation in top, central and bottom); KS-ml not included here*

This beidellitization of Ca-smectite at 35°C is linked with a very high octahedral Fe^{3+}-amount (> 0.8 per $(OH)_2$ O_{10}) (fig. 10) and a reduced octahedral Al (~ 1.0 per $(OH)_2$ O_{10}) (tab. 3). The degree of this beidellitization is lower at temperatures higher than 35°C with a BMI in average ~70:30:00 (tab. 3), but the "illitization" of diVS-ml started now (fig. 5). A reduction of expandability could be expected.

The additional contribution of KS-ml on expandability of the total sample is not really to evaluate. The rising mass of KS-ml (< 2 µm) by higher thermal load during the experiments (tab. 6; fig. 7) and the even rising smectite layer probability (tab. 6; fig. 8) let assume a certain degree of compensation of expected lost expandability by Ca-smectite and diVS-ml.

TEM-EDX: Illite-behaviour in experiments

Only few particles of illite could be measured in fraction < 2 µm by TEM-EDX. Because of these low numbers of measured illite particles, the following messages are not full valid by statistics.

The available TEM-EDX-measurements indicate the occurrence of two illite groups: (i) Al(VI)-rich with a low to moderate K-deficit and (ii) Fe(VI)-rich ($\geq$ 0.9 per $(OH)_2 O_{10}$) with a high K-deficit (tab. Illite_B25). Both groups are not to distinguish in all samples by clustering because of often low numbers of illite particles. The octahedral Fe seems to substitute Al in a certain degree in both groups in experiments ≤ 60°C. The opposite development in octahedral Al/Fe-ratio (again Fe-reduction) is to observe in experiments > 60°C. This observed variable result concerning illite could represented by alteration of composition, but also by degradation of larger illite particles than feeding the fraction < 2 µm.

	Ca (XII)	Mg (XII)	Na (XII)	K (XII)	Cr3+ (VI)	Al (VI)	Fe3+ (VI)	Mg (VI)	Ti (VI)	Al (IV)	Si (IV)	XII	n_VI	%S	K-deficit	charge-deficit
B25 original																
Cluster2 *(n=3)*	0.06	0.03	0.03	0.56	0.00	1.55	0.33	0.11	0.01	0.69	3.31	0.79	2.0	10	43%	7%
Cluster4 *(n=2)*	0.07	0.28	0.00	0.19	0.00	0.99	0.90	0.11	0.00	0.78	3.22	0.88	2.0	4	80%	-2%
B25 treated																
No4_T *35°C, 93.6h*																
Cluster2 *(n=6)*	0.01	0.03	0.08	0.71	0.00	1.28	0.60	0.10	0.01	0.78	3.22	0.87	2.0	4	24%	0%
No4_C *35°C, 93.6h*																
Cluster4 *(n=6)*	0.09	0.06	0.12	0.51	0.00	1.18	0.56	0.25	0.02	0.70	3.30	0.93	2.0	9	48%	-10%
No4_B *35°C, 93.6h*																
Cluster1 *(n=6)*	0.10	0.02	0.03	0.61	0.00	1.24	0.60	0.13	0.03	0.75	3.25	0.87	2.0	4	34%	0%
Cluster3 *(n=7)*	0.15	0.16	0.00	0.18	0.00	0.59	1.28	0.06	0.06	0.80	3.20	0.80	2.0	4	81%	7%
No5_T *60°C, 454h*																
Cluster1 *(n=3)*	0.03	0.25	0.00	0.35	0.00	0.88	0.95	0.10	0.07	0.87	3.13	0.90	2.0	0	61%	-2%
No5_C *60°C, 454h*																
Cluster3 *(n=8)*	0.08	0.23	0.00	0.18	0.00	0.57	1.29	0.10	0.04	0.75	3.25	0.81	2.0	6	81%	5%
Cluster5 *(n=6)*	0.03	0.05	0.00	0.59	0.00	1.13	0.72	0.13	0.03	0.68	3.32	0.77	2.0	11	41%	8%
No5_B *60°C, 454h*																
Cluster1 *(n=27)*	0.13	0.01	0.19	0.44	0.00	0.93	0.81	0.25	0.01	0.68	3.32	0.91	2.0	11	56%	-9%
No0_T *100°C, 110h*																
Cluster2 *(n=3)*	0.07	0.17	0.02	0.25	0.00	1.15	0.72	0.11	0.02	0.67	3.33	0.76	2.0	12	75%	9%
No0_C *100°C, 110h*																
Note: no illite detected																
No0_B *100°C, 110h*																
Cluster1 *(n=3)*	0.17	0.07	0.02	0.30	0.00	1.51	0.38	0.11	0.00	0.69	3.31	0.80	2.0	10	69%	5%
Cluster4 *(n=2)*	0.14	0.22	0.03	0.15	0.00	0.79	1.00	0.21	0.01	0.70	3.30	0.90	2.0	9	84%	-6%
No2_T *100°C, 35d*																
Cluster1 *(n=4)*	0.04	0.11	0.01	0.44	0.00	1.36	0.53	0.10	0.02	0.66	3.34	0.75	2.0	13	57%	10%
No2_C *100°C, 35d*																
Cluster1 *(n=4)*	0.07	0.24	0.02	0.28	0.00	0.92	0.82	0.24	0.02	0.69	3.31	0.91	2.0	10	72%	-9%
No2_B *100°C, 35d*																
Note: no illite detected																
No15 *125°C, 98.6h*																
Cluster2 *(n=9)*	0.07	0.08	0.02	0.49	0.00	1.35	0.51	0.13	0.01	0.70	3.30	0.81	2.0	9	50%	4%
No3_T *150°C, 4d*																
Cluster1 *(n=4)*	0.08	0.12	0.00	0.31	0.00	1.13	0.81	0.06	0.00	0.67	3.33	0.73	2.0	12	69%	13%
No3_C *150°C, 4d*																
Cluster2 *(n=4)*	0.07	0.10	0.09	0.43	0.00	1.39	0.49	0.11	0.01	0.75	3.25	0.85	2.0	6	55%	2%
No3_B *150°C, 4d*																
Cluster2 *(n=1)*	0.08	0.13	0.00	0.27	0.00	1.74	0.25	0.00	0.01	0.73	3.27	0.69	2.0	7	72%	19%

Tab. Illite_B25. *B25 bentonite: Illite in fraction < 2 µm (by TEM-EDX)*

Legend: *(n=3) – number of illite particles measured by TEM-EDX; XII – interlayer charge; n_VI – number of atoms in octahedral layer per $(OH)_2$ O_{10}; %S – probability of smectite layers in senso of Środon et al. (1992); K-deficit, charge-deficit – in senso of Środon et al. (1992) (normal K in illite = 0.89 per $(OH)_2$ O_{10})*

"Top – Central – Bottom" - Development of Reactions

The flow direction of adapted Opalinus solution during the experiments was arranged from bottom to top. Differences are only to observe in short term experiments for ≤ 100°C (figs. 9, 10). The Si-behaviour (fig. 9) mirrors probably a beidellitization of Ca-smectite (alteration into pure beidellite) (tab. 3) with a highest impact at the bottom area. This process is accompanied by enrichment of octahedral Fe (tab. 10), especially to see in experiment at 60°C.

2. Mineral matter in Friedland Clay

***Tab. 7**. Mineral matter of Friedland Clay-series (bulk sample)*

Sample	Ca-Smectite	IS-ml	Illite (1M)	Illite (2M1)	Chlorite	Kaolinite + KS-ml	Σ clay	Quartz	K-feldspar	Plagioclase	Pyrite	Calcite	Anatase	Σ total
orig., compact. **No19**	5% (±0.9)	14% (±0.3)	34% (±0.9)	6% (±0.3)	3% (±0.3)	16% (±0.6)	78%	15% (±0.6)	3% (±0.2)	3% (±0.2)	<1% (±0.1)		1% (±0.1)	100%
35°C, 46.3h, OPA **No10**	6% (±0.3)	13% (±1.6)	26% (±0.7)	7% (±0.3)	6% (±0.6)	11% (±0.5)	69%	22% (±0.8)	5% (±0.3)	3% (±0.2)	<1% (±0.1)	*<1% (±0.1)	1% (±0.1)	100%
60°C, 45.9h, OPA **No11**	5% (±0.5)	13% (±0.4)	28% (±0.9)	8% (±0.3)	5% (±0.6)	15% (±0.6)	73%	17% (±0.8)	5% (±0.3)	3% (±0.2)	<1% (±0.1)	*	1% (±0.1)	100%
100°C, 40h, OPA **No16**	6% (±0.8)	16% (±0.6)	26% (±0.6)	8% (±0.2)	5% (±0.4)	15% (±0.5)	75%	16% (±0.5)	4% (±0.3)	3% (±0.2)	<1% (±0.1)	*<1% (±0.2)	1% (±0.1)	100%
125°C, 40h, OPA **No20**	3% (±0.6)	16% (±1.0)	33% (±1.0)	7% (±0.4)	8% (±0.8)	12% (±0.8)	78%	15% (±0.9)	3% (±0.2)	3% (±0.3)	<1% (±0.1)		1% (±0.1)	100%
150°C, 68.3 h, OPA **No21**	8% (±1.6)	13% (±0.5)	30% (±1.2)	7% (±0.4)	3% (±0.6)	16% (±0.8)	76%	16% (±0.5)	3% (±0.2)	4% (±0.3)	<1% (±0.1)		1% (±0.1)	100%
without transport cell														
100°C, OPA **No12**	7% (±0.4)	7% (±0.5)	29% (±0.9)	8% (±0.4)	4% (±0.6)	18% (±0.7)	73%	19% (±0.5)	4% (±0.3)	3% (±0.3)	<1% (±0.1)	<1% (±0.1)	1% (±0.1)	100%

***Legend:** * - including indications by TG for additional amount of amorphous calcium carbonate; (±0.1) – standard deviation, absolute*

Smectite is mainly to find in Friedland Clay-series in illite-smectite mixed layers (a minor phase) with K- and/or charge deficiency (diVS-ml) and in Ca-smectite as well as kaolinite-smectite mixed layer phases (both are trace phases). Smectite in diVS-ml phases shows only a slight ratio of beidellite. Moreover, in Ca-smectite, beidellite is the dominating smectite component.

The main phase in Friedland Clay is illite accompanied by kaolinite and quartz as further minor phases. In traces, the Friedland Clay also contains chlorite, feldspar, pyrite, calcite and anatase. Calcite occurs as crystalline calcite and probably also as amorphous calcite carbonate. Compaction of clay material and the percolation and heating processes during the experiments don't cause any mineralogical neoformations (tab. 7).

Validation of Friedland Clay composition by literature

The validation of own Friedland Clay measurements with data from literature is difficult. The open cast mining company of deposit "Siedlungsscholle" has closed and covered the well-known old areas of this deposit and opened here a new exploitation field at the east margin. This material is located at the margin of deposit and was in contact with glacial water in Pleistocene. For this new opened Eastfield, no new published data were not to find. A comparison of published mineralogical results ("Siedlungsscholle"), the recent own measurement No19, and a former own measurement from neighboured deposit "Burgscholle" (tab. 8) shows a remarkable coincidence of mineral matter

Tab. 8. *Friedland Clay (initial) composition – own measurement of this project (No19) in comparison with literature and former own other measurements*

	|----	*Deposit: Siedlungsscholle*			----|	*|- Burgscholle -|*
Phase	***Henning (1971)***	**Hoang (2006)**	**Karnland et al. (2006)**	**FIM (2009)**	**own sample (No19)**	***Tonmehl, Juli 2021***
Ca-smectite					5%	
Illite-smectite mixed layer structure	44%	40%	56%	33-42%	14%	12%
Illite 2M1	12%	14%	7%	25-30%	6%	33%
Illite 1M					34%	9%
Kaolinite (+ Chlorite)	11%	12%				
Kaolinite			11%	10-13%	16%	17%
Chlorite				3-4%	3%	5%
Quartz	24%	27%	20%	16-20%	15%	16%
Feldspar	5%					
Plagioclase				0-2%	3%	2%
K-Feldspar		2%	1%	0-1%	3%	1%
Anatase, Rutile		1%			1%	1%
Gypsum			1%			2%
Pyrite	1%	traces	1%		<1%	1%

between sample No19 (belongs to “Siedlungsscholle” – new field at the east margin of this deposit) and the trade ware of deposit “Burgscholle”.

Glacitectonics in Pleistocene divided the occurrence of Friedland clay in few separate blocks (Schollen). The block “Siedlungsscholle” is the source of Friedland clay used in this project. Another block, “Burgscholle”, is located only few kilometres to east from “Siedlungsscholle”. The material from deposit “Burgscholle” is characterized by a higher degree of interaction with former glacial water.

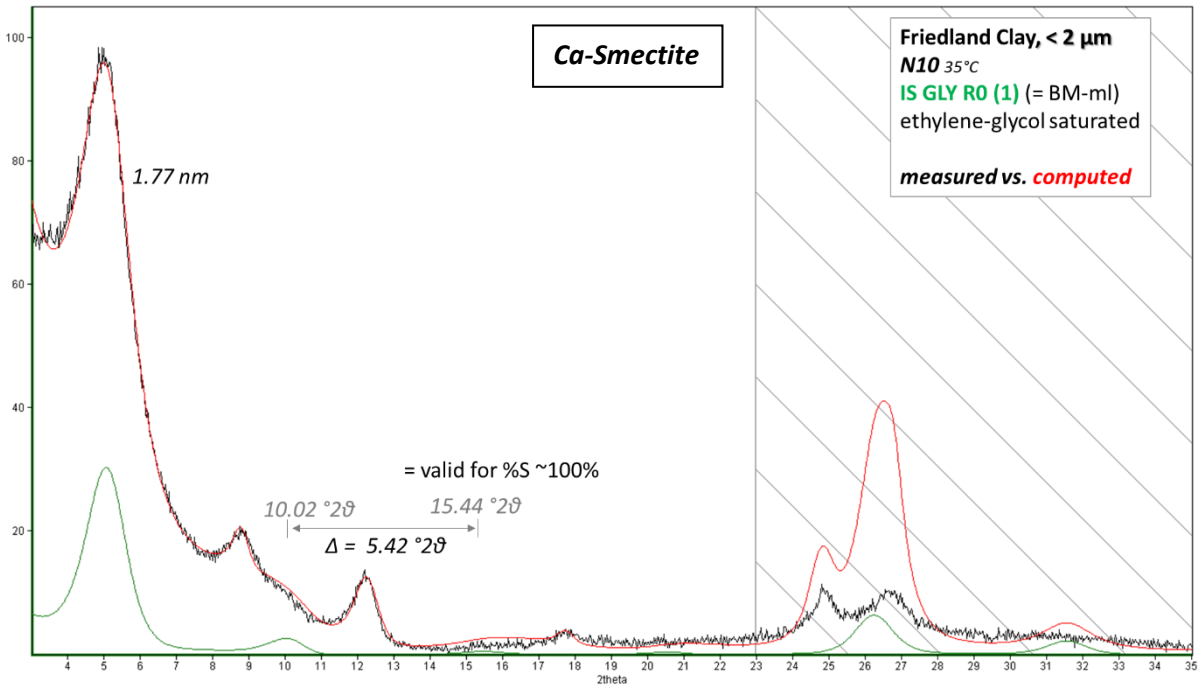

Fig. 11. *Friedland Clay No10, 35°C, 46.3 h (< 2 µm) - X-ray diffraction pattern of the ethylene-glycol saturated oriented specimen (with computing of Ca-smectite by Sybilla-software – green line)*

Beidellite-rich Ca-Smectite

Identification by XRD: The X-ray diffraction pattern of the ethylene-glycol saturated oriented specimen of samples "Friedland initial", "No10" (35°C) and "No11" (60°C) show an expandability closed to 1.7 nm or higher and a difference at 5.42-5.68°2θ between 2. and 3. order of smectite interferences (fig. 11). This distance is typically for full expandable smectite like montmorillonite (Moore & Reynolds, 1997) or beidellite.

The XRD-pattern of bulk samples show for all samples the occurrence of Ca-smectite ((tab. 7)). Otherwise, only for the above mentioned three samples were found phases with a full expandability in the clay fraction (< 2 µm).

Mineral formula by TEM-EDX and clustering: The full expandability of ethylene-glycol saturated oriented specimen let assume Si-values close to 4 per $(OH)_2\ O_{10}$ in computation of mineral formula by TEM-EDX-analyses, but values have been calculated between 3.53 - 3.56 e phuc. This situation is considered as intergrowth between beidellite (Si ~ 3.5), montmorillonite (Si ~ 4) and sometimes also in interstratification with illite (Si ~ 3.2).

Beidellite-ratio in Ca-smectite is dominating in all three mentioned samples. The BMI-ratios for these three samples indicate the occurrence of pure beidellite (but "Friedland initial" with 20% illite layer probability). The calculated structural formulae (tab. 9) show variable tetrahedral Si-values (from 3.53 - 3.56 e phuc), but the full expandability is stable nearby in all mentioned three samples (tab. 9).

Tab. 9. *Structural formulae for Ca-smectite in Frieland Clay-series with estimation of beidellite-ratio*

		phase (low illite)		mineral formula *(clustering of TEM-EDX-results)*										%S *(XRD-oriented)*	mass-% *(XRD-oriented)*
				Ca	Mg	Na	K	Al	Fe^{3+}	Mg	Ti	Al	Si		
Original	Friedland	BMI	60:20:20	0.02	0.10	0.00	0.29	1.30	0.58	0.11	0.02	0.45	3.55	82%	11%
orig., compr.	No19														
OPA, 35°C	No10	BMI	95:05:00	0.04	0.03	0.14	0.35	1.21	0.58	0.19	0.02	0.47	3.53	100%	11%
OPA, 60°C	No11	BMI	80:15:05	0.09	0.02	0.03	0.32	1.20	0.61	0.19	0.02	0.44	3.56	94%	17%
OPA, 100°C	No16														
OPA, 125°C	No20														
OPA, 150°C	No21														

Legend: *BMI – beidellite-montmorillonite-illite; %S – probability of smectite layer*

Further indications by FTIR: The Al-OH-Fe^{3+} band at 882 cm^{-1} had a low intensity reflecting the high Fe content of Friedland clay (Craciun, 1984; Russell & Fraser, 1994; Vantelon et al., 2001; Gates, 2005).

Development of mass-distribution: Ca-smectite shows a nearby constant mass distribution in all experimental stages (fig. 12) surrounding a level at 5-6%.

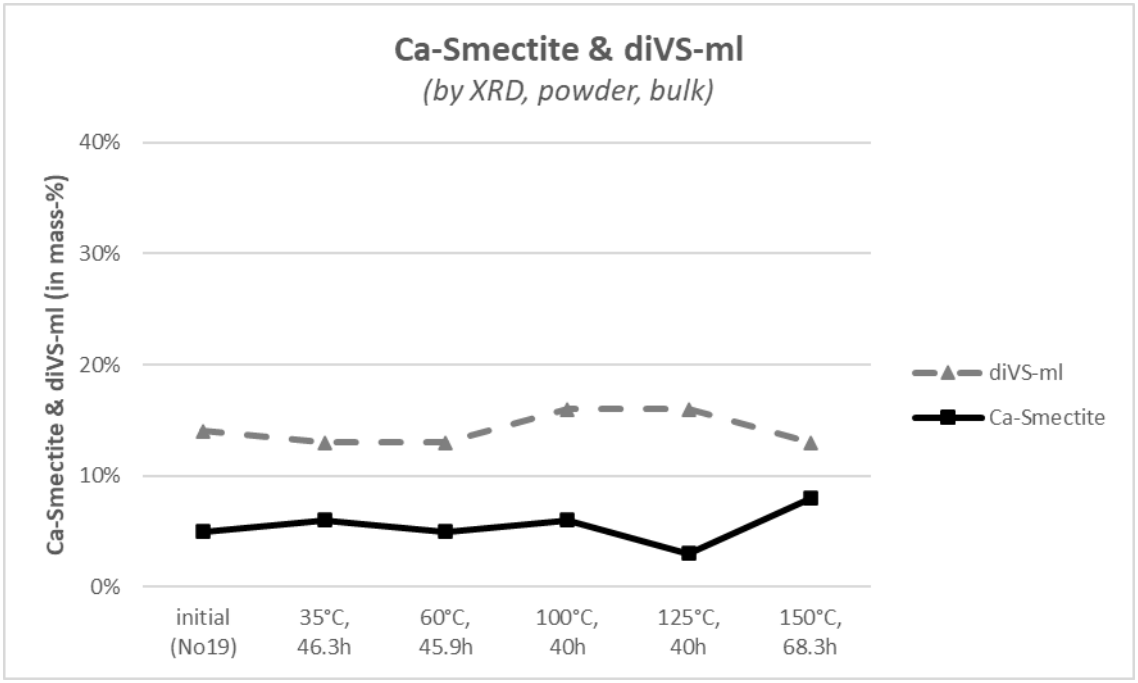

Fig. 12. *Mass distribution of Ca-smectite (black line) and diVS-ml (dashed line) in bulk samples of Friedland Clay-series*

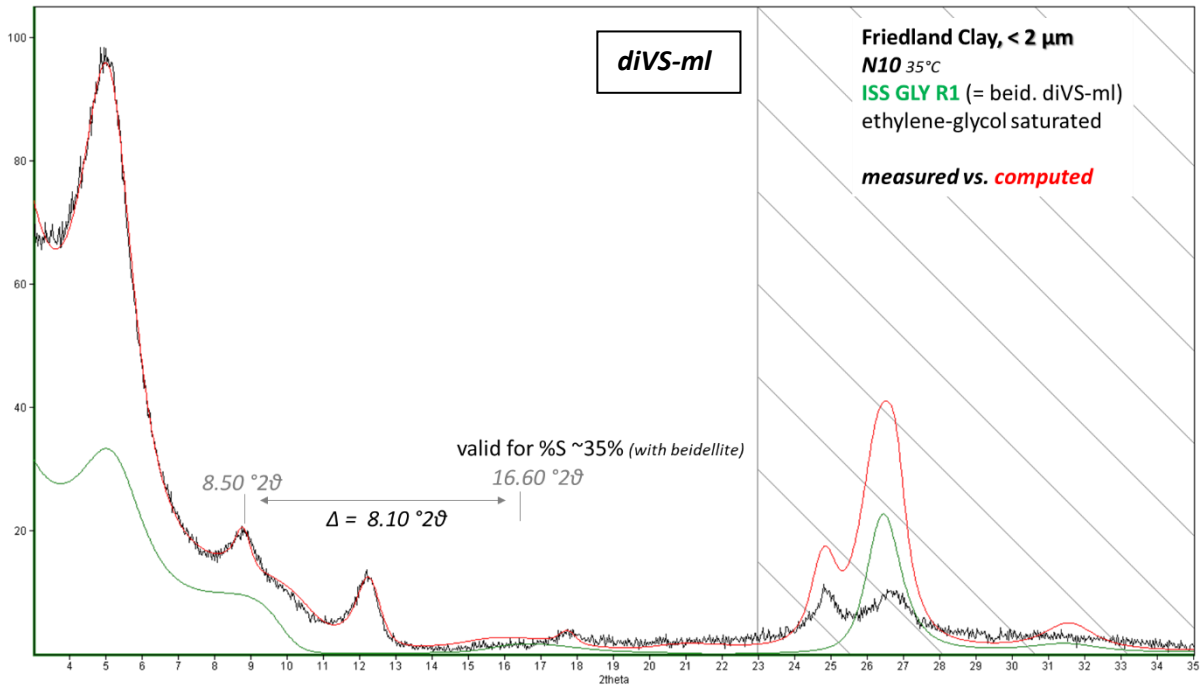

Fig. 13. *Friedland Clay N10, 35°C (< 2 µm) - X-ray diffraction pattern of the ethylene-glycol saturated oriented specimen (with computing of diVS-ml by Sybilla-software – green line)*

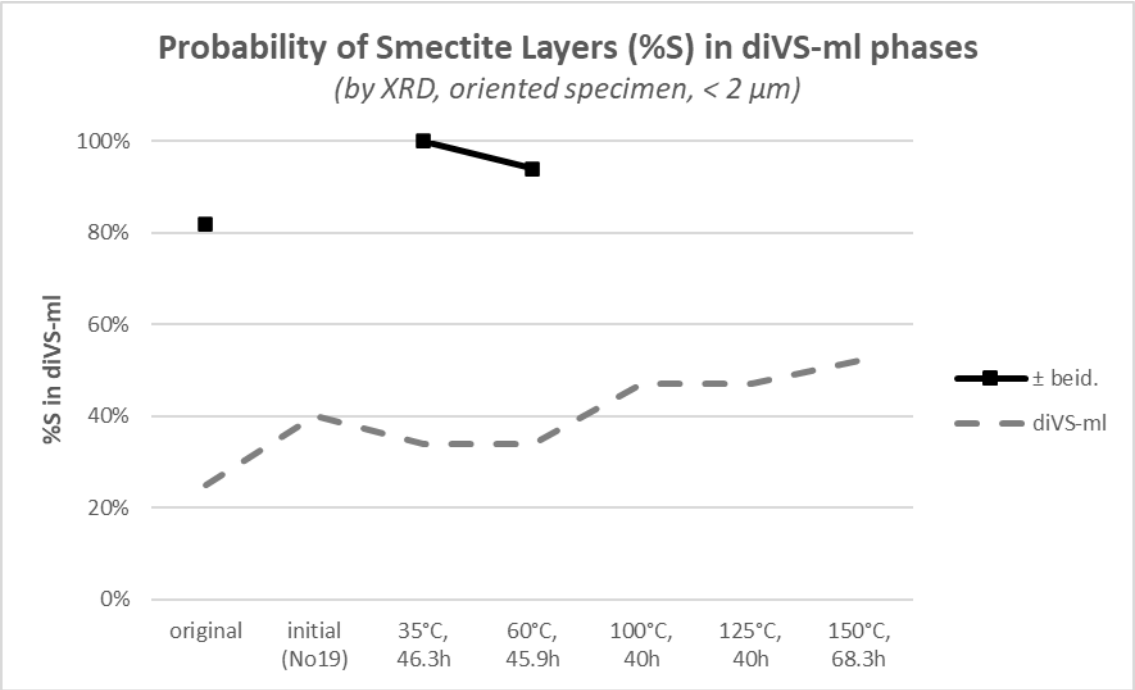

Fig. 14. *Smectite layer probability of beidellite (solid line) and diVS-ml (dashed line) in fraction < 2 µm of Friedland Clay-series*

Dioctahedral Vermiculite-Smectite Mixed-Layer (diVS-ml)

Identification by XRD: The X-ray diffraction pattern of the ethylene-glycol saturated oriented draws a further group of swelling clay mineral phases. The difference between 2. and 3. order of smectite interferences is variable representing smectite layer probabilities (%S) between 10 - 52% (see example: fig. 13). These diVS-ml phases are distributed in two groups: (i) %S at 40% (from %S = 34% to %S = 52%) and (ii) %S at 20% (from %S = 10% to %S = 30%) (tab. 10). The smectite layer probability (%S) of uncompacted original Friedland Clay is to find at %S = 25%.

Mineral formula by TEM-EDX and clustering: The cross-checking between phases with limited expandability of ethylene-glycol saturated oriented specimen and TEM-EDX-data (incl. clustering) shows illite-smectite mixed layer phase with K- and charge deficiency. These phases are mainly dominated by montmorillonite as smectite component. Beidellite occurs in diVS-ml only in traces (tab. 10). That means, increased tetrahedral Si-values after experiments are linked with rising swelling properties by a decreased illite layer probability (%I).

Development of mass-distribution: diVS-ml phases show with a slight variable mass distribution (13%-16%) close to the original composition (fig. 12, tab. 7).

Development of expandability: diVS-ml phases in fraction < 2 µm of Friedland Clay-series draw a slight increasing smectite layer probability with increasing thermal load in experiments from %S = 25% (Friedland initial) to 52% (150°C) (fig. 14).

Tab. 10. *Structural formulae for diVS-ml phases in Friedland Clay samples with estimation of beidellite-ratio*

		phase (high illite)	mineral formula (clustering of TEM-EDX-results)										%S (XRD-oriented)	mass-% (XRD-oriented)
			Ca	Mg	Na	K	Al	Fe^{3+}	Mg	Ti	Al	Si		
Original	Friedland	BMI 05:20:75	0.01	0.08	0.01	0.45	1.50	0.40	0.08	0.03	0.63	3.37	25%	2%
initial	No19	BMI 00:40:60	0.03	0.01	0.27	0.35	1.16	0.60	0.21	0.01	0.49	3.51	40%	54%
		BMI 30:10:60	0.02	0.03	0.20	0.48	1.42	0.42	0.14	0.01	0.63	3.37	40%	
OPA, 35°C	No10	BMI 15:20:65	0.04	0.09	0.13	0.31	1.43	0.46	0.10	0.01	0.59	3.41	34%	40%
OPA, 60°C	No11	BMI 00:35:65	0.10	0.05	0.03	0.31	1.24	0.58	0.15	0.03	0.52	3.48	34%	49%
OPA, 100°C	No16	BMI 15:20:65	0.01	0.04	0.12	0.49	1.40	0.45	0.14	0.01	0.59	3.41	36%	11%
		BMI 10:40:50	0.03	0.03	0.13	0.37	1.20	0.62	0.16	0.01	0.47	3.53	47%	57%
OPA, 125°C	No20	BMI 15:30:55	0.05	0.01	0.23	0.38	1.15	0.60	0.24	0.01	0.51	3.49	47%	67%
		BMI 00:10:90	0.05	0.07	0.16	0.34	1.54	0.37	0.08	0.01	0.68	3.32	10%	6%
OPA, 150°C	No21	BMI 05:45:50	0.03	0.02	0.12	0.35	1.20	0.61	0.18	0.01	0.42	3.58	52%	51%
		BMI 10:20:70	0.02	0.07	0.09	0.41	1.46	0.43	0.09	0.02	0.62	3.38	30%	7%

Legend: *BMI – beidellite-montmorillonite-illite; %S – probability of smectite layer*

Tab. 11. *Mineral matter of Friedland Clay-series (< 2 µm) – oriented specimen*

Sample	Ca-Smectite (BMI-ml) *(IS GLY R0_V1)*	beid. diVS-ml *(IS GLY R0_V2 or ISS GLY R1)*	Illite	Chlorite	Kao-linite	Kaolinite-Smectite-ml *(KS GL R0)*		*Σ total*
FRIEDLAND* original	11% *(%S = 82%)*	2% *(%S = 25%)*	13%	15%	48%	11% *(%S = 23%)*		*100%*
initial **No19**		54% *(%S = 39%)*	16%	2%	10%	17% *(%S = 48%)*		*99%*
35°C, 46.3h **No10**	11% *(%S = 100%)*	40% *(%S = 34%)*	11%		12%	27% *(%S = 51%)*		*101%*
60°C, 45.9h **No11**	17% *(%S = 94%)*	49% *(%S = 34%)*	7%		13%	14% *(%S = 48%)*		*100%*
100°C, 40h **No16**		11% *(%S = 36%)* 57% *(%S = 47%)*	16%		13%	4% *(%S = 50%)*		*101%*
125°C, 40h **No20**		6% *(%S = 10%)* 67% *(%S = 47%)*	11%		10%	6% *(%S = 48%)*		*100%*
150°C, 68.3h **No21**		7% *(%S = 30%)* 51% *(%S = 52%)*	24%	4%	9%	6% *(%S = 50%)*		*101%*
without transport cell *100°C* **No12**	35% *(%S = 79%)*	27% *(%S = 34%)*	11%		11%	16% *(%S = 40%)*		*100%*

Kaolinite-Smectite Mixed-Layer (KS-ml)

Identification by XRD: The occurrence of kaolinite-smectite mixed layer is mainly indicated by modelling of XRD-pattern of oriented specimen using Sybilla-software (developed by Chevron Inc.: Aplin et al., 2006) (tab. 11; fig. 15). Few particles, measured by TEM-EDX, indicated the occurrence of KS-ml phases, but it was not possible to calculate a valid structural formula.

Development of mass-distribution: KS-ml phases in fraction < 2 µm show a variable development without any significant trend with increasing thermal load (fig. 16).

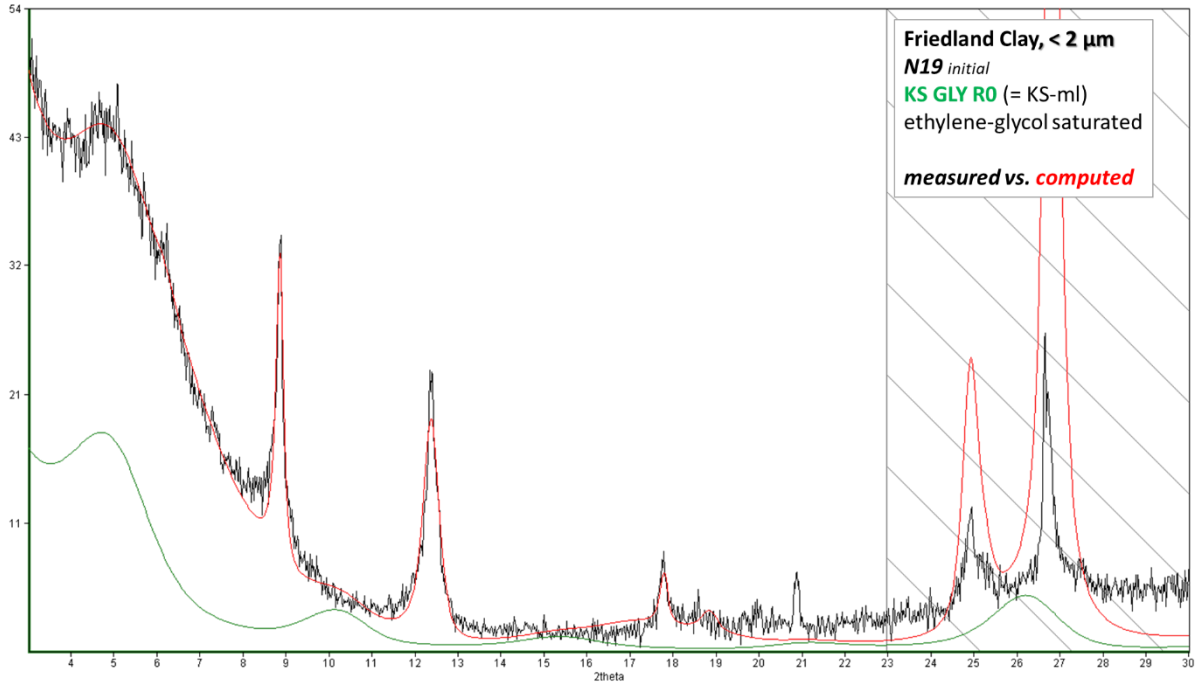

Fig. 15. *Friedland Clay No19, initial (< 2 µm) - X-ray diffraction pattern of the ethylene-glycol saturated oriented specimen (with computing of KS-ml by Sybilla-software – green line)*

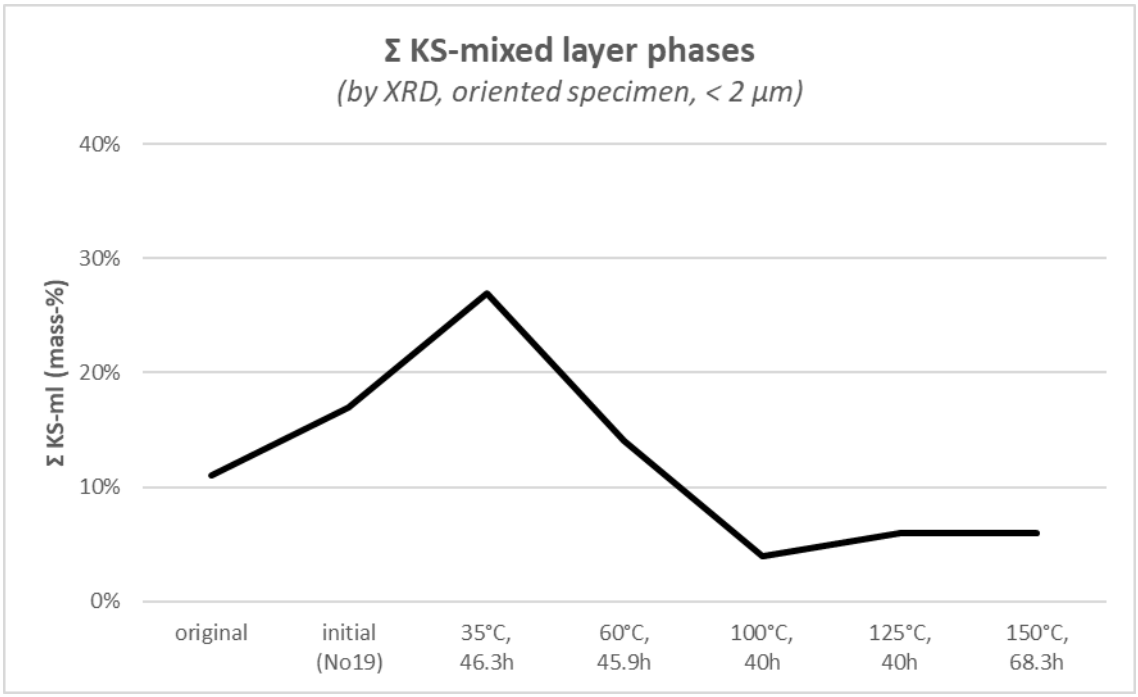

Fig. 16. *Mass distribution of KS-ml in samples of Friedland Clay-series (< 2 µm)*

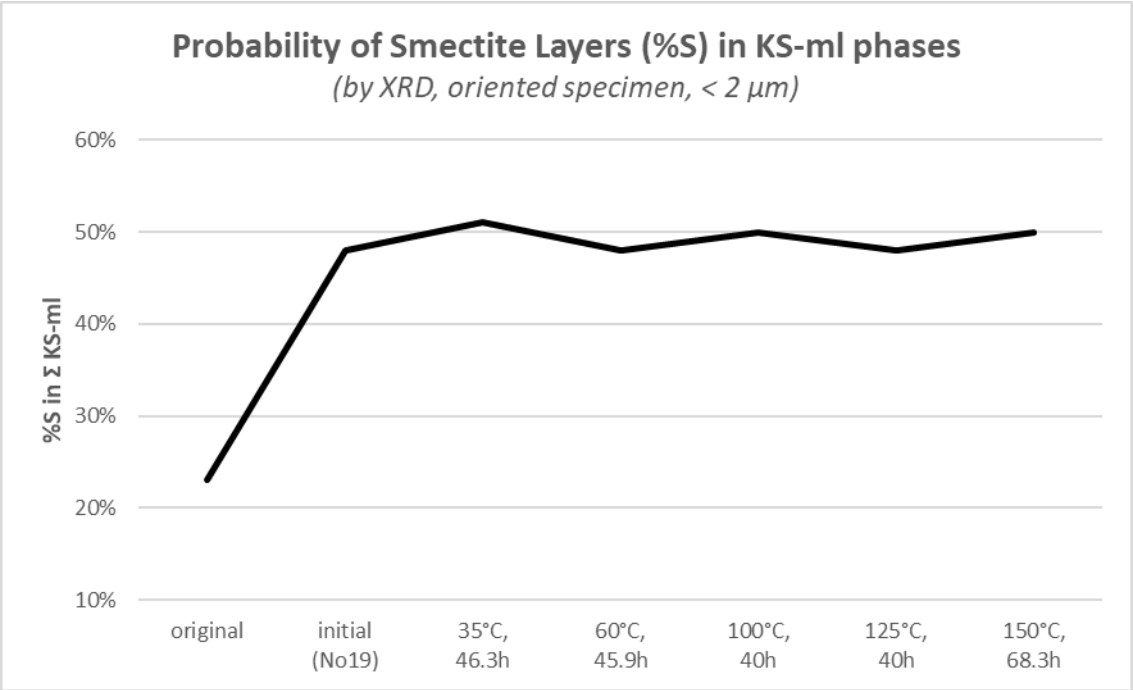

Fig. 17. *Smectite layer probability of KS-ml in fraction < 2 µm of Friedland Clay-series*

Development of expandability: KS-ml phases in Friedland Clay-series (< 2 µm) draw a higher smectite layer probability than %S=23% from original Friedland Clay staying to close to 50% (fig. 17). With increasing thermal load, the smectite layer probability is running nearby constant at %S= ~50%.

Smectite-behaviour in experiments

Smectite is the main responsible mineralogical phase, which determines the swelling behaviour of clays. In Friedland Clay, smectite is distributed in three different groups of phases (Ca-smectite, diVS-ml, KS-ml). Each group has shown a specific behaviour during the experiments (tab. 12).

Tab. 12. *Friedland Clay – Overview about different smectite behaviour (in direction of rising thermal load in experiments)*

	role of phase in bulk sample	smectite species	mass-% development	%S-development	assumptions to expandab.
Ca-smectite	minor phase, trace *(tab. 7)*	beidellite >> montm. *(tab. 9)*	± constant *(at 5% - 6%)* *(fig. 12)*	± constant *(at %S=100%, only ≤60°C)* *(tab. 9) (fig. 14)*	slight impact for increasing in low temperat. level
diVS-ml	minor phase *(tab. 7)*	montm. >> beidellite *(tab. 10)*	± stable *(variable 13%-16%)* *(fig. 12)*	rising *(from 25% to 52%)* *(fig. 14)*	impact for rising
KS-ml	minor phase *(tab. 7)*	not to determine	± stable *(< 2 µm: variable at 10 %) (fig. 16)*	constant *(< 2 µm: ~50%)* *(fig. 17)*	constant contribution for expanda-bility

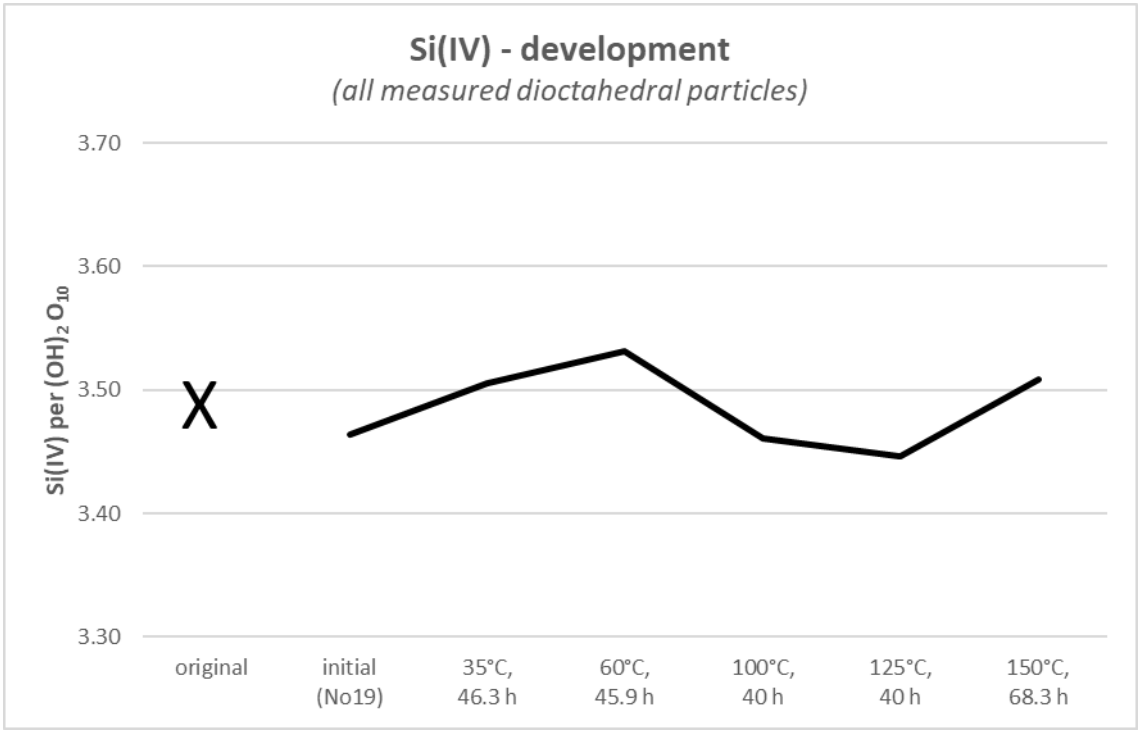

Fig. 18. *Behaviour of tetrahedral Si per $(OH)_2$ O_{10} in fraction < 2 µm of Friedland Clay*
Note: *KS-ml not included here*

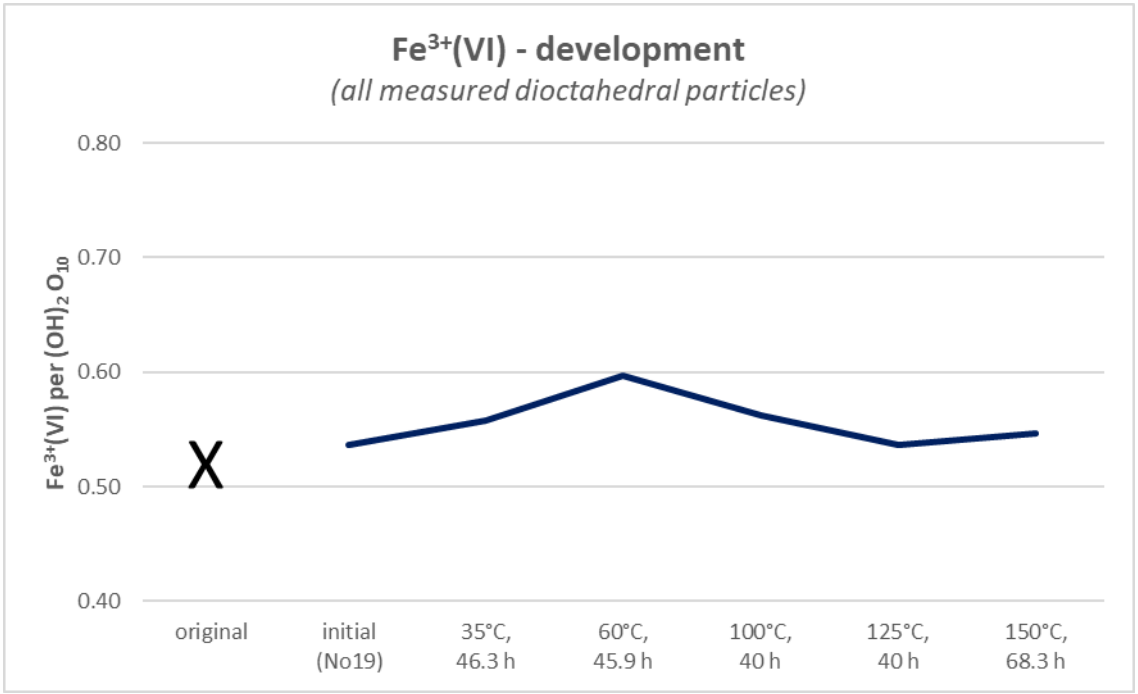

Fig. 19. *Development of octahedral Fe^{3+} per $(OH)_2$ O_{10} in fraction < 2 µm of Friedland Clay*
Note: *KS-ml not included here*

The summarizing impact of Ca-smectite including with diVS-ml on expandability is mirrored by TEM-EDX-measurements (fig. 18)/. The original material shows an average value for development of tetrahedral Si-value per $(OH)_2$ O_{10} with Si = 3.49. The tetrahedral Si-values of all measured particles from all experiments are constant with a slight variability from Si 3.45 – 3.53. A trend related to increasing thermal load by experiments is not to recognize.

The octahedral layer of all Ca-smectite and diVS-ml phases don't show real changes in all experiments (fig. 19).

The additional contribution of KS-ml on expandability of the total sample is not real to evaluate. The variable mass distribution of KS-ml (< 2 µm) by higher thermal load during the experiments (tab. 12; fig. 16) and the even constant smectite layer probability (tab. 12; fig. 17) let assume a more stabilizing contribution for expandability of sample.

TEM-EDX: Illite-behaviour in experiments

Ca. 20% of all measured particles in each sample were identified as illite. A very limited number of illite particles (N10 – 35°C) or a lack of illite particles (N11 – 60°C) was only detected in these two samples.

The available TEM-EDX-measurements indicate the occurrence of only one illite group: Al(VI)-rich, with a high to moderate K-deficit and Fe(VI) at 0.4 per $(OH)_2\ O_{10}$ (tab. Illite_Friedland). The composition of this illite group is stable in all experiments – exception: experiment at 125° (sample N20). Illite in sample N20 shows an octahedral Al-enrichment substituting Fe(VI).

The reduced number or the lack of illite in samples N10 and N11 could be caused by a slight smectitization of illite particles (fig. 18). The Al-development of illite in sample N20 (125°C) let assume a degradation of larger illite particles, which than feed the fine fraction < 2 µm.

	Ca (XII)	Mg (XII)	Na (XII)	K (XII)	Cr3+ (VI)	Al (VI)	Fe3+ (VI)	Mg (VI)	Ti (VI)	Al (IV)	Si (IV)	XII	n_VI	%S	K-deficit	charge-deficit
Friedland original																
Cluster1 *(n=15)*	0.01	0.07	0.01	0.54	0.00	1.49	0.39	0.08	0.05	0.70	3.30	0.72	2.0	9	45%	15%
No19 *initial*																
Cluster2 *(n=15)*	0.03	0.03	0.25	0.47	0.00	1.42	0.42	0.13	0.02	0.71	3.29	0.83	2.0	9	52%	2%
Opalinus treated																
N10 *35°C, 48.3h*																
Cluster1 *(n=4)*	0.02	0.07	0.14	0.45	0.00	1.49	0.41	0.09	0.00	0.67	3.33	0.76	2.0	12	56%	8%
N11 *60°C, 45.9h*	Note: No illite measured by TEM-EDX.															
N16 *100°C, 40h*																
Cluster1 *(n=20)*	0.01	0.03	0.10	0.65	0.00	1.46	0.40	0.12	0.02	0.75	3.25	0.84	2.0	6	31%	2%
No20 *125°C, 40h*																
Cluster1 *(n=21)*	0.05	0.08	0.17	0.34	0.00	1.61	0.33	0.07	0.01	0.74	3.26	0.77	2.0	7	65%	11%
No21 *150°C, 68.3h*																
Cluster2 *(n=16)*	0.02	0.07	0.09	0.49	0.00	1.48	0.40	0.09	0.04	0.72	3.28	0.75	2.0	8	49%	12%

Tab. Illite_Friedland. *Friedland Clay: Illite in fraction < 2 µm (by TEM-EDX)*

Legend: *(n=4) – number of illite particles measured by TEM-EDX; XII – interlayer charge; n_VI – number of atoms in octahedral layer per $(OH)_2\ O_{10}$; %S – probability of smectite layers in senso of Środon et al. (1992); K-deficit, charge-deficit – in senso of Środon et al. (1992) (normal K in illite = 0.89 per $(OH)_2\ O_{10}$)*

3. Mineral matter in Opalinus Clay

Tab. 13. *Mineral matter of Opalinus Clay-series (bulk sample)*

Sample	Ca-Smectite	diVS-ml	Illite (1M)	Illite (2M1)	Chlorite	Kaolinite + KS-ml	Σ clay	Quartz	K-feldspar	Plagioclase	Pyrite	Calcite	Siderite	Dolomite	Anatase	Σ total
Opalin. Clay original, BLT-A7		3% (±0.4)	4% (±0.3)	18% (±0.9)	12% (±0.7)	25% (±3.0)	*61%*	13% (±0.5)	1% (±0.2)	4% (±0.2)	1% (±0.1)	17% (±0.6)	1% (±0.1)	2% (±0.1)		*100%*
. Opalin. Clay original, BFS-B12 **No6**		9% (±0.5)	2% (±0.2)	13% (±0.6)	4% (±0.3)	50% (±1.6)	78%	9% (±0.3)	1% (±0.2)	2% (±0.2)	<1% (±0.1)	8% (±0.3)	<1% (±0.1)	<1% (±0.1)	<1% (±0.1)	*100%*
35°C, 144h, OPA **No22** BFS-B12		12% (±0.7)	2% (±0.5)	22% (±0.8)	7% (±0.4)	25% (±1.2)	67%	14% (±0.5)	2% (±0.3)	3% (±0.3)	1% (±0.1)	10% (±0.1)	1% (±0.1)	1% (±0.1)	1% (±0.1)	*100%*
60°C, 45.4h, OPA **No9** BFS-B12		12% (±0.7)	1% (±0.3)	19% (±0.9)	3% (±0.3)	35% (±2.2)	69%	13% (±0.7)	1% (±0.2)	2% (±0.2)	1% (±0.1)	*10% (±0.3)	<1% (±0.1)	1% (±0.1)		*99%*
60°C, 95.3h, OPA **No7** BFS-B12		9% (±0.5)	1% (±0.4)	3% (±0.3)	<1% (±0.1)	13% (±0.8)	28%	6% (±0.4)	1% (±0.2)	1% (±0.2)	<1% (±0.1)	***60%** (±0.6)	<1% (±0.1)	1% (±0.1)		*98%*
100°C, 69.3h, OPA **No8** BFS-B12		12% (±1.0)	3% (±0.5)	11% (±0.4)	8% (±0.7)	27% (±1.2)	61%	14% (±0.6)	3% (±0.3)	4% (±0.3)	2% (±0.1)	*14% (±0.3)	2% (±0.1)	1% (±0.1)		*100%*
125°C, 48.5h, OPA **No14** BFS-B12		16% (±0.7)	5% (±0.5)	10% (±0.4)	7% (±0.9)	25% (±1.2)	63%	14% (±0.6)	3% (±0.3)	4% (±0.3)	1% (±0.1)	*11% (±0.3)	2% (±0.1)	<1% (±0.1)		*99%*
150°C, 48.6 h OPA **No13** BFS-B12		8% (±0.9)	<1% (±0.1)	16% (±1.1)	4% (±0.4)	53% (±3.2)	81%	8% (±0.5)	1% (±0.2)	1% (±0.1)	1% (±0.1)	*7% (±0.4)	<1% (±0.1)	<1% (±0.1)		*99%*
without transport cell																
35°C, OPA **No9a** BFS-B12		10% (±0.3)	2% (±0.2)	25% (±0.6)	4% (±0.5)	29% (±0.8)	70%	15% (±0.4)	1% (±0.2)	3% (±0.2)	1% (±0.1)	*9% (±0.2)	<1% (±0.1)	1% (±0.1)		*99%*
125°C, OPA **No9b** BFS-B12		10% (±0.4)	3% (±0.3)	20% (±0.6)	1% (±0.2)	32% (±0.9)	65%	14% (±0.3)	2% (±0.2)	2% (±0.2)	1% (±0.1)	*11% (±0.2)	<1% (±0.1)	1% (±0.1)		*96%*

Legend: ** - including indications by TG for additional amount of amorphous calcium carbonate; (±0.1) – standard deviation, absolute; BLT-A7, BFS-B12 - boreholes*

Note: *sample No7 ("white" clay) is composed mainly by calcite = indication for sometimes inhomogeneous distribution of calcite in sample body; all other samples belong to the so-called "grey" clay*

Smectite is to find in Opalinus Clay-series in illite-smectite mixed layers (a minor phase) with K- and/or charge deficiency (diVS-ml) and especially in kaolinite-smectite mixed layer phases (a main phase). Montmorillonite is the dominating smectite component.

Illite and kaolinite (incl. KS-ml) are the main phases in Opalinus Clay, accompanied by diVS-ml, quartz, and calcite as minor phases and in traces by chlorite, feldspar, pyrite, siderite, dolomite and anatase. Calcite occurs as crystalline calcite (see values in tab. 13) and additionally also as amorphous calcite carbonate. The percolation and heating processes during the experiments don't cause any mineralogical neoformations (tab. 13).

Validation of Opalinus Clay composition

The measured composition of original Opalinus Clay from the borehole BLT-A7 is in a good agreement (tab. 14) with already published data from literature (Gaucher et al., 2003; Bossart & Thury, 2008; Nagara, 2002). Differences between here presented own measurements and literature references are to recognize in the amount of diVS-ml (lower for own measurement). Thermogravimetric investigations of Opalinus Clay support the here reported results of diVS-ml, kaolinite, and carbonate amount (tab. 14). The differences in mass loss values of original sample BFL-B12 between measured by thermogravimetry and calculated from XRD-results indicate the occurrence of amorph calcium carbonate (ACC) (tab. 14).

Tab. 14. *Opalinus Clay (original) composition – own measurement in comparison with literature*

	Opalinus				
	own results				
	BLT-A7	BFL-B12	Pearson et al., 2003	Bossart & Thury, 2008 *(min-best-max)*	NAGRA, 2002
Ca-smectite					
IS-ml	3%	9%	11 - 20%	5 - 11 - 20%	11%
Illite_1M	4%	2%	17 - 40%	15 - 23 - 30%	23%
Illite_2M1	18%	13%			
Chlorite	12%	4%	5 - 20%	3 - 10 - 18%	10%
Kaolinite	25%	50%	15 - 32%	15 - 22 - 37%	22%
Σ clay	***61%***	***78%***		***28 - 66 - 93%***	***66%***
Quartz	13%	9%	6 - 17%	10 - 14 - 32%	14%
Orthoclase	1%	1%	1 - 2%	0 - 1 - 6%	1%
Albite	4%	2%	1 - 2%	0 - 1 - 2%	1%
Pyrite	1%	<1%	1 - 2%	0 - 1 - 3%	1%
Calcite	17%	8%	11 -28%	4 - 13 - 22%	13%
Siderite	1%	<1%	1 - 4%	0 - 3 - 6%	3%
Dolomite	2%	<1%	≤ 2%	≤ 1%	
Rutile		<1%			
Gypsum				≤ 0.5%	
Σ total	***100%***	***100%***			***99%***

DTG/TG, mass loss (as proof)			
300-1000°C *(as check for all phases)*			
meas. by TG	13.90%	13.73%	
calc. by XRD	13.89%	11.60%	
650-1000°C *(as check especially for calcite+dolomite)*			
meas. by TG	7.75%	7.23%	*This difference between TG and XRD let assume the additional occurrence of 6% ACC in BFL-B12.*
calc. by XRD	7.89%	4.35%	

Generally, the here reported compositions of untreated and treated bentonite were verified by combination of following methods:

- TEM-EDX results, cross-checked by oriented specimen (XRD) after Sybilla-modelling of probability of smectite layers, also offer indications to the occurrence of beidellite

- XRD of powder samples (bulk) has been cross-checked by thermogravimetry using the mass loss to verify especially the XRD-results to kaolinite, indications to kaolinite-smectite mixed layer phases, and carbonates (see example: tab. 2, tab. 14).

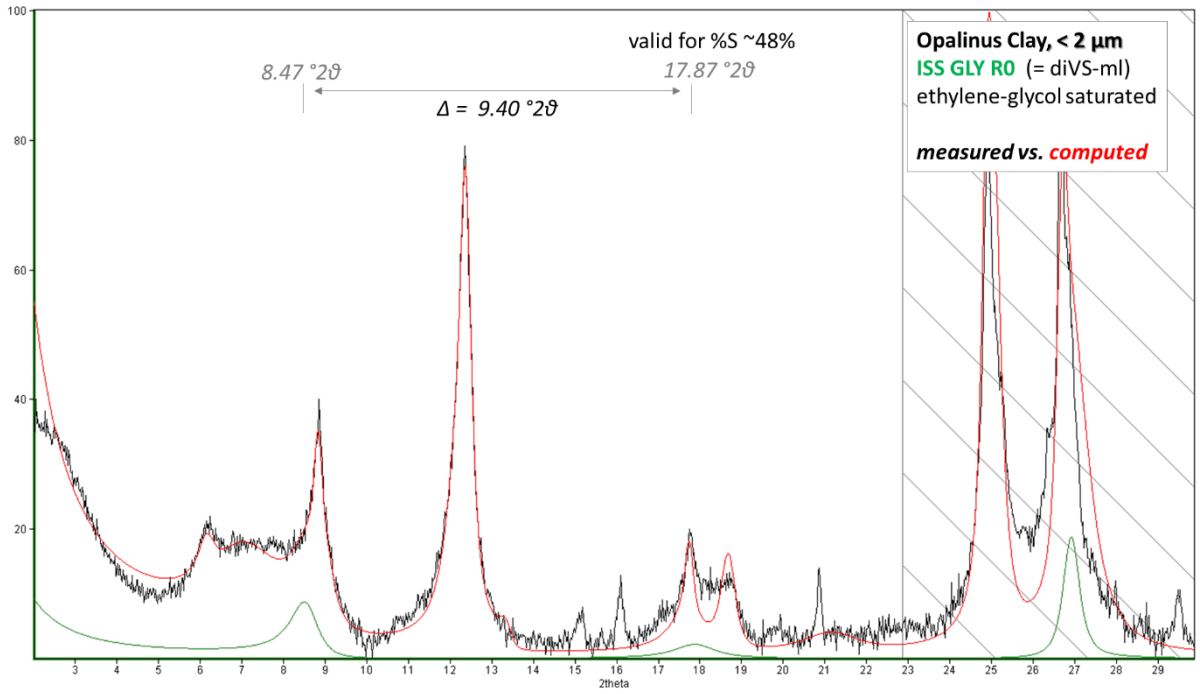

Fig. 20. *Opalinus Clay, original (< 2 µm) - X-ray diffraction pattern of the ethylene-glycol saturated oriented specimen (with computing of diVS-ml group I by Sybilla-software – green line)*

Tab. 15. *Structural formulae for diVS-ml phases (group I) in Opalinus Clay samples with estimation of beidellite-ratio*

		phase (low smectite)		mineral formula (clustering of TEM-EDX-results)										%S (XRD-oriented)	mass-% (XRD-oriented)
				Ca	Mg	Na	K	Al	Fe^{3+}	Mg	Ti	Al	Si		
Original	OPAL_40µm	BMI	10:40:50	0.08	0.04	0.00	0.44	1.39	0.41	0.20	0.00	0.47	3.53	48%	11%
		BMI	00:09:91	0.11	0.12	0.01	0.28	1.42	0.45	0.10	0.03	0.71	3.29	11%	18%
OPA, 35°C	No22	BMI	00:15:85	0.10	0.03	0.03	0.56	1.42	0.39	0.18	0.01	0.67	3.33	16%	44%
OPA, 60°C	No9	BMI	00:20:80	0.10	0.00	0.04	0.56	1.34	0.42	0.24	0.00	0.58	3.42	23%	21%
OPA, 100°C	No8	BMI	00:20:80	0.06	0.04	0.00	0.55	1.40	0.40	0.19	0.00	0.56	3.44	26%	22%
OPA, 125°C	No14	BMI	00:20:80	0.08	0.00	0.05	0.59	1.27	0.46	0.28	0.00	0.55	3.45	24%	31%
OPA, 150°C	N013	BMI	00:15:85	0.05	0.00	0.09	0.68	1.36	0.42	0.22	0.00	0.65	3.35	16%	42%

Legend: *BMI – beidellite-montmorillonite-illite; %S – probability of smectite layer*

Dioctahedral Vermiculite-Smectite Mixed-Layer (diVS-ml)

Identification by XRD: The X-ray diffraction pattern of the ethylene-glycol saturated oriented specimen draw for diVS-ml phases two groups of swelling. First group is characterized with a smectite layer probability (%S) at 15-20%. Exception: Opalinus clay, original contain two diVS-ml phases (tab. 15): (i) with %S = 50% (fig. 20) and (ii) with %S = 11%, both basing on the differences between 2. and 3. order of smectite interferences.

Second group of diVS-ml contains only traces of smectite (%S ≤ 5%) (tab. 16), even basing on the difference between 2. and 3. order of smectite interferences, close to pure illite.

Tab. 16. *Structural formulae for diVS-ml phases (group II) in Opalinus Clay samples with estimation of beidellite-ratio*

		phase (~ illite)	mineral formula (clustering of TEM-EDX-results)										%S (XRD-oriented)	mass-% (XRD-oriented)
			Ca	Mg	Na	K	Al	Fe^{3+}	Mg	Ti	Al	Si		
Original	OPAL_40µm													
OPA, 35°C	No22	BMI 00:05:95	0.10	0.14	0.03	0.33	1.58	0.37	0.05	0.01	0.80	3.20	0%	14%
		BMI 00:05:95	*0.10*	*0.10*	*0.02*	*0.51*	*1.26*	*0.55*	*0.16*	*0.03*	*0.82*	*3.18*		
OPA, 60°C	No9	BMI 00:05:95	0.15	0.07	0.04	0.43	1.41	0.43	0.14	0.02	0.81	3.19	0%	14%
OPA, 100°C	No8	BMI 00:05:95	0.12	0.13	0.04	0.32	1.56	0.38	0.07	0.00	0.82	3.18	0%	29%
OPA, 125°C	No14	*BMI 00:05:95*	*0.08*	*0.15*	*0.00*	*0.44*	*1.28*	*0.57*	*0.13*	*0.02*	*0.79*	*3.21*	0%	26%
		BMI 00:05:95	0.12	0.13	0.04	0.32	1.56	0.38	0.07	0.00	0.82	3.18		
OPA, 150°C	N013	*BMI 00:05:95*	*0.10*	*0.03*	*0.14*	*0.57*	*1.33*	*0.45*	*0.21*	*0.01*	*0.77*	*3.23*		
		BMI 00:00:100	*0.06*	*0.16*	*0.06*	*0.45*	*1.21*	*0.64*	*0.11*	*0.05*	*0.92*	*3.08*	0%	14%
		BMI 00:00:100	0.20	0.05	0.13	0.34	1.67	0.24	0.09	0.00	0.88	3.12		

Legend: *BMI – beidellite-montmorillonite-illite; %S – probability of smectite layer*

Mineral formula by TEM-EDX and clustering: The cross-checking between phases with limited expandability using ethylene-glycol saturated oriented specimen and TEM-EDX-data (incl. clustering) shows illite-smectite mixed layer phase with K- and charge deficiency. For these phases, montmorillonite is the only smectite component. Beidellite is to assume in traces (BMI 10:40:50) only in one sample, in diVS-ml of group I of untreated Opalinus Clay, original (tab. 15).

Further indications by FTIR: The $AlFe^{3+}OH$ band at 874 cm^{-1} shows a high intensity in comparison with 831 cm^{-1} of AlMgOH band. This is a sign of high content of Fe in octahedral sheet of dioctahedral minerals (e.g. smectite, illite, IS-ml) in Opalinus clay (Craciun, 1984; Gates, 2005).

Development of mass-distribution: diVS-ml phases (group I) show with increasing thermal load a broader variable mass distribution (absolute ± 10%) at the original composition of 29% (fig. 21).

Development of expandability: diVS-ml phases (group I) draw with increasing thermal load at the beginning a rising smectite layer probability from %S=11% (original Opalinus Clay) to close to 26% (100°C) and higher 100°C again a downfall to 16% (16%) (fig. 22). Otherwise, the high smectite diVS-ml phases of sample Opalinus original are immediately removed by the experiments.

Kaolinite-Smectite Mixed-Layer (KS-ml)

Identification by XRD: The occurrence of kaolinite-smectite mixed layer is mainly indicated by modelling of XRD-pattern of oriented specimen using Sybilla-software (developed by Chevron Inc.: Aplin et al., 2006) (tab. 17; fig. 23). Few particles, measured by TEM-EDX, indicated KS-ml phases, but it was not possible to calculate a valid structural formula.

Development of mass-distribution: KS-ml phases in fraction < 2 µm show as trend with increasing thermal load a slight decreasing ratio to the original composition (fig. 24). A cross-check between XRD powder analysis of bulk sample and thermogravimetry (bulk sample) indicates for sample "Opalinus, original" 20 % kaolinite and 5% KS-ml phases.

Development of expandability: KS-ml phases in Opalinus Clay (< 2 µm) draw with increasing thermal load a ± constant smectite layer probability at %S=40% (fig. 25).

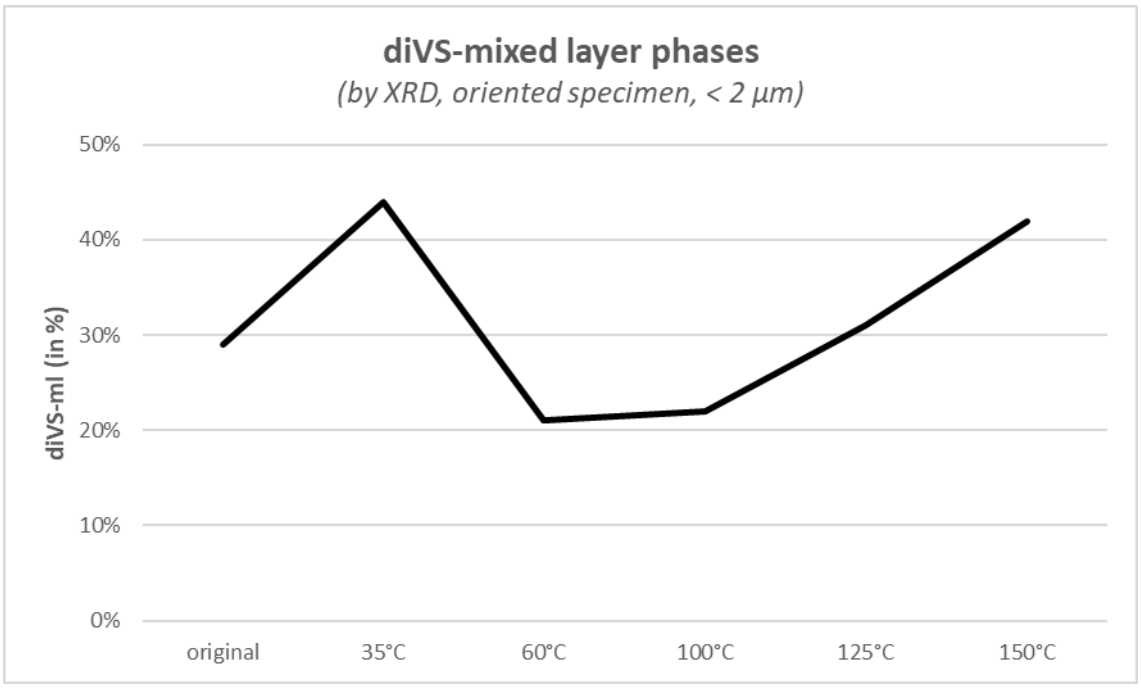

Fig. 21. *Mass distribution of diVS-ml (group I) in bulk samples of Opalinus Clay*

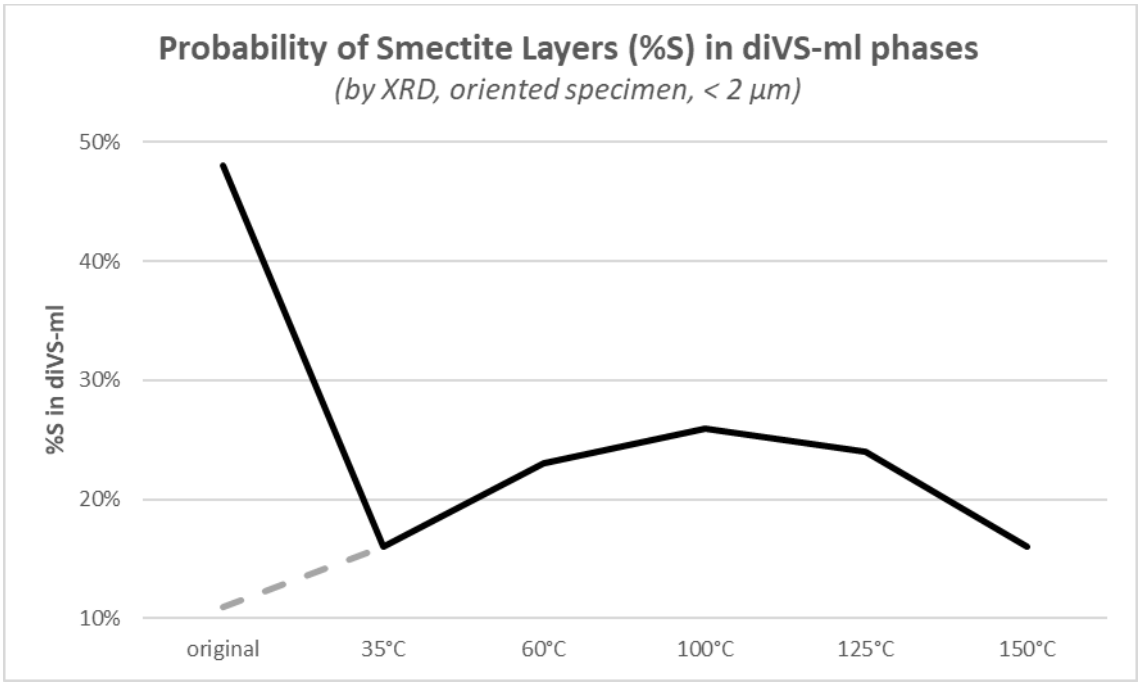

Fig. 22. *Smectite layer probability of diVS-ml (group I) in fraction < 2 µm of Opalinus Clay*

Tab. 17. *Mineral matter of Opalinus Clay (< 2 µm) – oriented specimen*

Sample	diVS-ml *(IS GLY R0)*	diVS-ml *(ISS GLY R0)*	Illite	Chlorite	Kao-linite	Kaolinite-Smectite-ml *(KS GL R0)*	Kaolinite-Smectite-ml *(KSS GL R0)*	*Σ total*
OPALINUS original	18% *(%S = 11%)*	11% *(%S = 48%)*	8%	8%	8%	20% *(%S = 14%)*	27% *(%S = 61%)*	*100%*
35°C, 144h **No22**	44% *(%S = 16%)*		14%	4%	7%		32% *(%S = 37%)*	*100%*
60°C, 45.4h **No9**	21% *(%S = 23%)*		14%	5%	16%	10% *(%S = 14%)*	34% *(%S = 53%)*	*100%*
60°C, 95.3h **No7**	32% *(%S = 20%)*		12%	5%	12%	13% *(%S = 9%)*	26% *(%S = 55%)*	*100%*
100°C, 69.3h **No8**	22% *(%S = 26%)*		29%	5%	12%	6% *(%S = 14%)*	27% *(%S = 53%)*	*101%*
125°C, 48.5h **No14**	31% *(%S = 24%)*		26%	5%	8%	12% *(%S = 26%)*	19% *(%S = 35%)*	*101%*
150°C, 48.6h **No13**	42% *(%S = 16%)*		14%	4%	8%	2% *(%S = 28%)*	30% *(%S = 45%)*	*102%*
Without transport cell *35°C* **No9a**	25% *(%S = 20%)*		14%	4%	15%	10% *(%S = 9%)*	31% *(%S = 55%)*	*99%*
125°C **No9b**	13% *(%S = 29%)*		30%	4%	13%	7% *(%S = 14%)*	35% *(%S = 56%)*	*102%*

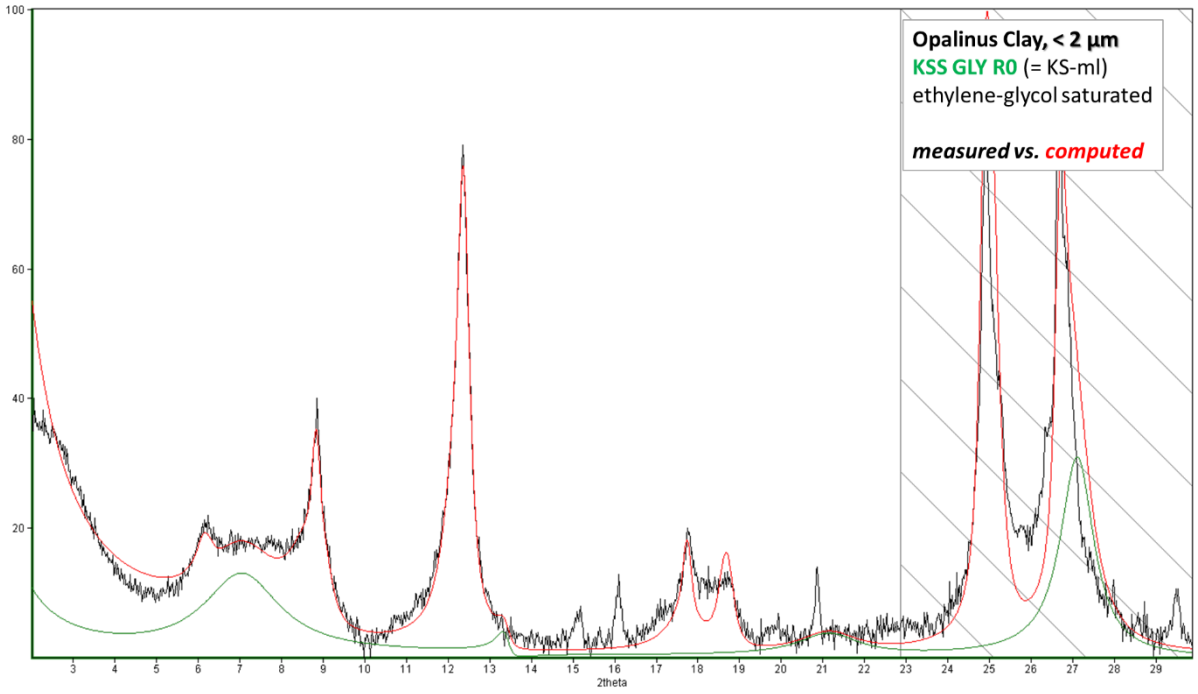

Fig. 23. *Opalinus Clay, original (< 2 µm) - X-ray diffraction pattern of the ethylene-glycol saturated oriented specimen (with computing of KS-ml by Sybilla-software – green line)*

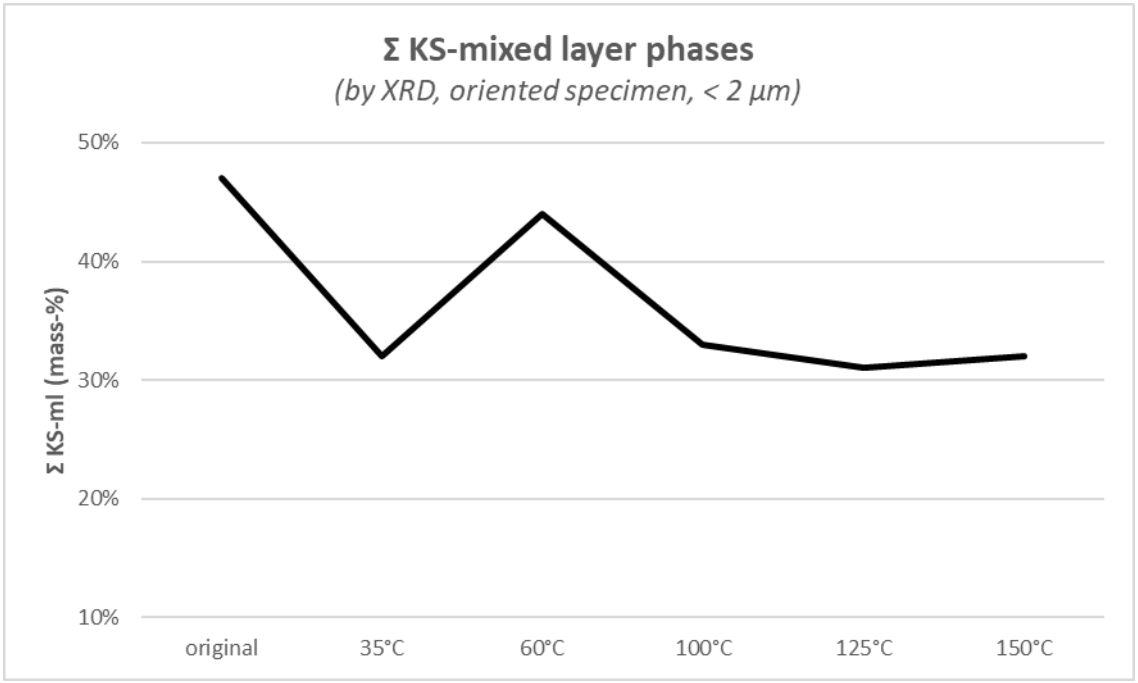

***Fig. 24**. Mass distribution of KS-ml in samples of Opalinus Clay (< 2 µm)*

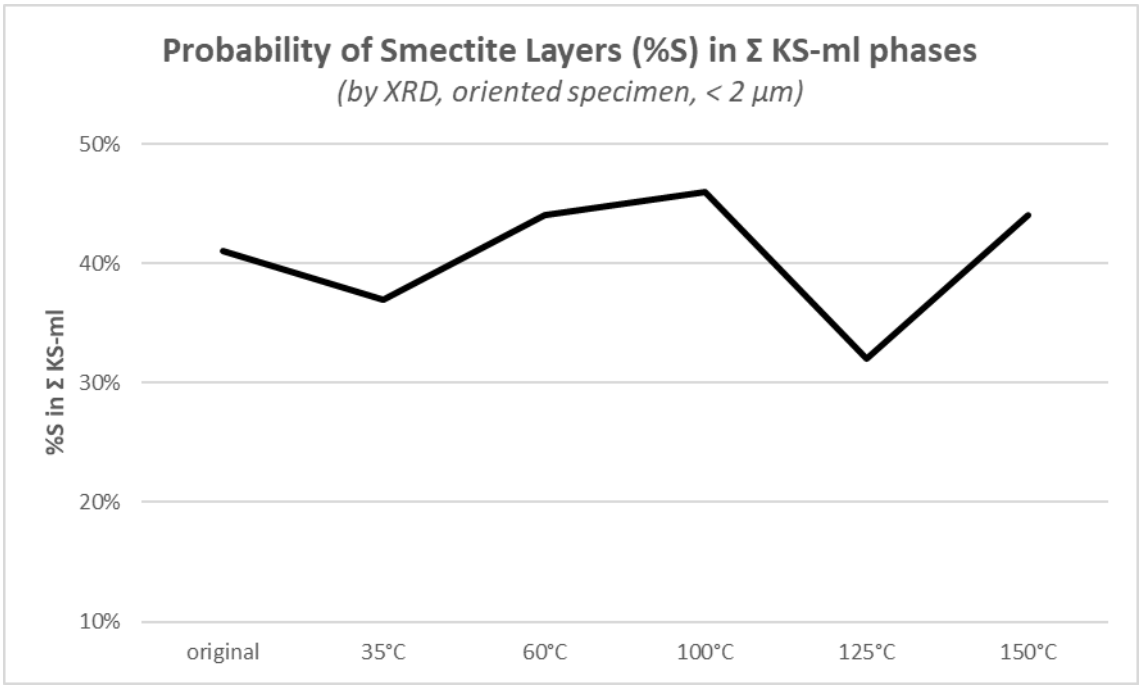

***Fig. 25.** Smectite layer probability of KS-ml in fraction < 2 µm of Opalinus Clay-series*

Smectite-behaviour in experiments

Smectite is the main responsible mineralogical phase, which determines the swelling behaviour of clays and bentonites. In Opalinus Clay, smectite is distributed in only two different groups of phases (diVS-ml, KS-ml). Each group has shown a specific behaviour during the experiments (tab. 18).

Tab. 18. *Opalinus Clay – Overview about different smectite behaviour (in direction of rising thermal load in experiments)*

	role of phase in bulk sample	smectite species	mass-% development	%S-development	assumptions to expandab.
diVS-ml *(%S ~ 50%)*	minor phase *(tab. 13)*	montm. >> beidellite *(tab. 15)*	destroyed by each experim. *(fig. 21)*	destroyed by each experim. *(fig. 22)*	reduction
diVS-ml *(%S ~ 20%)*	minor phase *(tab. 13)*	montm. *(tab. 15)*	no trend *(variable at 30% ±10%) (fig. 21)*	≤100°C: rising *(from 11% to 26%) (fig. 22)*	slight rising impact
KS-ml	minor phase *(tab. 13)*	not to determine	slight decreas. *(< 2 µm: 47% → 32%) (fig. 24)*	± stable *(< 2 µm: at 40% ±8%) (fig. 25)*	slight decreasing

The summarizing impact of diVS-ml phases on expandability is mirrored by TEM-EDX-measurements (fig. 26). The original material shows the highest tetrahedral Si-value per $(OH)_2\ O_{10}$ with Si = 3.46. The first Si-downfall to 35°C is caused by the loss of diVS-ml with %S~50% from untreated sample "Opalinus, original" (tab. 17). Following the %S-development of diVS-ml with %S ~ 20%, a rising smectite ratio is to observe also by Si-development until 100°C.

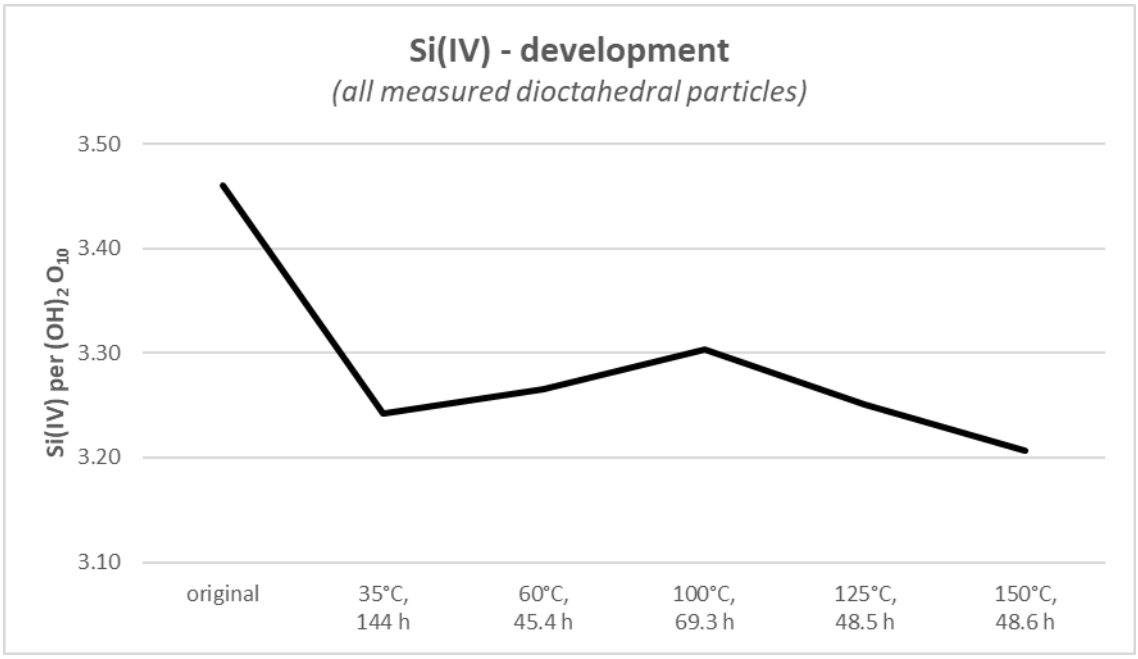

Fig. 26. *Behaviour of tetrahedral Si per $(OH)_2\ O_{10}$ in fraction < 2 µm of Opalinus Clay*
Note: *KS-ml not included here*

TEM-EDX: Illite-behaviour in experiments

All samples are dominated in fraction < 2 µm by illite and offer that's why a sufficient number of illite particles for TEM-EDX-measurements.

The available TEM-EDX-measurements indicate the occurrence of three illite groups: (i) Al(VI)-rich (> 1.5 per $(OH)_2\ O_{10}$), Fe(VI) ≤ 0.4 per $(OH)_2\ O_{10}$ and low Mg(VI) (< 0.1 per $(OH)_2\ O_{10}$), with a high K-deficit; (ii) Al(VI)-rich (< 1.5 per $(OH)_2\ O_{10}$), Fe(VI) ≤ 0.4 per $(OH)_2\ O_{10}$ and moderate Mg(VI) (~ 0.2 per $(OH)_2\ O_{10}$), with only a moderate K-deficit; (iii) Al(VI)-reduced (< 1.3 per $(OH)_2\ O_{10}$), Fe(VI)-rich > 0.5 per $(OH)_2\ O_{10}$ and moderate Mg(VI) (~ 0.2 per $(OH)_2\ O_{10}$), with a moderate K-deficit. These three illite

groups are well to recognize in experiments at 35°C (sample No22), at 125°C (sample No14) and at 150°C (sample No13) (fig. Illite_Opalinus). Cluster1 of sample No22 represents illite group (i), Cluster2 mirrors illite group (ii) and Cluster3 shows the illite group (iii). Cluster2 of sample No14 represents illite group (i), Cluster3 mirrors illite group (ii) and Cluster1 shows the illite group (iii). Cluster2 and Cluster4 of sample No13 represent illite group (i), Cluster3 mirrors alteration in illite group (ii) and Cluster1 shows the illite group (iii). Experiments at 60°C (sample No9) and at 100°C (sample No8) show a reduced differentiation of illite particles. Cluster1 of sample No9 seems to mix illite groups (ii) and (iii). In sample No8, illite group (ii) was not identified here.

Following the above introduced division of clusters in this system of illite groups, illite group (i) is nearby unchanged in composition in all experiments. Only a slight substitution of Al by Fe in octahedral layer is to observe with increasing thermal load in experiments. Illite group (ii) is few times not to differentiate after treatment of clay (60°C, 100°C) and shows in experiment at 150°C (No13) a slight substitution of Fe by Al, now with a higher K-deficit. Illite group (iii) shows the same development (enrichment of octahedral Fe by Al-substitution) with increasing thermal load as illite group (i) but linked with slight continuous changes in composition. All these mentioned low-changed compositions in illite groups (i) + (iii) and the more variable behaviour of illite group (ii) could be caused by alteration processes and/or by changes in the thickness of particles. Thinner particles offer a higher surface in interaction with solutions than thicker particles and aggregates. So, thinner particles resist in solutions better, if they contain a higher octahedral Al-ratio and less Fe and Mg (less sheet stress by effect of Fe, Mg-cation diameter).

	Ca (XII)	Mg (XII)	Na (XII)	K (XII)	Cr3+ (VI)	Al (VI)	Fe3+ (VI)	Mg (VI)	Ti (VI)	Al (IV)	Si (IV)	XII	n_VI	%S	K-deficit	charge-deficit
Opalinus original																
BLT-A7																
Cluster1 *(n=14)*	0.13	0.13	0.01	0.25	0.00	1.39	0.48	0.09	0.04	0.76	3.24	0.76	2.0	6	74%	12%
Opalinus treated																
BFS-B12																
No22 *35°C, 144h*																
Cluster1 *(n=22)*	0.10	0.14	0.03	0.33	0.00	1.58	0.37	0.05	0.01	0.80	3.20	0.83	2.0	3	64%	5%
Cluster2 *(n=30)*	0.10	0.03	0.03	0.56	0.00	1.43	0.39	0.17	0.01	0.68	3.32	0.84	2.0	11	44%	-1%
Cluster3 *(n=34)*	0.10	0.10	0.02	0.51	0.00	1.26	0.55	0.16	0.03	0.82	3.18	0.95	2.0	2	44%	-8%
No9 *60°C, 45.4h*																
Cluster1 *(n=64)*	0.15	0.07	0.04	0.43	0.00	1.41	0.43	0.14	0.02	0.81	3.19	0.93	2.0	3	53%	-6%
Cluster2 *(n=20)*	0.10	0.01	0.03	0.62	0.00	1.37	0.39	0.23	0.01	0.68	3.32	0.88	2.0	11	38%	-5%
No8 *100°C, 69.3h*																
Cluster1 *(n=38)*	0.08	0.15	0.00	0.44	0.00	1.28	0.57	0.13	0.02	0.79	3.21	0.90	2.0	4	52%	-3%
Cluster2 *(n=52)*	0.06	0.08	0.00	0.54	0.00	1.52	0.35	0.12	0.01	0.69	3.31	0.81	2.0	10	45%	4%
No14 *125°C, 48.5h*																
Cluster1 *(n=33)*	0.11	0.10	0.06	0.47	0.00	1.18	0.59	0.19	0.04	0.82	3.18	0.96	2.0	2	48%	-9%
Cluster2 *(n=38)*	0.12	0.13	0.04	0.32	0.00	1.56	0.38	0.07	0.00	0.82	3.18	0.87	2.0	2	65%	1%
Cluster3 *(n=50)*	0.12	0.02	0.06	0.57	0.00	1.36	0.40	0.23	0.01	0.70	3.30	0.91	2.0	9	42%	-8%
No13 *150°C, 48.6h*																
Cluster1 *(n=10)*	0.06	0.16	0.06	0.45	0.00	1.21	0.64	0.11	0.05	0.92	3.08	0.97	2.0	-2	48%	-8%
Cluster2 *(n=9)*	0.05	0.00	0.09	0.68	0.00	1.39	0.40	0.21	0.00	0.68	3.32	0.88	2.0	11	32%	-5%
Cluster3 *(n=15)*	0.20	0.05	0.13	0.34	0.00	1.67	0.24	0.09	0.00	0.88	3.12	0.97	2.0	0	61%	-9%
Cluster4 *(n=38)*	0.10	0.03	0.14	0.57	0.00	1.33	0.45	0.21	0.01	0.77	3.23	0.98	2.0	5	39%	-13%

Tab. Illite_Opalinus. *Opalinus Clay: Illite in fraction < 2 µm (by TEM-EDX)*

Legend: *(n=22) – number of illite particles measured by TEM-EDX; XII – interlayer charge; n_VI – number of atoms in octahedral layer per $(OH)_2$ O_{10}; %S – probability of smectite layers in senso of Środon et al. (1992); K-deficit, charge-deficit – in senso of Środon et al. (1992) (normal K in illite = 0.89 per $(OH)_2$ O_{10})*

References

Aplin, A.C., Matenaar, I.F., McCarty, D.K., van der Pluijm, B.A. (2006). Clays Clay Miner 54, 500-514. DOI: 10.1346/CCMN.2006.0540411

Bergmann, J., Friedel, P., Kleeberg, R., 1998. BGMN — a new fundamental parameter based Rietveld program for laboratory X-ray sources, its use in quantitative analysis and structure investigations. CPD Newsl. 20, 5–8.

Bossart, P., Tury, M. (Ed.) (2008. Mont Terri Rock Laboratory. Project, Programme 1996 to 2007 and Results, Federal Office of Topography

Cliff, G. & Lorimer, G. W. (1975). J. Microsc. 103, 203–207.

Döbelin, N., Kleeberg, R. (2015). Journal of Applied Crystallography 48, 1573-1580. DOI: 10.1107/S1600576715014685

Henning, K.-H. (1971): Mineralogische Untersuchung des eozänen Tones der Lagerstätte Friedland (Bezirk Neubrandenburg).- In: Ber.dtsch.Ges.geol.Wiss., B.- 16 (5), 5-39.

Henning, K.-H. & Störr, M. (1986). Electron Micrographs (TEM, SEM) of Clays and Clay Minerals, p. 325. Akademie-Verlag Berlin.

Hoang-Minh, T., Kasbohm, J., Nguyen-Thanh, L., Nga, P. T., Lai, L. T., Duong, N. T., Thanh, N. D., Thuyet, N. T. M., Anh, D. D., Pusch, R., Knutsson, S. & Ferreiro Mahlmann, R. (2019). J. Appl. Cryst. 52, 133-147. DOI: 10.1107/S1600576718018162

Karnland, O., Olsson, S., and Nilsson, U. (2006) Mineralogy and sealing properties of various bentonites and smectite-rich clay materials. In: Technical Report of SKB TR-06-30, SKB, Stockholm, Sweden, 112 pp.

Kaufhold, S., Hein, M., Dohrmann, R., and Ufer, K. (2012). Quantification of the mineralogical composition of clays using FTIR spectroscopy. Vibrational Spectroscopy 59, 29 – 39. DOI: 10.1016/j.vibspec.2011.12.012

Kleeberg, R., Ufer, K., and Bergmann, J. (2010) Rietveld analysis with BGMN Rietveld method physical basics profile modelling quantification. In: BGMN workshop Freiberg 2010. Technische Universität Bergakademie Freiberg. Freiberg, Germany, 87 pp.

Lee, B.D., Sears, S.K., Graham, R.C., Amrhein, C., Vali, H., 2003. Secondary mineral genesis from chlorite and serpentine in an ultramafic soil toposequence. Soil Sci. Soc. Am. J. 67, 1309–1317. http://dx.doi.org/10.2136/sssaj2003.1309.

Lorimer, G. W. & Cliff, G. (1976). Electron Microscopy in Mineralogy, edited by H. R. Wenk, pp. 506–519. Berlin: Springer Verlag.

Matschiavelli N, Kluge S, Podlech C, Standhaft D, Grathoff G, Ikeda-Ohno A, Warr LN, Chukharkina A, Arnold T, Cherkouk A. (2019). The Year-Long Development of Microorganisms in Uncompacted Bavarian Bentonite Slurries at 30 and 60 °C. Environ Sci Technol. 53(17),10514-10524. DOI: 10.1021/acs.est.9b02670.

Mellini, M. & Menichini, R. (1985). R. Soc. Ital. Miner. Petrol. 40, 261–266.

Moore, D.M., Reynolds, R.C., 1997. X-ray Diffraction and the Identification and Analysis of Clay Minerals, 2nd ed. Oxford University Press.

NAGRA (2002). Project Opalinus Clay - Safety Report – Demonstration of disposal feasibility for spent fuel, vitrified high-level waste and long-lived intermediate-level waste (Entsorgungsnachweis). TECHNICAL REPORT 02-05. ISSN 1015-2636

Nguyen-Thanh, L., Herbert, H.-J., Kasbohm, J., Hoang-Minh, T. & Mählmann, R. F. (2014). Clays Clay Miner. 62, 425–446.

Pearson, F.J., Arcos, D., Bath, A., Boisson, J.-Y., Fernández, A. M., Gäbler, H.-E., Gaucher, E., Gautschi, A., Griffault, L., Hernán, P., and Waber, H. N. (2003. Mont Terri Project – Geochemistry of Water in the Opalinus Clay Formation at the Mont Terri Rock Laboratory. No. 5, Berichte des BWG, Serie Geologie – Rapports de l'OFEG, Série Géologie – Rapporti dell'UFAEG, Serie Geologia – Reports of the FOWG, Geology Series.

Środoń, J., Elsass, F., McHardy, W. J. & Morgan, D. J. (1992). Clay Miner. 27, 137–158.

Ufer, K., Roth, G., Kleeberg, R., Stanjek, H., Dohrmann, R., Bergmann, J., 2004. Description of X-ray powder pattern of turbostratically disordered layer structures with a Rietveld compatible approach. Z. Krist. 219, 519–527. doi.org/10.1524/zkri.219.9.519.44039.

Ufer, K., Stanjek, H., Roth, G., Dohrmann, R., Kleeberg, R., Kaufhold, S. (2008) Quantitative phase analysis of bentonites by the Rietveld method. Clays and Clay Minerals, 56, 272-282. dx.doi.org/10.1346/CCMN.2008.0560210.

Part III. SUPPLEMENTS

S1. Overhead shaking experiments of B25-bentonite and Opalinus clay

(p. 96- p. 166)

S2. X-ray Diffraction (XRD)

(p. 167- p. 383)

S3. Fourier Transform Infared Spectroscopy (FTIR)

(p. 384- p. 414)

S4. Thermal Analysis (DTA-TG)

(p. 415- p. 457)

S5. Cation exchange capacity (CEC), Specific surface area (SSA), and surface charges

(p. 458- p. 460)

S6. Scanning Electron Microscopy (SEM)

(p. 461- p. 491)

S7. Transmission Electron Microscopy coupled Energy-dispersive X-ray Spectroscopy (TEM-EDX)

(p. 492- p. 902)